

Human and Machine Learning in Myoelectric Control

By

KENNETH ROBERT LYONS

DISSERTATION

Submitted in partial satisfaction of the requirements for the degree of

DOCTOR OF PHILOSOPHY

in

Mechanical and Aerospace Engineering

in the

OFFICE OF GRADUATE STUDIES

of the

UNIVERSITY OF CALIFORNIA

DAVIS

Approved:

Sanjay S. Joshi, Chair

Stephen K. Robinson

Anthony S. Wexler

Committee in Charge

2018

CONTENTS

List of Figures	v
List of Tables	xi
Abstract	xii
Acknowledgments	xiii
1 Electromyography and Myoelectric Control	1
1.1 Why Record the Music of Muscles?	1
1.2 Why is it Difficult?	3
1.3 How is it Done?	4
2 First Experiments with Myoelectric Control	6
2.1 Using a Single EMG Sensor to Control a Mobile Robot	6
2.1.1 Introduction	6
2.1.2 Mapping a Single Signal to Two Dimensions	8
2.1.3 Control Interface	9
2.1.4 Experiment Setup	10
2.1.5 Results	12
2.1.6 Conclusions	15
2.2 Initial Venture into Multi-Channel EMG	16
2.2.1 Introduction	16
2.2.2 Building a Multi-Channel EMG Platform	16
2.2.3 MATLAB GUI for Collecting Data	17
2.2.4 Gesture Recording	18
2.2.5 Processing	20
2.2.6 Manifold-Based Classification	21
2.2.7 Results	23
2.2.8 Conclusions	25
2.3 Outcomes	27

3 Classification of Leg Gestures for Prosthetic Arm Control	28
3.1 Literature Review	29
3.2 Mapping Between the Arm and Leg	31
3.3 Experiment: Feasibility of Classifying Leg Gestures with EMG	32
3.3.1 Introduction	32
3.3.2 Experiment Design	33
3.3.3 Signal Processing and Analysis	35
3.3.4 Results	38
3.3.5 Conclusions	40
3.4 Experiment: Initial Real-Time Control Testing	44
3.4.1 Introduction	44
3.4.2 The Target Achievement Control Test	45
3.4.3 Experiment Design	46
3.4.4 Results	48
3.4.5 Conclusions	49
3.5 Experiment: TAC Test with Two-Dimensional Targets	51
3.5.1 Introduction	51
3.5.2 Improved Simulation	51
3.5.3 Experiment Design	51
3.5.4 Results	54
3.5.5 Conclusions	60
3.6 Outcomes	64
4 Visuomotor Adaptation with Proportional Myoelectric Control	66
4.1 Bayesian Integration Theory of Motor Adaptation	67
4.2 Proportional Myoelectric Control	69
4.3 Experiment: Adaptation Following Training with Mapping Noise	70
4.3.1 Introduction	70
4.3.2 Experiment Design	71
4.3.3 Experimental Tasks	72

4.3.4	Analysis	75
4.3.5	Results	76
4.3.6	Conclusions	77
4.4	Experiment: Rotational and Randomized Mapping Noise	79
4.4.1	Introduction	79
4.4.2	Experiment Design	79
4.4.3	Results	83
4.4.4	Conclusions	88
4.5	Outcomes	89
	Conclusion	91

LIST OF FIGURES

1.1	Depiction of the concept of myoelectric control. Electromyography sensors detect signals generated by muscles, allowing for estimation of a user's intentions in controlling an machine interface.	2
1.2	Common processing pipeline in myoelectric control.	4
2.1	Diagram of hardware connections made to input the sEMG signal to the tablet computer.	8
2.2	Screenshots of the user interface while the robot is navigating the course. Video from the robot's camera is shown in the background (with an obstacle in view), while the brain-computer interface regions overlay it. The cursor's path in time is obtained from logged data and is applied on top of the screenshot in (b).	10
2.3	Photo of the "Second Eyes" mobile robot developed for this project. . .	11
2.4	Photo of the subject performing the mobile robot control task. The tablet computer was placed on the table in front of him. The differential electrode pair can be seen placed behind the ear over the auricularis posterior muscle.	12
2.5	A map of robot locations while completing the course. Numbers next to the points indicate that the robot turned in place at that location the corresponding number of times before moving to the next point. Point locations are estimated based on overhead video footage taken throughout the trial.	15
2.6	EMG bridge (left): a custom circuit board made to convert a DC power source to positive and negative power rails, distribute this power to multiple EMG sensors, and route the EMG signals through a single cable. The cable can then be connected to any suitable data acquisition system (right).	17
2.7	Screenshot of MATLAB graphical user interface for prompting the subject to produce a specific gesture and record the EMG signals generated during the movement.	18

2.8	The seven gestures being performed. These are the same photos displayed in the graphical interface to prompt the subject to perform the gesture.	19
2.9	Three different perspectives of the 3-dimensional projection produced by LPP.	25
3.1	Illustration of targeted muscle reinnervation. Based on a figure from [RRFA14].	29
3.2	The mapping between upper and lower limb degrees of freedom. Elbow extension and flexion were not performed in these experiments, but these movements could be more useful for high-level amputees than radial and ulnar deviation.	31
3.3	Example electrode positioning on the arm and leg. Capital letters in the shaded areas indicate muscles that have similar primary action on the corresponding limb (see Table 3.1).	36
3.4	Screenshot of the graphical user interface used to collect gesture data. The image of the gesture to perform is the main component. A progress bar beneath that prompts the subject to contract and rest at the correct time.	37
3.5	Classification accuracy for each participant distributed across gesture classes (top) and for each gesture class distributed across participants (bottom) in the four experimental conditions. Whiskers show the full extent of the data (no outliers for clarity). Stars in the “avg” column indicate significant differences between conditions (*: $p < 0.05$, **: $p < 0.01$, ***: $p < 0.001$).	39
3.6	Confusion matrix for the leg configuration in P1 including the two “problematic” gestures: foot adduction (AD) and abduction (AB). The matrix is generated by cross validation (two cycles for training data, two cycles for testing data) averaged across subjects. The main sources of error are the off-diagonals outlined. For clarity, numerical values less than 1% are not shown.	41

3.7 Example classifier predictions over time illustrating poor recognition of the foot inversion (FI) gesture being performed (leg P1 data shown here). Most participants had trouble producing foot inversion and foot adduction gestures distinguishably from one another. This plot illustrates that the correct and incorrect predictions take place mostly on a whole <i>trial</i> basis, hinting that feedback could be a way to improve the poor classification accuracy of the problematic gestures.	42
3.8 Target achievement control test environment simulated with V-REP. The subject is being prompted to supinate the forearm in this image.	46
3.9 Summary of results averaged across participants. Error bars indicate standard error of the mean. Results from comparable studies are also shown: AB (inexperienced able-bodied subjects with sensors on the arm, 3-DOF active [SHLK11a, SHLK11c]), AMP (experienced amputees with sensors on the residual limb, 3-DOF active [SHLK11b]), TMR (experienced TMR subjects, 4-DOF active [SHLK09]).	48
3.10 Cumulative completion rates averaged over participants. Filled areas represent ± 1 standard error of the mean.	49
3.11 Progression of a 2-DOF TAC test trial depicted using serial screenshots of the V-REP interface. A translucent, multi-colored “reference arm” was shown to the subject to display the resting (target) posture. Each DOF involved in the trial was initially displaced by 60 degrees and the task involved bringing the arm back to the resting posture with ± 10 -degree tolerances in each joint. Arm segments corresponding to joints outside the target were colored grey and turned green when the joint reached the target.	52

3.12 Subject performance in the target achievement control task. Each subject's performance is shown with a translucent grey dot, and across-subject means are indicated as squares. Completion time and path efficiency correspond only to successful trials. Data from comparable studies are also shown near the corresponding configurations: AB (inexperienced able-bodied subjects with sensors on the arm [SHLK11a]), TMR (experienced TMR subjects [SHLK11a, SHLK09]), AMP (experienced amputees with sensors on the residual limb [SHLK11b]).	56
3.13 Cumulative completion rate: the percentage of trials completed across the range of completion times. Kernel density estimates of completion rates are plotted below to highlight the time at which most of the trials were completed for each condition.	57
3.14 Subject performance in the target achievement control task across trial blocks. Each point is the mean over subjects and target DOFs, and error bars indicate standard deviation of the mean across subjects. Only completion rate in the leg configuration with 4-DOF active showed a significant change over the session (marked with *).	58
4.1 Illustration of the Bayesian update. The prior represents the subject's initial prediction of reach position. When an observation is made that is incongruent with the prior, the estimate is shifted away toward the observation, depending on the relative strength of the prediction from the forward model and the feedback received.	68
4.2 Illustration of the cursor following process. The subject watches a cursor on the screen move out to some target location and back while following it with the hand. The assumption is that windows of EMG signals correspond to the cursor position at each moment.	70
4.3 Electrode placement in the adaptation experiments. Six Delsys wireless sensors were spaced equidistantly around the forearm.	72

4.4	(a) Cursor control mapping from a representative subject. Each arrow represents a single EMG channel's effect on the cursor position. For the noise group, new mappings were formed on each trial by perturbing the mapping vectors vertically. (b) Wrist movements subjects used to move the cursor in the four cardinal directions (assuming right hand dominant). .	73
4.5	Illustration of an adaptation trial to the target at 0°. The cursor begins at the starting location (center of the screen) then disappears as the subject moves in the target direction. Once the cursor passes an invisible line perpendicular to the target direction, its position is perturbed and displayed. .	74
4.6	Path efficiency by block in the familiarization task. Each block consists of two repetitions of each target. Points represent subject averages and filled regions represent \pm one standard error of the mean. .	76
4.7	Adaptation rates for the two groups and two targets in the adaptation task. Each subject's data for the given condition is averaged, then subject means are combined to form the boxes. .	77
4.8	The three types of variability added, corresponding to the three different experimental groups. Mapping variability refers to sampling mapping vectors randomly from a symmetric 2D Gaussian. Direction variability refers to the entire mapping matrix being rotated randomly. Target variability refers to the target being rotated about the center of the interface randomly. .	81
4.9	Representative mappings generated by subjects. The solid lines are the mapping vectors in the prone (default) position, and the dashed lines are the corresponding vectors fit to data generated while the subject had the arm in the supine position. Each color is a different EMG channel named after the primary muscle being recorded (extensor carpi ulnaris, brachioradialis, flexor carpi ulnaris, flexor carpi radialis, extensor digitorum minimi, extensor digitorum). .	83

4.10	Absolute errors across target directions in the pre and post test tasks, averaged across subjects in all groups. Boxes extend to the upper and lower quartiles, while the whiskers show the full extent of the data.	84
4.11	Absolute endpoint errors made averaged across subjects in each group in the pre-test, all practice blocks, post-test, and transfer tasks. Error bars indicate standard deviation across subjects.	85
4.12	Slope and Pearson correlation coefficient of the linear regression between endpoint errors and midpoint errors in the practice task.	86
4.13	Adaptation rates for each group, split into trials with and without feedback uncertainty (scattered cursors). This adaptation rate is defined by the change in endpoint error as a function of previous perturbation.	87
4.14	Observation adaptation rate. Here, the adaptation rate is the change in endpoint error as a function of the previously observed error.	88

LIST OF TABLES

2.1	Evaluation of Target Selection	13
2.2	Evaluation of Performance Inefficiencies	14
2.3	Comparison of feature-based classifiers	23
2.4	LDA confusion matrix	24
2.5	SVM confusion matrix	24
2.6	Comparison of manifold-based classifiers	25
3.1	Arm and Leg Muscles Used for Gesture Classification	33

ABSTRACT

Human and Machine Learning in Myoelectric Control

Muscles are responsible for generating the forces that move the body, but if a limb is missing or some part of the body is unable to move, it is sometimes possible to remap muscle outputs to a machine through an engineered human-machine interface. By recording the electrical potentials that muscles generate when they contract, known as electromyography (EMG), we can bring biological data into the world of computing and robotics. Opening this communication channel from muscle to machine makes it possible to replace lost or diminished capabilities in disabled individuals via devices like prosthetic limbs or powered wheelchairs.

A primary task in bringing these kinds of interfaces to fruition is in recognizing the intentions of the user in commanding the machine, and due to the nature of EMG signals, this is a challenging problem. Over the last several decades, focus has been primarily directed toward development of sophisticated signal processing and machine learning techniques to extract user intentions from EMG. More recently, however, research in myoelectric control interfaces and brain-computer interfaces has emphasized the role of the human in the human-machine interface and the fact that we are particularly capable of adapting to various kinds of change. While machine learning algorithms can be made to operate adaptively, the kinds of adaptation achieved are rigid compared to the capabilities of humans, who perform an entire lifetime of accurate movements despite noisy sensors, noisy transmission lines, and delays.

Presented here are several branches of work aimed at improving the state of myoelectric control. Having designed and tested different approaches to myoelectric control for various applications, I am convinced that future EMG-based interfaces need to more explicitly take the user into account as an active learning agent. Accordingly, the common thread in the research presented here is the desire to understand how to improve myoelectric control by considering both of these perspectives on learning and adaptation.

ACKNOWLEDGMENTS

Overall, I want to acknowledge the fact that a good number of people put up with and supported me while I wrestled with this... interesting life chapter that I look forward to looking back on fondly. I'd like to recognize the following people for their roles in making this work possible.

My advisor, Sanjay Joshi, always provided a reliable source of optimism and encouragement to balance my tendency to dwell on the suboptimal. I couldn't imagine a better person to share rejection with. Of course, there's no way I would've gotten through this without him.

Desmona Brooks, my partner through this entire process, deserves most of the credit for keeping me grounded and seeing me through all of the peaks and valleys. Putting up with someone that keeps saying "just one more year" could not have been easy, but she did it anyway.

My friends and fellow lab members Ben Margolis and Ida-Maria Skavhaug were always willing to listen to my ideas and struggles. It's important to have friends that understand, and both of them understood better than most.

Thanks to my committee members for taking the time to review this document and provide feedback on it.

Finally, credit belongs to my parents, Bob and Sue, for instilling in me at an early age the idea that I can do whatever I put my mind to. So far, so good.

Chapter 1

Electromyography and Myoelectric Control

1.1 Why Record the Music of Muscles?

Electromyography (EMG) is the measurement of electrical potentials generated by skeletal muscles when they contract. It is used in a variety of clinical contexts such as diagnosis of neuromuscular disorders and gait analysis, and it is commonly used as a control signal for powered prosthetic devices. Surface electromyography, in which muscle signals are measured by electrodes on the surface of the skin, has several important features for practical use: it is noninvasive, it is relatively large in magnitude compared to other bioelectric signals measured from the skin (e.g. electroencephalography—measurement of cortical potentials at the scalp which are orders of magnitude smaller than EMG), and it represents a very *functional* output of the human body that is easy to manipulate in many situations. These features make it an attractive target of study for providing control of external devices as a means of replacing lost functionality (e.g. prosthetic arm control) or augmenting existing functionality (e.g. powered exoskeleton control). All of these control applications utilize a myoelectric interface—the signal acquisition, signal processing, algorithms, and actuation between volitional production of muscle activity and external device action.

Perhaps the most well-known use of electromyography is in the control of prosthetic limbs. With the loss of a limb, there may be residual musculature that can be recorded

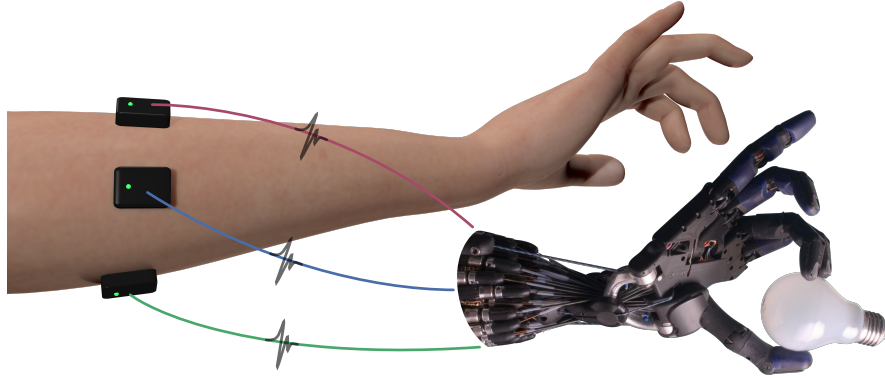


Figure 1.1: Depiction of the concept of myoelectric control. Electromyography sensors detect signals generated by muscles, allowing for estimation of a user’s intentions in controlling a machine interface.

from and used as a means of controlling a robotic replacement. The genius of this idea lies in the fact that the muscles of the limbs tend to be located “upstream” of the joint they’re responsible for actuating. For example, the muscles that move the hand up and down if you hold your arm out in front of you (wrist extension and flexion) are located in the forearm near the elbow. Hence, in the case of an amputation between the elbow and the wrist (transradial), these muscles may remain and can be contracted to generate an EMG signal even though the wrist and hand are missing. A common goal in the use of EMG in this application is to allow the user to contract the residual muscles and map the generated signals to the prosthesis such that it moves similarly to how the missing limb *would have moved* (Figure 1.1). The ideal outcome would be to perfectly replace the lost limb. This problem can be broken down into two main components: robotics technology capable of moving with the amazing dexterity of the human arm and hand, and the human-machine interface technology to recognize the intentions of the device operator.

1.2 Why is it Difficult?

The amplitude of an EMG signal is representative of the “strength” of the underlying muscle contraction, but it doesn’t correlate well with useful variables like force output (except in very specific conditions) or joint velocity. Furthermore, it is usually difficult or impossible to isolate specific muscles with current surface electromyography technology. In general, a single sensor detects the electrical potentials of many muscle fibers of any muscles near the electrodes. In addition, there are various sources of non-stationarity and variability inherent in surface EMG recording. For example, accumulation of sweat in a prosthetic limb socket can cause the skin-electrode interface to degrade. Another example is the well-known limb position effect [FSC⁺11], which arises on short time scales as a result of simply changing limb position (e.g. from arm out in front of the user to reaching overhead). To overcome some of these issues, research in the last decade has focused primarily on machine learning techniques for accurately decoding user intent from EMG signals produced during natural movements. This involves a training procedure in which a user performs these natural movements while EMG is recorded in order to *train* the system, then the system can predict those natural movements given novel inputs. In laboratory settings, where an individual’s training data can be carefully recorded and testing occurs in the same environment, this approach provides extremely accurate recognition of gestures (> 95%). However, it remains difficult to keep this performance when conditions change, and it turns out that there are many changes at various time scales that can do influence performance. Inter-electrode distance [YH11], electrode shift [HEH08, YHK12], day-to-day (inter-session) changes [Liu15] and changing arm position [FSC⁺11] are all examples that have been studied and resolved with limited success for specific systems. All of these changes make the design of robust and highly functional myoelectric control schemes a challenging problem, and this seems to be the reason that advanced myoelectric control interfaces are still not viable clinically.

Another fundamental challenge in myoelectric control is a chicken-and-egg problem: we want the user to generate data so that a machine can learn the association between the EMG signals and the user’s intended action, but a novice user may not be capable

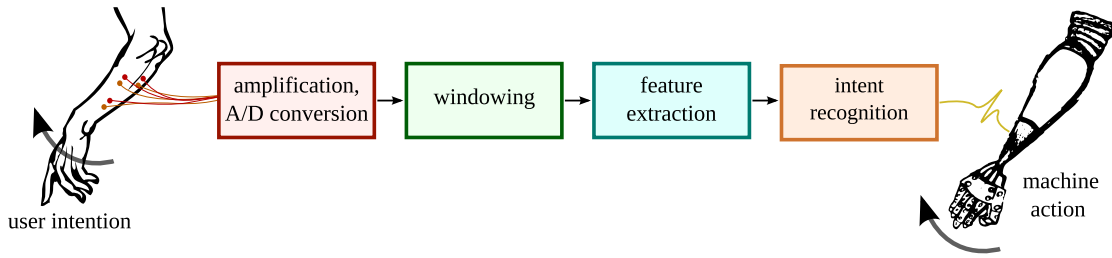


Figure 1.2: Common processing pipeline in myoelectric control.

of producing EMG signals that represent their intentions accurately. This problem is exemplified by the primary candidates for myoelectric control: amputees. Since they are missing part or all of a limb, it can be challenging to produce muscular contractions that are representative of, say, wrist extension and not hand opening. Co-adaptive systems, where the human and machine work together toward a common “understanding” of the mapping from muscle activation to intended action, is one promising approach to this problem [HDH⁺15].

1.3 How is it Done?

Essentially all myoelectric control schemes employ a common set of operations to map user intentions to some effect on the world, shown in Figure 1.2. First, electrodes placed on the surface of the skin pick up the millivolt-level potentials generated by the propagation of motor unit action potentials traveling down the muscle fibers. These electrodes are usually directly connected to an amplifier that increases the signal amplitude, and usually at this point the signals are sampled in order to bring them into the digital domain. The samples are then read in frames, or windows, and this is the point from which different approaches to myoelectric control diverge. What they all seem to have in common, however, is a process of extraction of features from the signals and some method of mapping these features to a device controller.

In proportional control, the features are usually some measure of signal amplitude, like the root mean square or mean absolute value. Since the amplitude of an EMG signal increases with contraction strength, this maps well to things like a robotic wrist joint velocity or a grasp force, so the intent recognition in this case is a simple mapping.

Proportional control is discussed in more detail in Chapter 4. Another approach is to extract more complex features like the signal spectrum and to let a machine learning algorithm learn the mapping from user intent to output. This approach to myoelectric control is discussed in Chapter 3.

Yet another approach is to forgo attempting to recognize intent at all and let the user *learn* how to generate desired outputs. Recently, researchers in myoelectric interfaces and brain-computer interfaces have emphasized that the human is half of the human-computer interface and that humans are particularly adaptable to multiple interferences at various time scales [CAW⁺14, SC14]. While machine learning algorithms can be made to operate adaptively, the kinds of adaptation achieved are rigid compared to the capabilities of humans, who perform an entire lifetime of accurate movements despite noisy sensors, noisy transmission lines, and delays [SSK10]. Having designed and tested a variety of myoelectric control systems, I am convinced that future myoelectric interfaces need to more explicitly take the user into account as an active learning agent.

The remainder of this text is split into three chapters. In Chapter 2, I discuss a couple very different styles of myoelectric control as a historical account of my initial exposure to the field. In Chapter 3, I discuss several experiments utilizing machine learning techniques in an attempt to bring highly functional upper limb prosthesis control to people with high-level amputations. Finally, in Chapter 4, I discuss a series of experiments aimed at better understanding the nature of human adaptation with myoelectric control as an approach to human-machine co-adaptive control.

Chapter 2

First Experiments with Myoelectric Control

Preface

This chapter describes my initial study of and experience with electromyography for myoelectric control. First, I extended the use of an existing single-sensor interface to allow a person with a high-level spinal cord injury to remotely control a telepresence mobile robot. After this introduction to the measurement, processing, and mapping of EMG to external devices, I became interested in working with multiple sensors and using machine learning techniques to recognize complex gestures. This required new hardware and software, so development of this infrastructure will be described as well as some initial experiments with gesture classification.

2.1 Using a Single EMG Sensor to Control a Mobile Robot

2.1.1 Introduction

EMG is most commonly used in clinical applications (e.g. gait analysis) and prosthesis control applications, but it has additional applications for mobility-impaired individuals. For example, people with high-level spinal cord injury (SCI) typically are able to contract the muscles in the head and face because those muscles are innervated at the brain stem

rather than the spinal cord. With this ability, EMG can be recorded and mapped to an abstract interface like a cursor on a screen, which can in turn be connected to a device like a wheelchair controller or a telepresence mobile robot. Most of the content of this section is also presented in [LJ13].

In the EMG interface described here, the neuromuscular system is trained to generate an electrical signal from the auricularis posterior, a small muscle behind the ear. This muscle is vestigial in humans, meaning it serves no known purpose, though many individuals are capable of contracting this and other auricular muscles to “wiggle” the ears. Interestingly, the auricular muscles are known to contract involuntarily in response to rapid-onset sounds like clicks [OP99]. Aside from that, not much is known about these muscles, including who can or can’t voluntarily contract them. In the interface described here, the user is tasked with continuously manipulating the power in two different bands of the spectrum of a single EMG signal recorded from the auricularis posterior. Each frequency band gives a control channel, provided the user can manipulate them independently. In this study, a paralyzed subject guided a computer cursor in two dimensions to hit three available buttons on the screen to command a telepresence mobile robot to perform discrete driving actions (move forward, turn left in place, turn right in place). The subject guided the robot through an obstacle course using a live video feed from the robot as feedback. The foundation for this study is presented briefly here but is based on previous work in our lab [PMWJ10, VJ11], where the technique of utilizing the power in two frequency bands of a single EMG signal to control a cursor in two-dimensional space was established.

There has been some previous work done on control of mobile robots using brain-computer interfaces, most of which is based on electroencephalography (EEG). Millán et al. [MRMG04] used a classification-based approach to recognize mental states based on EEG recordings. These states were then used in the discrete function control of Khepera robots to go forward, turn left, turn right, etc. Escolano et al. [EAM12] used EEG to control a mobile robot with some autonomy and image processing capabilities by allowing the user to select from a scanning grid of robot locations viewed from the

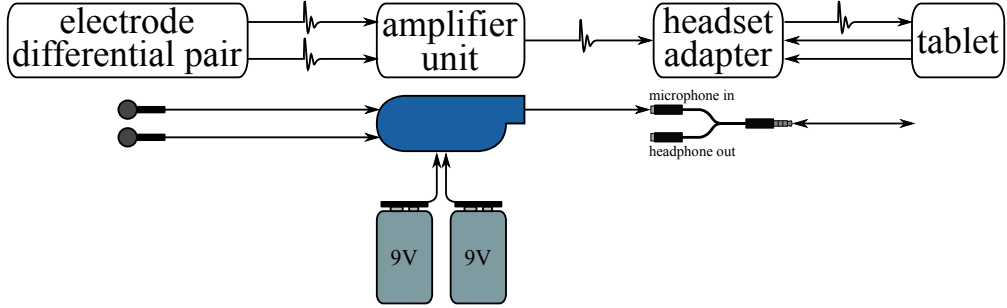


Figure 2.1: Diagram of hardware connections made to input the sEMG signal to the tablet computer.

robot's perspective. Note that all EEG systems use multiple signals measured from the scalp, whereas the EMG system used here needs only a differential pair of electrodes at a single muscle site located behind the ear, making the interface discreet and allowing it to be completely mobile since currently available mobile devices are capable of processing single-channel EMG. EMG is also a fairly robust signal in comparison to EEG, which is 10–100 times smaller in magnitude due to attenuation of the skull.

2.1.2 Mapping a Single Signal to Two Dimensions

The hardware used to implement this interface is depicted in Figure 2.1. It is similar to the setup described in previous work in our lab [VJ11], but it uses a tablet with a standard 3.5 mm TRRS phone connector rather than the power and data cable used in the Android phone system. This setup is completely mobile since it is battery-powered and self-contained. A differential pair of 4 mm shielded Ag-AgCl electrodes from BIOPAC were connected to a Motion Lab Systems Y03 EMG preamplifier. An off-the-shelf headset adapter split the headset signals to mono microphone input and stereo headphone output. The single amplified signal was then directly sent to the tablet's microphone input hardware while still allowing for the use of headphones or speakers.

With the EMG signal routed to the microphone port, a custom application on the tablet recorded the signal at an 8 kHz sample rate and downsampled to 4 kHz. A buffer of samples was copied and each copy underwent separate signal processing to extract two frequency bands from the signal. Each copy had a Butterworth filter applied (80–100 Hz cutoffs and 130–150 Hz cutoffs) and the power (sum of squares of samples) was

computed after filtering, P_1 and P_2 . With the power in each frequency band, the values were normalized according to calibration values by having the subject produce a strong (though not necessarily maximal) contraction, $P_{1\text{max}}$ and $P_{2\text{max}}$. After normalization, the values were further adjusted by what we called “effort” values, set manually by the researcher. These parameters were implemented to help avoid fatigue, since the inputs were normalized with respect to a strong contraction that the subject would not be able to generate for long periods of time. The overall calculation for the normalized and adjusted band power values are given by

$$b_1(n) = \frac{P_1(n)}{P_{1\text{max}}} \frac{100}{e_1}, \quad b_2(n) = \frac{P_2(n)}{P_{2\text{max}}} \frac{100}{e_2} \quad (2.1)$$

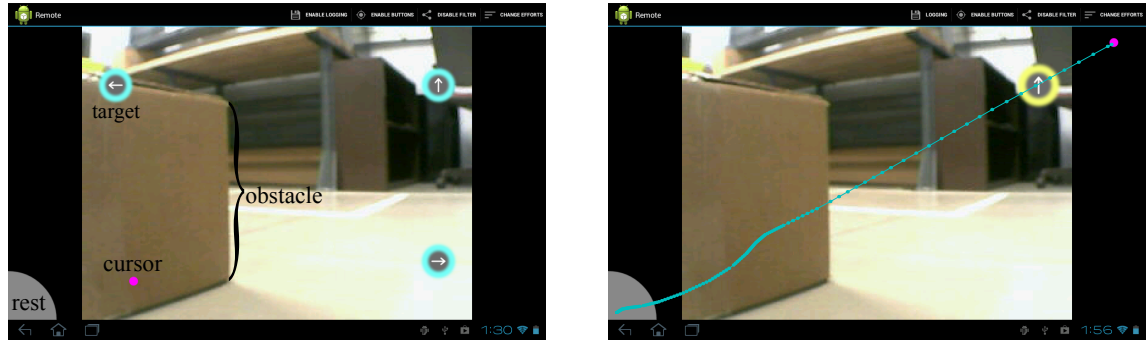
Note that because the power values are always positive and the effort values are always between 1 and 100, the coordinate pair, (b_1, b_2) , will always exist in the first quadrant of the Cartesian plane. The region of the quadrant that the point lies in is further constrained because zero power is not achievable in practice due to noise, etc. and because increasing the power in one band will lead to at least some increase in the other. A linear transformation to expand the achievable space was then applied:

$$\begin{bmatrix} x(n) \\ y(n) \end{bmatrix} = \begin{bmatrix} 1.75 & -0.75 \\ -0.75 & 1.75 \end{bmatrix} \begin{bmatrix} b_1(n) \\ b_2(n) \end{bmatrix} \quad (2.2)$$

where $x(n)$ and $y(n)$ are the transformed coordinates at time n . These coordinates were then filtered with a moving average filter and then used as the coordinates of the cursor on the screen. In addition, the positions were linearly interpolated between the calculated cursor positions (at 4 Hz) so that the perceived update rate of the cursor position was 32 Hz.

2.1.3 Control Interface

The graphical user interface implemented on the tablet is shown in Figure 2.2. The cursor interface was drawn on top of a video feed from the robot. The cursor starts in the lower left corner when the subject relaxes. As the subject contracts the muscle, the cursor leaves the rest area. Once a cursor intersects with a target, that target is selected. In order to confirm the target and have the robot perform the corresponding action, the subject



(a) Cursor on its way to a target.

(b) Forward target selected

Figure 2.2: Screenshots of the user interface while the robot is navigating the course. Video from the robot’s camera is shown in the background (with an obstacle in view), while the brain-computer interface regions overlay it. The cursor’s path in time is obtained from logged data and is applied on top of the screenshot in (b).

relaxes again to move the cursor back to the rest area. A selection timeout was also implemented such that the subject could keep the cursor out of the rest area to de-select a target if it was selected by mistake. The tablet recorded the cursor positions at each update event as well as the sequence of commands sent for analysis of the robot control session.

The robot was developed through an undergraduate senior design project, pictured in Figure 2.3. The robot was not implemented with any autonomy, so it was the sole responsibility of the user to drive it through the obstacle course. When a target was confirmed, a message was sent from the tablet to the robot via a TCP message through a local WiFi network. The three commands were: move forward one meter, rotate in place (differential drive) to the right 15° , and rotate to the left 15° . The robot also sent back command completion status messages as well as a continuous video feed from its video camera. In this study, the subject controlled the robot from across the room (separated by a partition), but the system could also be controlled totally remotely over the Internet.

2.1.4 Experiment Setup

To validate the BCI-robot system, a simple obstacle course was created, and the subject was tasked with navigating the robot through it using only the video from the robot’s perspective. The participant was a 30 year old male with an incomplete C3-C4 spinal

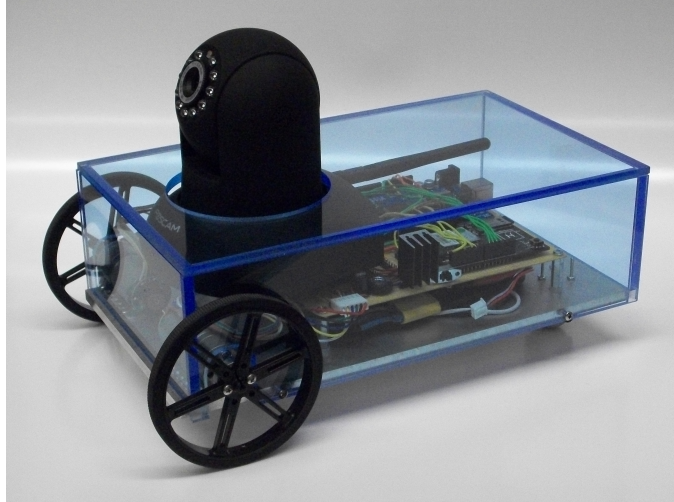


Figure 2.3: Photo of the “Second Eyes” mobile robot developed for this project.

cord injury (over 15 years since injury) who had been involved in previous studies in the lab using the mobile phone version of the cursor-to-target interface (no robot, only cursor control). His experience amounted to approximately four visits per month over the past nine months. An experienced participant was selected in order to eliminate potentially confounding issues involved in learning and focus the study on the end-to-end integration of the robot system and the interface. Characterization of the learning time to use the interface was the focus of other studies in the lab.

The course, seen in Figure 2.5, was approximately 4.25 m long and 2 m wide. Two obstacles blocked the direct path to the goal area, and they were placed to force the subject to use all three motion commands available. One obstacle split the course so that there were at least some navigation decisions required to complete the task. The task was defined as sending a series of robot commands in order to get the robot from the start location to the goal location without hitting obstacles or going outside the course boundaries. Optimally, the robot would be capable of traversing the course using approximately 15 commands. However, because of encoder-based odometry errors from wheel slippage and bumps in the path, a more realistic minimum was determined experimentally to be about 20 commands.

The participant was allowed to see the course before beginning the trial and was instructed on how target selection and confirmation works. He then moved to a location

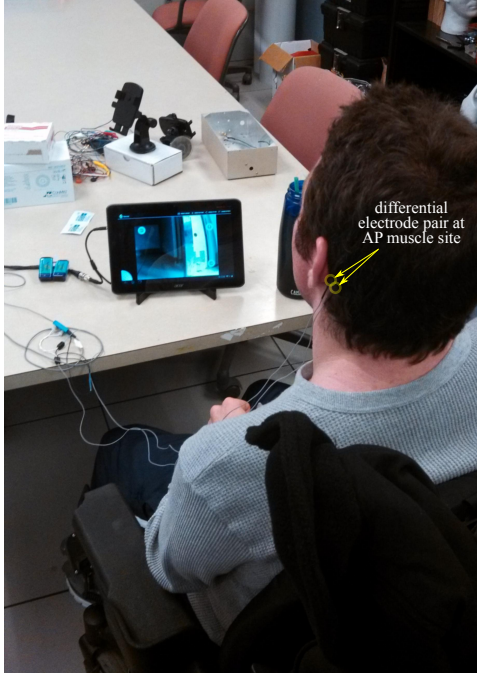


Figure 2.4: Photo of the subject performing the mobile robot control task. The tablet computer was placed on the table in front of him. The differential electrode pair can be seen placed behind the ear over the auricularis posterior muscle.

about 10 m from the robot site with a partition blocking the view of the course. The only feedback from the robot thereafter was the robot’s camera image displayed on the control tablet as shown in Figures 2.4 and in Figure 2.2. After calibration, the participant was given some time to practice sending commands, primarily to see how the robot moves with each command. Following this, the trial began, and the data collected during the single trial is presented below.

2.1.5 Results

Several performance metrics were defined to evaluate the suitability of the interface for mobile robot control. Perhaps the most important metric in a system such as this is the total amount of time taken to complete the navigation task. This encompasses all aspects of the system including efficiency of interface usage, command selection, and robot performance. If considering only robot travel time, the course could be completed in approximately one minute. However, this does not include time required to activate the interface or account for errant commands by the user. It took the subject in this case

study 8 minutes and 30 seconds to complete the course. Other numerical values of general interest are given in Table 2.1. The number of target attempts is simply the number of times the cursor entered a target region on the screen. Time to target is defined as the amount of time measured from the moment the cursor leaves rest to the moment it hits a target. The number of commands sent is the same as the number of targets confirmed. The total number of commands sent is in the range expected, especially considering that the participant had no overhead view of the course during the trial. Command completion time represents the amount of time between the control device sending a motion control message and the robot responding with a completion message. This can be thought of as travel time, since transmission delays are normally very small. Note that forward travel time is inherently greater because of the much larger wheel rotation needed to complete the motion command. Target deselections occurred when the subject selected a target erroneously and held the cursor outside the rest area to avoid confirming it, and deselection time is simply the elapsed time during the deselection process. Note that the number of target deselections was not insignificant compared to the number of commands actually sent and compared to the number of target attempts.

Table 2.1: Evaluation of Target Selection

Metric	Target			
	forward	right	left	all
target attempts	20	15	12	47
avg. cursor to target time (s)	1.57	2.45	2.92	2.20
commands sent	12	8	8	28
avg. command completion time (s)	4.09	1.45	1.64	2.64
deselections	8	7	4	19
avg. deselection time (s)	3.69	4.68	5.38	4.41

The three main performance inefficiencies were identified as *cursor wandering*, *cursor resting*, and *target deselection*. Cursor wandering is a common cycle in which the cursor leaves rest, fails to hit any target, then returns to rest. The amount of time for a given

“wander” is defined as the time from leaving rest to entering it. The amount of time spent in rest is a weak indicator of inefficiency as there will always be some non-zero resting time due to the nature of the target confirmation process. Also, the user is expected to spend some time relaxing to avoid muscle fatigue and to plan the next command to send to the robot. Deselection time is a strong indication of performance inefficiency, however. Note that it is more than simply the number of deselections multiplied by the selection timeout value because of the time taken to reach the target from rest. Not including cursor rest, the inefficiencies noted here accounted for 48% of the total course navigation time.

Table 2.2: Evaluation of Performance Inefficiencies

Metric	Times			
	min (s)	max (s)	mean (s)	total (min:sec)
cursor wander	0.09	9.14	2.57	2:44
cursor rest	0.11	20.08	1.52	2:40
target deselection	—	—	—	1:23

A visual depiction of the results of the study are shown in Figure 2.5. This shows the positions in the course in which the robot stopped between successive commands executed during the telerobotic task. A wide-angle camera mounted above the course captured video of the robot as it travelled through the course and this was used to estimate the robot’s location after each command was completed. Curved arrows next to the location points in the figure indicate the directions, if any, that the robot turned in place at that location. Numbers next to the points indicate the number of times the robot turned in place. Note that several of the points have no number, which means the robot only stopped at that location and moved forward at the very next command. This shows that only a few extraneous commands were used to complete the task. The two yellow points indicate that the robot contacted an obstacle. In both cases, it simply caused the robot to stop moving, but it did not cause the robot to become stuck at that location, so the trial continued. The red line going outside the boundary of the course is the result of

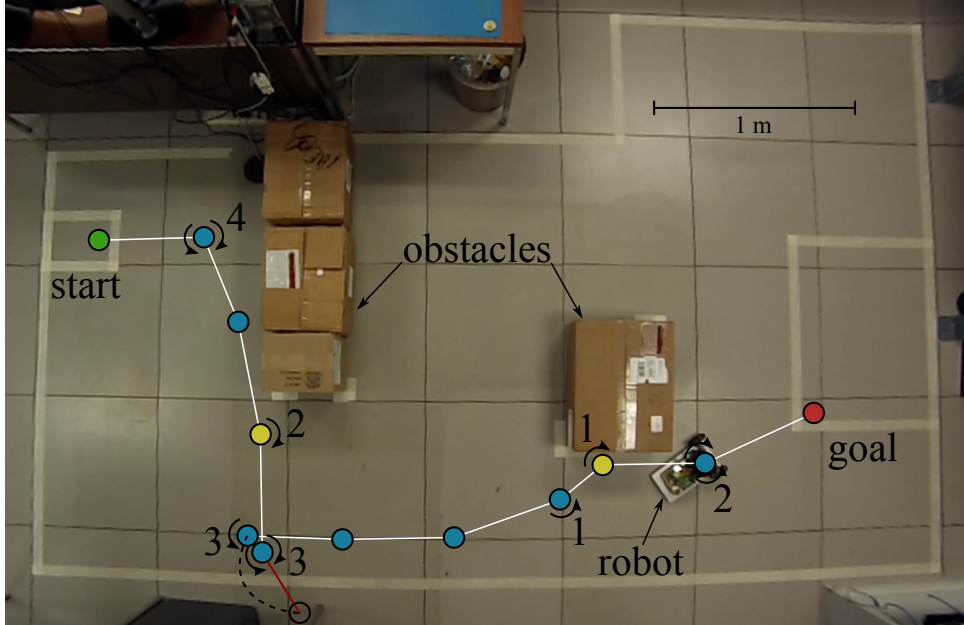


Figure 2.5: A map of robot locations while completing the course. Numbers next to the points indicate that the robot turned in place at that location the corresponding number of times before moving to the next point. Point locations are estimated based on overhead video footage taken throughout the trial.

the user hitting an undesired target, causing the robot to go out of bounds. To keep the trial running, the robot was reset to its previous location (indicated by the dashed line) and the trial continued. The participant would have been capable of continuing toward the goal without being reset to the previous location, but we wanted to contain the trial within the specified boundaries. If the boundary had been established with a physical object, the trial would have likely continued just as with the collisions with the obstacles. Obstacle detection was added to the robot’s capabilities after this experiment, but as it stands, the results show more accurately the level of control the user had in operating the robot via the interface.

2.1.6 Conclusions

Based on the experience of running this study, it became clear that this interface based on manipulating the power in two different frequency bands of a single EMG signal was interesting from the viewpoint of human motor learning and adaptation, but it took considerable training and was still difficult to use in a practical system. At this point,

I had became interested in how mainstream EMG research, based primarily on gesture classification, was done. I decided then to pursue development of a multi-channel EMG recording system, composed of the EMG sensors we had in the lab, a custom circuit board for routing all of the signals, and an inexpensive data acquisition device.

2.2 Initial Venture into Multi-Channel EMG

2.2.1 Introduction

Research involving the use of multi-channel EMG is typically aimed at classifying gestures, with prosthesis control being the primary application. In this application domain, there are essentially two primary measures of quality that must be taken into consideration. The first is accuracy (correct classification of the current gesture) and the second is time lag between user input (initiation of movement) and system output (the predicted gesture class). Most research in this area addresses these two ideas, but there is a somewhat large range of variability in the results, even when the same classifier is used. This is due to there being a large number of variables that the researcher must decide on when doing physiological research. In nearly all cases, a new paper in this research area implies a new data set measured with different instrumentation, processed with different systems, and generated by different subjects. Herein lies one of the biggest difficulties in using machine learning in physiological research: if you create a system that works well, it might not work well with different amplifiers, different electrode materials, different muscles, different participants, etc. One of the aims of this experiment was to find a suitable amalgam of previous gesture recognition efforts and build a system that approximates it. This facilitates a nearly direct comparison as a way to verify that my own custom system works as expected. A second aim was to work toward a novel method of recognizing gestures that utilizes the rich temporal information that most previous work in the area discards.

2.2.2 Building a Multi-Channel EMG Platform

The EMG recording setup described in the previous section was aimed at creating a completely mobile interface, and the basic design idea of using a microphone constrains

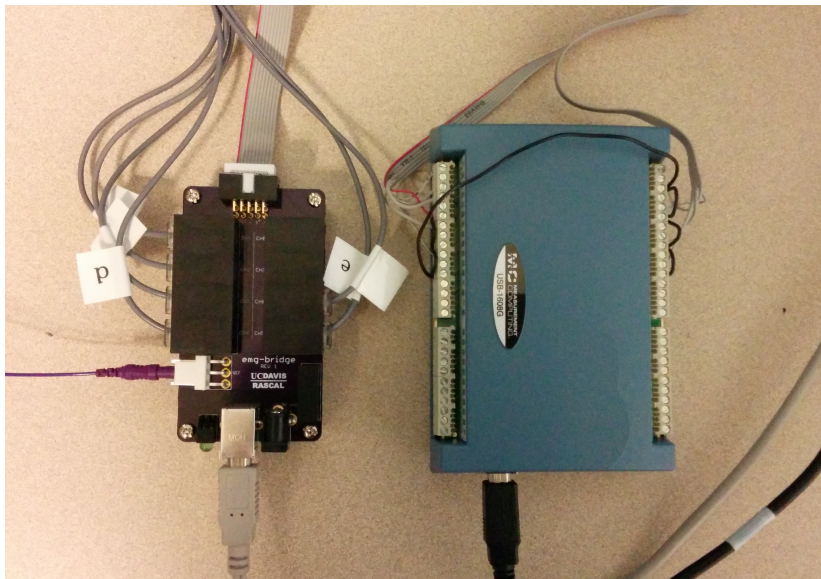


Figure 2.6: EMG bridge (left): a custom circuit board made to convert a DC power source to positive and negative power rails, distribute this power to multiple EMG sensors, and route the EMG signals through a single cable. The cable can then be connected to any suitable data acquisition system (right).

the interface to a single sensor (in most tablets and personal computers). In order to expand the lab’s capabilities to use of multiple EMG channels, a custom printed circuit board was created, shown in Figure 2.6. After terminating the cables of our Motion Labs Y03 amplifiers with J25 (6p6c modular jack) connectors, up to eight of them could be plugged into the board. Power was supplied through a standard USB-B cable or a “wall wart” style power supply with a barrel connector, and an off-the-shelf DC-DC converter generated positive and negative power rails to distribute power to the instrumentation amplifiers inside the EMG sensors. Finally, the analog signals from the sensors were routed to a flat ribbon cable which could in turn be connected to a data acquisition system. This hardware platform became the basis of a majority of my work with EMG.

2.2.3 MATLAB GUI for Collecting Data

With this hardware setup, data from the data acquisition unit can be streamed and processed in real time. In favor of rapid development and in order to leverage available code for locality preserving projections (described later), a simple MATLAB graphical user interface (GUI) was built for recording gestures, shown in Figure 2.7. There are a couple

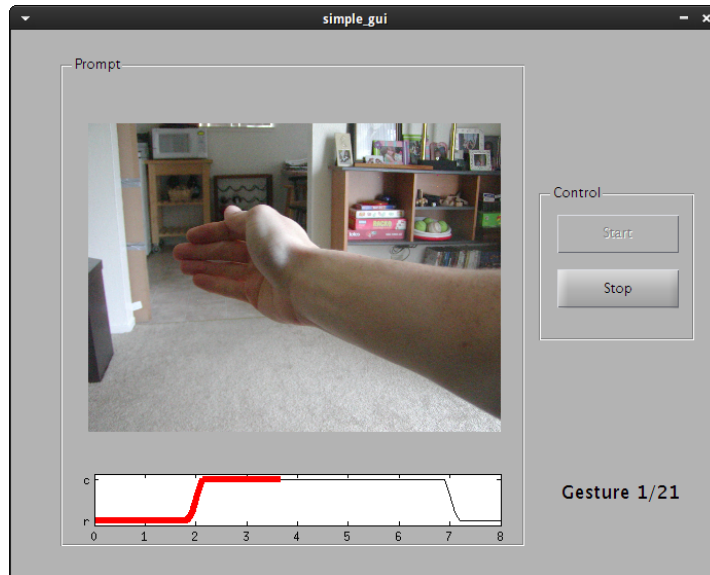


Figure 2.7: Screenshot of MATLAB graphical user interface for prompting the subject to produce a specific gesture and record the EMG signals generated during the movement.

reasons a GUI is needed. A picture of the gesture being performed is useful to ensure there is no risk of performing an incorrect gesture, and it is important to minimize reaction time (user doesn't have to recall what a gesture name means). A small rectangular plot window under the gesture picture in the GUI also provided instruction for onset and offset of the gesture so that labeling of the data (rest vs. active) could be done automatically. While the gesture was displayed, data from the USB data acquisition device was streamed and then written to WAV files for offline analysis. The timing parameters were all configurable and were set as described below.

2.2.4 Gesture Recording

Six electrode pairs (one pair gives one EMG signal) were placed around the circumference of the forearm at approximately one third the distance from the elbow to the wrist (more precisely, one third of the way between the medial epicondyle of the humerus to the head of the ulna). Placement of the electrodes along this line was done by marking the flexor digitorum profundus and the brachioradialis as key points with respect to which the remaining electrode pairs are to be placed (evenly spaced between the two marks). Although a more accurate system could be built by placing the electrodes at optimal

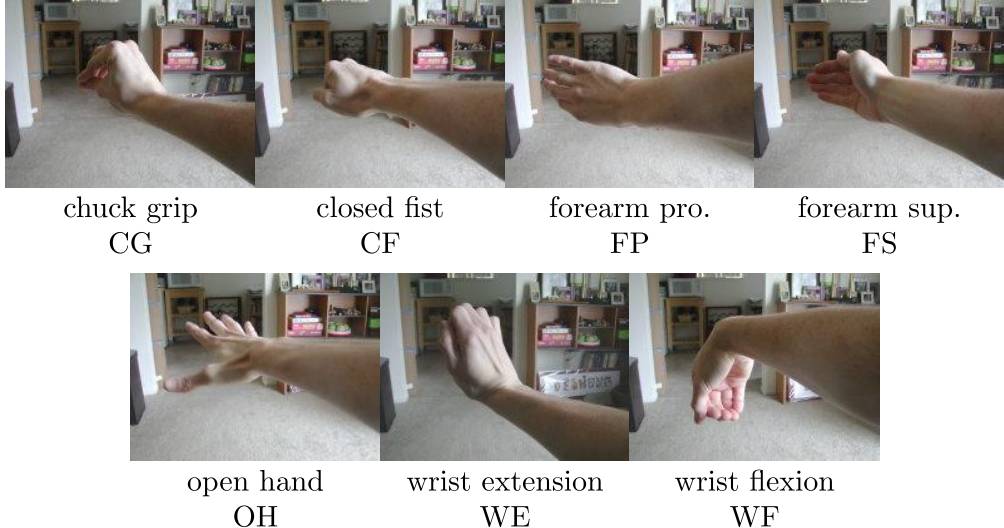


Figure 2.8: The seven gestures being performed. These are the same photos displayed in the graphical interface to prompt the subject to perform the gesture.

locations (i.e. on muscles relevant to the gestures being recognized), a ring of electrodes in an arm-band type configuration is much closer to a device that could be used in practice like a prosthetic socket with embedded electrodes.

Six different gestures were performed: chuck grip, closed fist, forearm pronation, forearm supination, open hand, wrist extension, or wrist flexion. The images displayed in the GUI are shown in Figure 2.8. Each run of the GUI constituted a session made up of 21 trials (three of each gesture type) in randomized order. Every trial followed the sequence: display of the prompted gesture type, 2 seconds of rest, onset of the gesture, static holding of the posture for 5 seconds, release back to rest, then 1 second of rest. Each trial was separated by 3 seconds. The data acquisition device recorded each of the six EMG channels at a 1 kHz sample rate, pulled into MATLAB in 100 ms windows. A digital low pass filter is often implemented before writing the data to disk, but no such processing was done, so all processing and analysis occurred after recording the raw data.

Despite the ability to record multiple sessions in a row, it is important for the sessions used for classifier training to be performed on separate occasions so that there is natural variability in electrode placement and gesture performance, as this is what would occur in a realistic scenario. For the testing data, however, this constraint was somewhat relaxed in favor of collecting more data. In all, three sessions were run on consecutive days for

the training data set, and four more sessions (spread over two days) were created for the testing set. Since this was a preliminary study and the purpose was mostly to validate the new hardware and software platform, I was the sole subject.

2.2.5 Processing

For each segment of the recording, features were calculated for each of the channels, and these features were concatenated into a feature vector \mathbf{v}_k , corresponding to gesture with label y , which was used to either train or test the classifier. The features used were the “standard” time domain features from Hudgins, Parker, and Scott [HPS93], namely mean absolute value (MAV), waveform length (WL), zero crossings (ZC) and slope sign changes (SSC). Each segment of an EMG channel is denoted by $\mathbf{x}[n]$, where n is a time index.

1. Mean absolute value is the mean value of the rectified signal over the current window. This provides a measure of the activation level of the muscle of interest, and it is probably the most important feature of the set for discriminating between gestures.

$$\text{MAV} = \frac{1}{N} \sum_{n=1}^N |\mathbf{x}[n]| \quad (2.3)$$

2. Waveform length is the term used for summing over the change in value of the signal from sample to sample. It gives a sense of waveform complexity.

$$\text{WL} = \sum_{n=1}^N |\mathbf{x}[n] - \mathbf{x}[n-1]| \quad (2.4)$$

3. Zero crossings is a count of the number of times the signal crosses zero. It is another measure of waveform complexity, but in a different sense than WL.

$$\text{ZC} = \sum_{n=1}^N \mathbf{1}_{ZC}[n] \quad (2.5)$$

where $\mathbf{1}_{ZC}$ is an indicator function that is one if the current sample and previous sample have opposite sign and the absolute value of their difference is larger than some threshold (to remove the effect of noise).

4. Slope sign changes is another feature that takes frequency content into account as a measure of signal complexity.

$$\text{SSC} = \sum_{n=1}^N \mathbf{1}_{SSC}[n] \quad (2.6)$$

where $\mathbf{1}_{SSC}$ is an indicator function that is one if the current sample is either greater than both the previous sample and next sample or less than the previous sample and next sample. A threshold is also used here just like in the calculation of ZC.

As simple as these features are, they seem to encapsulate a great deal of the relevant information of an EMG signal, and they ended up being useful in much of my work with EMG. With a set of feature vectors with known labels, a supervised classifier can be trained. Four different standard classifiers were compared in this study: linear discriminant analysis (LDA), quadratic discriminant analysis (QDA), support vector machine (SVM), and k -nearest neighbors (KNN).

Two more details require attention. The first is that MAV and WL are very different in numerical scale from ZC and SSC. To alleviate this issue, the training data as a whole was used to scale both the training and testing data sets (in a realistic situation, we cannot know all of the testing data *a priori*, so we have to use only the training data for scaling). The scaling parameters were computed such that each feature in the training set had zero mean and unit variance. This step is crucial especially for the SVM classifier. The second detail is gesture onset/offset detection. For the analysis described above, the data used to generate the feature vectors corresponds only to the portions of the recordings between 2 s and 7 s (where the user is prompted to transition from/to rest), so no rest state was involved in the offline analysis. In an online application, a simple threshold method can be implemented relatively easily. One implementation of such a technique is described later.

2.2.6 Manifold-Based Classification

As a second, somewhat novel, approach to processing EMG, I implemented a classification scheme that does not require selection of features. Everything was the same as in the

feature-based setup until feature calculation. Instead of forming a feature vector, the raw EMG signals were filtered with a 5th-order Butterworth filter with cutoff frequency at 200 Hz, rectified, and then each channel was concatenated into a single 600-dimensional vector for each recording window. Each vector was then mapped to a lower-dimensional space using locality preserving projection (LPP) [HN03] in an attempt to find a low-dimensional manifold that the lightly-processed EMG data lies on. The idea behind LPP is to find projection vectors which map the training data to a low-dimensional space such that neighbors in the original feature space remain neighbors in the manifold space. Importantly, LPP produces a method for projecting new inputs to the low-dimensional space (out-of-sample projection), so it can be used in real time applications. The projected data can then be input to a classifier.

An adjacency graph was computed using Euclidean distances between all of the 600-dimensional training vectors. The graph was then filtered so that connections only between nearest neighbors remain ($k = 100$ used here). Edge weights were calculated using the heat kernel $w_{ij} = \exp(-\|\mathbf{x}_i - \mathbf{x}_j\|)$ where \mathbf{x}_i and \mathbf{x}_j are instances of the training set. With the edge weights, the graph Laplacian can be formed, and the projection vectors which map our 600-dimensional vectors to lower-dimensional space in a neighborhood-preserving way are the eigenvectors of the generalized eigenvalue problem:

$$XLX^T \mathbf{a} = \lambda XDX^T \mathbf{a} \quad (2.7)$$

where X is a matrix with the training instances as columns, L is the graph Laplacian, and D is the degree matrix. An arbitrary number of eigenvectors can be used to project the data—six were used here.

In contrast to the feature-based classification system, the recording segments corresponding to the rest state were included for the manifold-based approach. In order to label the rest state segments, a threshold was applied to the weighted sum of the total mean absolute value (MAV) of all channels and the Teager-Kaiser operator

(TKO) [DQK93, SRS⁺10] of all channels:

$$A = \sum_{i=1}^C \left(10 \underbrace{\frac{1}{N} \sum_{n=1}^N |\mathbf{x}_i[n]|}_{\text{MAV}} + \sum_{n=1}^N \underbrace{\mathbf{x}_i^2[n] - \mathbf{x}_i[n]\mathbf{x}_i[n-1]}_{\text{TKO}} \right) \quad (2.8)$$

where C is the number of channels used (6) and N is the length of the segment of interest (100 ms at 1 kHz gives 100 samples). If A was smaller than the threshold, the label of the current segment was set to 0 (rest), and if it was greater than the threshold, the label of whole recording was used. The threshold was determined using only the training data, and it was set such that all segments between 0 s and 1.8 s (up until just before gesture onset prompt) of all recordings were below it.

2.2.7 Results

In the feature-based approach, four different supervised classifiers were evaluated. The performance of each of the four is shown in Table 2.3. Note that the algorithms with parameters (SVM, KNN) were tuned. In the case of the SVM, a grid search was performed over a range of kernel types and parameters. The linear kernel with $C = 50$ gave the best performance and had a moderate number of support vectors (about 6% of class size). Optimizing k for KNN was easy enough to do by hand. It is interesting to note that the performance of LDA and KNN is exactly the same, though this is just a coincidence that the number of correct classifications were the same (they did not make the same predictions).

Table 2.3: Comparison of feature-based classifiers

classifier	accuracy
SVM (linear, $C = 50$)	93.79%
QDA	91.21%
LDA	90.07%
KNN ($k = 20$)	90.07%

LDA is relatively popular in practical EMG gesture recognition studies, so the confusion matrix is given for comparison with that in [BK12]. For a novice user, these results

are actually quite good. Note that the machine is not the only thing learning the gestures, and the referenced work shows massive improvement with participant experience. Since the SVM was the highest-performing classifier, its confusion matrix is also given for comparison. The SVM performed better overall, of course, but it also more evenly spread the success to the seven gesture classes, ensuring that all classes had at least 90% of their instances correctly predicted.

Table 2.4: LDA confusion matrix

	CG	CF	FP	FS	OH	WE	WF
CG	0.985	0.002	0.007	0.003	0.003	0	0
CF	0.023	0.927	0.028	0.018	0	0	0.003
FP	0.010	0	0.827	0.017	0.002	0.003	0.142
FS	0.022	0.002	0.033	0.942	0	0	0.002
OH	0.073	0	0.025	0.022	0.867	0.002	0.012
WE	0.008	0.002	0.028	0.030	0.032	0.900	0
WF	0.032	0.070	0.025	0.015	0	0	0.858

Table 2.5: SVM confusion matrix

	CG	CF	FP	FS	OH	WE	WF
CG	0.960	0.010	0	0.007	0.015	0	0.008
CF	0.005	0.923	0.008	0.017	0.005	0.003	0.038
FP	0.010	0.008	0.900	0.003	0.005	0.007	0.067
FS	0.003	0.018	0.028	0.932	0.002	0.008	0.008
OH	0.003	0.013	0.013	0.018	0.940	0.010	0.002
WE	0.003	0.007	0.022	0.022	0.005	0.938	0.003
WF	0	0.008	0.003	0.017	0	0	0.972

After projecting the testing data to 6-D space using the eigenvectors from LPP on the training data (first three components shown in Figure 2.9), the same classifiers as in the previous section were used. The performance of each is shown in Table 2.6. Note

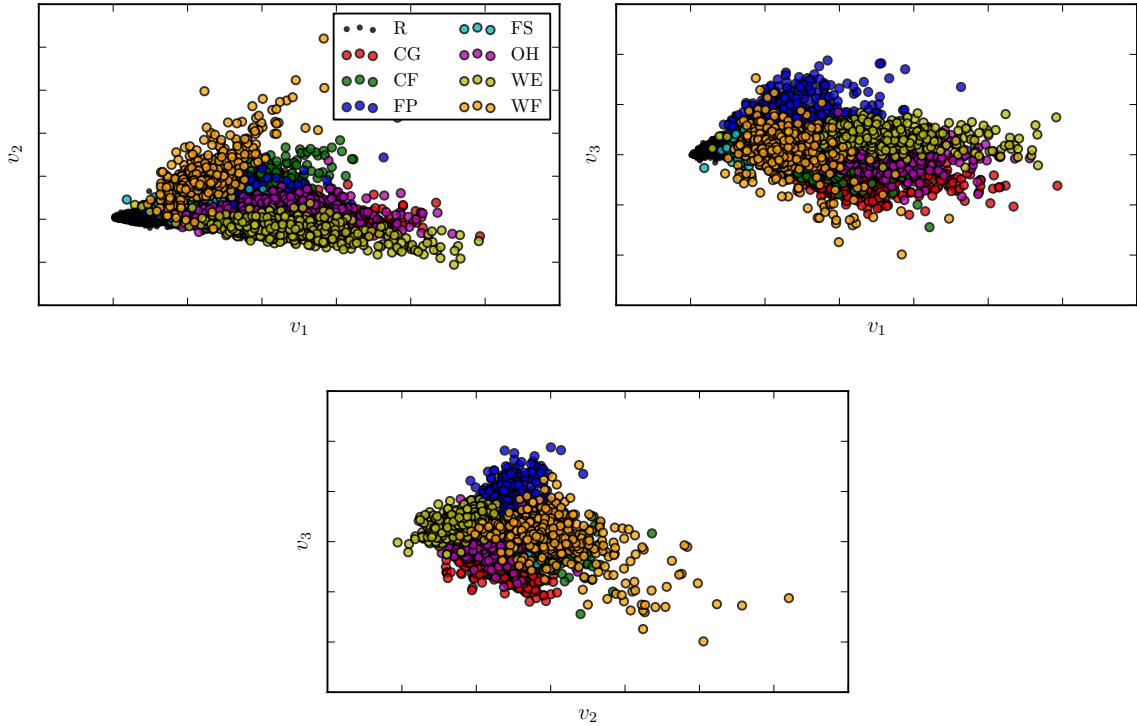


Figure 2.9: Three different perspectives of the 3-dimensional projection produced by LPP.

that although the SVM had the highest performance, it had somewhat high numbers of support vectors, indicating that there may have been some overfitting. KNN was fairly stable, with the accuracy staying within 2% of the performance shown for a wide range of values of k (about 5 to 100).

Table 2.6: Comparison of manifold-based classifiers

classifier	accuracy
SVM (RBF, $\gamma = 0.1$, $C = 10$)	90.13%
QDA	87.37%
LDA	85.04%
KNN ($k = 20$)	88.00%

2.2.8 Conclusions

The perspectives shown in Figure 2.9 do not give the full picture of how nicely formed the clusters actually are. Though the clusters are overlapping, there are certainly specific

regions of space that each of the clusters occupy. There seems to be an intuitive explanation for much of the content of the projection plot. First of all, there is a “ball” of points at the origin (in the non-normalized data, which is what is plotted) corresponding to the rest state. If a single recording is plotted, there is actually a temporal progression from this rest region out to the corresponding gesture class cluster. One of the problematic gestures is forearm supination. Although it has good recognition rates, several of the gesture recordings corresponding to forearm supination had very low signal amplitude, making gesture onset detection difficult. Though it is not easy to see in the projection plots, the forearm supination cluster turned out to be quite close to the rest region. It is clear that distance from the rest region is in one way or another representative of signal amplitude. The meaning of the direction or location, though, is not readily interpretable, and adjacent classes do not seem to imply similarity of gesture generally.

One possible improvement on the LPP idea would be to try different metrics for generating the graph affinity matrix. The Euclidean distance step for finding k nearest neighbors actually worked better than expected, but there are other distance metrics that may be more suitable to projecting raw physiological signals, like cross-fuzzy entropy [XZGC10]. The same argument holds for the metric used to calculate the graph weights. There are also more traditional stochastic signal comparison methods such as coherence, but these are not really suited to nonstationary signals such as EMG.

Although the manifold approach did not yield classification results as high as the feature-based approach, the idea of projecting the raw EMG data to a manifold is powerful. It seems as though the boundaries between classes are not as nice and distinct as we might want them to be for very high classification accuracy, but perhaps this uncovers a natural property of the data. It would be interesting, to investigate the boundaries of the classes in the LPP projection further. One possible application would be to relax the classification decision boundary to something akin to a fuzzy set. That is, a given test segment of a recording has at least some nonzero “belonging” to all of the classes, and we can utilize this information to detect transitions from one gesture to another. Smooth, quick transitions between gestures is a poorly studied problem, and this idea is one possible approach.

Overall, the idea of projecting the raw EMG data is attractive because it removes the burden of choosing features. Feature selection is a somewhat sensitive process, and it seems that certain features do very well sometimes, but not others. Sample entropy [RM00] is an illustrative example. It is a feature that has been shown to be very effective for EMG data [PQC⁺13]. However, as the analysis window (segment) becomes small, Samp-En blows up to infinity, becoming useless for rapidly-responding systems (like the one used here) with 100-sample window lengths. The tradeoff is that we now have to decide on parameter values (number of nearest neighbors, soft margin parameter), as well as metrics (k -nearest neighbors vs. ϵ -ball, heat kernel versus binary weights, etc.). Some of this can be taken care of automatically, but some of it may be more difficult to do without expert intervention. Before worrying about such a practical detail, however, there is still a significant amount of work left to bring EMG gesture recognition to offering fluid, fast, intuitive control.

2.3 Outcomes

As a result of these two projects, I gained competency in recording and processing EMG using both mobile hardware and a lab-based system which the lab also gained. I also ended up with graphical user interface software to perform further studies with multi-channel EMG. While both experiments were case studies, they offered distinct and valuable experience getting started with myoelectric control. In the future, it may be interesting to continue along the lines of the locality preserving projections method of mapping raw EMG to a lower-dimensional space, especially if combined with a training protocol that encourages the user to explore and learn what can be done with this control scheme. I have also always thought it would be interesting to investigate how many people can voluntarily contract the auricularis muscles and to what extent this ability can be improved with training.

Chapter 3

Classification of Leg Gestures for Prosthetic Arm Control

Preface

One of the fundamental problems in controlling upper limb prostheses with electromyography (EMG) is the scarcity of available muscle sites for control output. Many techniques have been developed for prosthesis control via EMG, but the typical assumption is that muscles of the forearm are available as with individuals having transradial (between the elbow and the wrist) or more distal amputations (wrist disarticulation, partial hand amputation). This chapter describes several experiments aimed at testing the feasibility and performance of a control scheme wherein a user can control a prosthetic arm using movements of the lower leg, recognized by techniques similar to those discussed in the second part of Chapter 2. The idea is based on the concept of the homology between the arm and the leg. For example, the wrist can flex and extend just as the ankle can, and the toes can move similarly to the fingers, albeit with less dexterity. In this work, a full mapping between movements of the arm and leg was established, and both offline and online experiments were performed to test the idea as fully as possible. The contents of this chapter are, for the most part, also presented in my published works [LJ16, LJ18b].

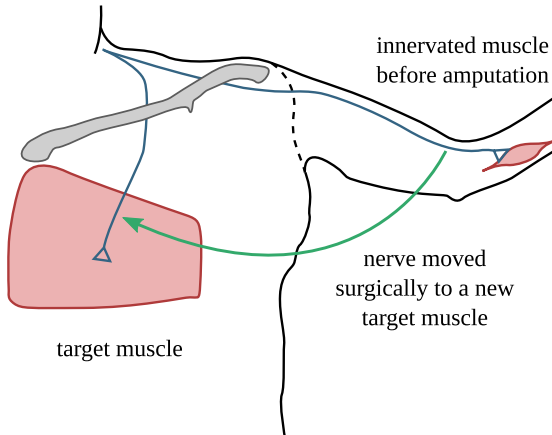


Figure 3.1: Illustration of targeted muscle reinnervation. Based on a figure from [RRFA14].

3.1 Literature Review

For individuals with amputation proximal to (above) the elbow, EMG-based control methods offer few advantages over traditional body-powered prostheses which are actuated by actuating a cable and pulley mechanism via movements of the shoulder, for example. This can lead to higher rates of prosthesis rejection and abandonment [BC07]. There is, however, one EMG-based method that offers intuitive myoelectric control of arm, wrist, and hand movements for individuals with amputations proximal to the elbow, called targeted muscle reinnervation (TMR). This is a surgical technique in which nerves from the amputation site are relocated to other muscles of the body such as the pectoral muscles of the chest, as in Figure 3.1, allowing users to imagine moving the missing limb to produce muscle activations that can be recognized as distinct gestures to control a prosthetic arm [KLL⁺09]. Despite the major advantages of TMR, eligibility for the surgery is limited to those whose amputation occurred within the last 10 years [tmr], and a recovery time of several months in addition to extensive rehabilitation and EMG testing is required before operating a prosthetic arm [KML⁺07]. Not all eligible amputees are open to additional surgery and the associated recovery and training time [ECK⁺15].

It turns out that the idea of controlling a prosthetic arm with the lower limb has been sparingly studied for several decades. A range of techniques have been used, including measuring toe movement with strain gauges [Gra74], measuring toe and foot movements

with resistor strips [Luz00], detecting foot movements with pressure sensors built into a shoe insole [CPL⁺07], and measuring foot movements with inertial measurement unit (IMU) sensors [RKEF14]. Each of these approaches involved a different mapping from lower limb movements to upper limb prosthesis function with different levels of intuitiveness. The IMU-based method of Resnik et al. is one of the most comprehensive approaches to upper limb prosthesis control for high-level amputees, providing control of shoulder, elbow, wrist, and hand movements. This is achieved by combining a number of techniques to create a complex system which requires significant training, in addition to requiring movement of both feet to control a single prosthetic arm. Despite the control complexity and the need to “re-zero” the IMU sensors after repositioning the body (e.g. standing to reclined sitting), users have reported positive experiences with using foot controls for prosthetic arm control [RKEF14].

Surface electromyography has been applied to the leg in a number of clinical and research settings, such as motor coordination (gait analysis), sport science, and neurological disease. In the context of gait analysis, for example, the rich temporal information in EMG signals may be used in combination with joint angle measurements to detect abnormalities in muscle activations during the gait cycle [FC09]. Leg EMG is also used in lower limb prosthetics research, which has recently been taking advantage of leg EMG as an additional sensor for improved control over other active devices which work only with “kinesthetic” and “proprioceptive” sensors [GLS13]. In all of these applications, EMG sensors are applied primarily to muscles above the knee, with exceptions including larger lower leg muscles [RMC04]. There has also been some recent work using supervised classification of leg EMG signals for volitional control of lower limb prostheses in non-weight-bearing situations [HVG11, HSL⁺13]. Interestingly, Hargrove et al. found that a small number of lower leg movements (plantarflexion/dorsiflexion and external/internal tibial rotation) can be recognized with EMG sensors placed only on upper leg muscles in both able-bodied subjects and transfemoral (above the knee) amputees [HSL⁺13]. That group has also investigated the use of TMR for improving recognizability of ankle movements from EMG signals of reinnervated thigh muscles [HSY⁺13].

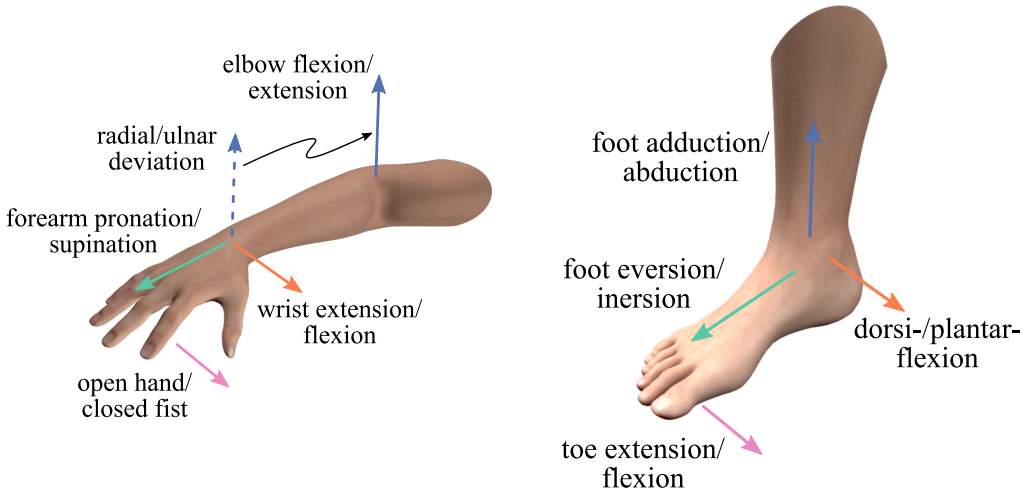


Figure 3.2: The mapping between upper and lower limb degrees of freedom. Elbow extension and flexion were not performed in these experiments, but these movements could be more useful for high-level amputees than radial and ulnar deviation.

3.2 Mapping Between the Arm and Leg

While the wrist and the ankle have diverged in humans due to their drastically different tasks in everyday life, there is still a natural alignment of their degrees of freedom. This idea is shown in Figure 3.2. Specifically: forearm pronation/supination maps to foot eversion/inversion, wrist extension/flexion maps to dorsiflexion/plantarflexion, and radial/ulnar deviation maps to foot adduction/abduction. This forms the basis of the proposed upper limb prosthesis control method. In addition to movements about the wrist and ankle, there are analogous movements of the fingers and toes. While the hallux (big toe) can be independently extended (corresponding to thumb extension), the lesser toes are not readily controlled independently so they are grouped together in flexion/extension (corresponding to open hand/closed fist). For high-level amputees, elbow flexion/extension is likely a more important degree of freedom than radial/ulnar deviation. In this case, foot adduction/abduction could serve as a suitable analog without significantly impacting the intuitiveness of the mapping, as it is often aligned with elbow flexion/extension depending on shoulder abduction angle.

In addition to the mapping between movements of the arm and leg, musculature of the two limbs can be identified as having similar primary functions on the corresponding limb.

It is common in EMG gesture recognition studies to arrange the sensors in a ring around the forearm (as in the experiments in Chapters 2 and 4), as this arrangement is suitable for the largest subset of patients with an amputation distal to the elbow and it creates a simple and repeatable electrode positioning procedure [SE11]. We found in preliminary testing, however, that with sensors placed circumferentially around the lower leg (approximately one third the distance from the medial condyle of the tibia to the medial malleolus), toe movements produced essentially no signal and were unrecognizable. To solve this problem, the muscles contributing to extension and flexion of the toes were targeted. For a fair comparison between the arm and leg configurations, we decided to target specific muscle sites in both. Although fewer EMG gesture recognition studies apply sensors to specific muscle sites, there is at least some work to serve as a reference for our arm gesture recognition results [EH03,KLL⁺09]. The muscles used and their primary actions are listed in Table 3.1. While these muscles were chosen to enhance the analogy between the arm and leg and to make the arm and leg configurations as comparable as possible, it should be noted that a classifier trained on data from leg gestures could not be naïvely applied to recognizing arm gestures, or vice versa. Despite each muscle pair having a similar action on the corresponding limb, the EMG characteristics are not matched and the co-activation of several muscles in producing a gesture would not generally be the same.

3.3 Experiment: Feasibility of Classifying Leg Gestures with EMG

3.3.1 Introduction

The goal of this study was to explore whether electromyographic gesture recognition from muscles below the knee can be applied to prosthetic arm control by determining whether or not gestures of the lower leg and foot can be decoded from EMG using current standard methods. We compared the classification accuracy of two EMG sensor configurations: one for the arm and one for the leg. In the leg configuration, three different body positions were tested: sitting, standing with both feet on the floor (partially closed kinematic chain), and standing with the gesturing foot lifted from the floor (open kinematic chain).

Table 3.1: Arm and Leg Muscles Used for Gesture Classification

	Muscle	Primary Action
Arm	A extensor carpi radialis longus	wrist extension
	B pronator teres	forearm pronation
	C flexor carpi radialis	wrist flexion
	D extensor pollicis longus	thumb extension
	E extensor digitorum	finger extension
	F flexor digitorum superficialis	finger flexion
Leg	A tibialis anterior	dorsiflexion
	B peroneus longus	foot eversion
	C gastrocnemius lateralis	plantarflexion
	D extensor hallucis longus	hallux extension
	E extensor digitorum longus	lesser toe extension
	F flexor digitorum longus	lesser toe flexion

All EMG recordings were taken by having subjects perform gestures with no feedback and the data collected was analyzed afterward, making it an offline study.

3.3.2 Experiment Design

Nine able-bodied subjects (four male and five female, 18 to 23 years old) with no myoelectric control experience participated in a single experimental session each. Able-bodied subjects were needed in order to compare performance between the arm and leg configurations. Eight of the participants were right-hand dominant, and one was left-hand dominant. For the left-handed subject, images prompting the subject to perform specific gestures were mirrored and the subject completed the task using the left arm and leg.

All subjects produced gestures with the dominant arm and then the dominant leg while EMG signals from six muscle sites on each limb were recorded. The term *cycle* is used to describe a continuous set of recording trials, lasting approximately five minutes. Each *trial* consisted of six seconds of EMG recording in which the participant rested for the first two seconds, produced the gesture and held the final position for three seconds, then returned

to the rest position. Three unrecorded seconds separated each trial. The gestures shown in Figure 3.2 (except elbow flexion/extension) were each performed three times per cycle in randomized order. Twelve cycles made up the experimental session. First, sensors were placed on the arm (arm configuration) and four consecutive cycles of wrist/hand gestures were performed. Then sensors were placed on the leg (leg configuration) and participants completed four cycles of ankle/foot gestures while sitting (P1), two cycles while standing (P2), and two cycles standing with the foot lifted from the floor (P3). Only two cycles were completed in P2 and P3 in order to keep the overall session to approximately two hours, and comparisons between leg configuration positions were secondary to the principal aim of comparing the arm and leg configurations in ideal conditions.

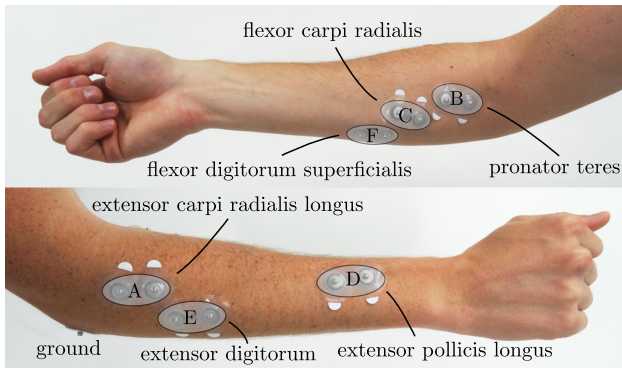
Subjects were first shown the recording equipment and the user interface while key components of the system were described. Before recording arm gestures, subjects viewed each of the arm/hand gesture images they would be seeing throughout the session and practiced each gesture several times. During recording, subjects sat in a chair with the dominant hand resting on a table. For the leg configuration, footwear was removed to ensure consistent conditions (note that the foot gestures can be performed with shoes on assuming the toe box is not overly restrictive). Subjects then viewed the same arm/hand gesture images, but here they were asked to produce the *lower limb* movements they thought should naturally correspond to the pictures of *upper limb* movements displayed. Any confusion with respect to a given gesture mapping was discussed with the researcher and verbally clarified (typically little clarification was needed) and each gesture was practiced several times. The first two cycles were completed in position P1: sitting with knees bent to a 90-degree angle and feet flat on the ground. Here, subjects were instructed to keep at least some part of the foot in contact with the ground while performing the gestures. For P2, subjects stood up and were instructed to produce the gestures in the same manner as in P1, with the additional instruction that they try not to shift their weight between the two feet in order to control for the effects of stabilization. In P3, subjects were asked to raise the dominant foot from the floor while performing the gesture such that the foot had no interaction with the floor while performing the gesture. This served

as a model for other positions in which the foot makes no contact with the ground, such as lying down. Each time a new position was introduced, subjects were allowed to practice the gestures several times.

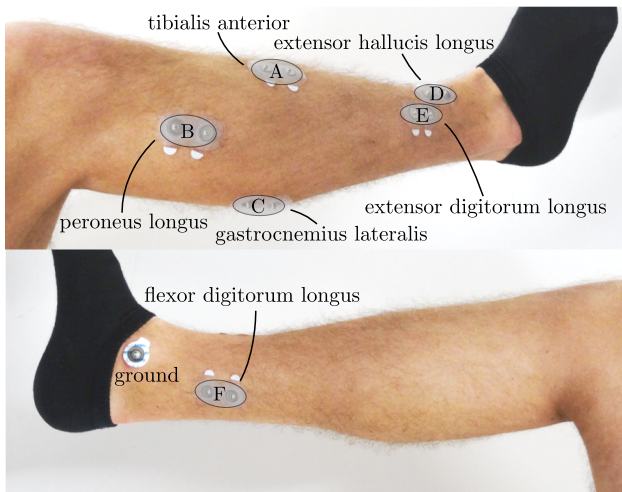
Twelve disposable Ag/AgCl center snap electrodes (ConMed 1620) were placed in bipolar pairs approximately 2.5 cm apart at specific sites of the arm or leg. An example electrode configuration for each limb is shown in Figure 3.3. Muscles that have sensor locations recommended by SENIAM (gastrocnemius lateralis, peroneus longus, tibialis anterior) were positioned as recommended [HFM⁺99]. The remaining sensors were placed using a combination of palpation and a moveable surface EMG “probe” (an EMG amplifier with Ag/AgCl electrode disks embedded). The probe was used to optimize sensor placement, helping to avoid the innervation zone and muscle-tendon junction [RMC04]. The locations of central points between electrode pairs were measured as distances from anatomical landmarks (e.g. styloid process of the ulna, head of the fibula) and recorded for each participant. The extrinsic muscles involved in toe movement presented the main practical difference between the setup for the arm and for the leg. While it is generally not recommended to place surface EMG sensors at or near the muscle-tendon junction, activity of the extensor digitorum longus, extensor hallucis longus, and flexor digitorum longus muscles can really only be measured by surface EMG near their corresponding distal tendons because the bulk of the muscles lie mostly or entirely beneath more superficial, larger muscles. Special attention was required in using the EMG probe to ensure a quality signal for these muscles. To my knowledge, no one has used surface EMG to record from these muscles before.

3.3.3 Signal Processing and Analysis

The multi-channel recording setup discussed in the previous chapter was used along with a new data collection program written in Python. The program displayed three primary elements: an image of the prompted gesture being performed, a horizontal sliding bar for prompting the user when to transition from rest to the desired gesture final position and back to rest, and an indicator of the progress through the current cycle. This is shown in Figure 3.4. The EMG signals were amplified by Motion Labs Systems Y03 differential



(a) Arm sensor locations



(b) Leg sensor locations

Figure 3.3: Example electrode positioning on the arm and leg. Capital letters in the shaded areas indicate muscles that have similar primary action on the corresponding limb (see Table 3.1).

amplifiers ($\times 300$ gain, 100 dB CMRR, -3 dB bandwidth from 15 Hz to 2 kHz), sampled at 8 kHz by a Measurement Computing USB-1608G data acquisition unit (16-bit), and recorded directly to disk in WAV format via the custom program. The raw data was conditioned with a digital fourth-order Butterworth bandpass filter with cutoff frequencies at 10 Hz and 450 Hz, then downsampled to 2 kHz.

Signals were recorded in 150 ms windows with 50 ms overlap, which is in the 150–250 ms range deemed optimal [SHLK11c]. Segments between 1 and 1.5 seconds of each recording were labeled as instances of the rest class (to avoid having trials in which the user simply rests the entire time), and segments between 2 and 4 seconds were labeled

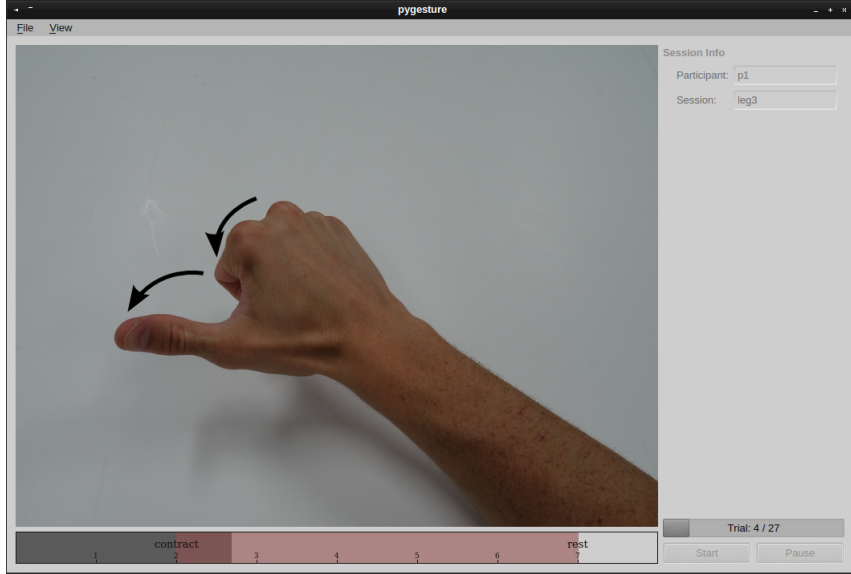


Figure 3.4: Screenshot of the graphical user interface used to collect gesture data. The image of the gesture to perform is the main component. A progress bar beneath that prompts the subject to contract and rest at the correct time.

with the prompted gesture class. Although the participants were prompted to hold the gesture between 2 and 5 seconds, there was some variability in the actual onset and offset timing for each trial. It was found that participants often anticipated the prompts, and the portion of the recordings between 2 and 4 seconds generally captured the static portion of most recordings. The same four time domain features introduced in Chapter 2 (mean absolute value, waveform length, slope sign changes, and zero crossings) were used in combination with a linear discriminant analysis (LDA) classifier to test offline classification accuracy. This configuration is well established in arm gesture recognition [SE11] and TMR [KLL⁺09] studies, and it is commonly used as a reference with respect to which more sophisticated feature sets and classification techniques are compared [PQC⁺13].

Classification accuracies were obtained by splitting the data into training and testing sets based on *whole cycles* rather than trials or instances (individual recording segments). This simulates how the classifier might perform (on average) in a realistic setting in which the training always occurs as a separate occasion from system use. For the arm configuration and leg configuration in P1, the four cycles of the given set were split into all possible combinations of two cycles for training and two cycles for testing. An LDA

classifier was built for each and their results were concatenated. We find this to be the most reasonable way of obtaining an accurate average classifier accuracy because there can actually be large differences in the accuracies of two classifiers trained with different sets of cycles. Because there were only two cycles for the leg configuration in P2 and P3, one cycle from the corresponding position was augmented with one cycle from P1 and the remaining cycle was used for testing. All possible combinations under this scheme were tested and the results were concatenated to produce the P2 and P3 results. In all cases, the average classification accuracies presented reflect the number of correct classifications divided by the total number of testing instances. While it would be ideal to evaluate the leg configuration in P2 and P3 the same way as in P1, we assume that both evaluation schemes are fair and comparable.

3.3.4 Results

The first set of results exclude the radial/ulnar deviation (mapped to foot adduction/abduction) gestures. The offline classification accuracies across participants and across gesture classes are given in Figure 3.5. The overall average accuracies (i.e. the means in the “avg” columns of both plots) are: 93.3% for the arm configuration, 89.5% for leg P1 (sitting), 87.3% for leg P2 (standing closed kinematic chain), and 81.9% for leg P3 (standing open kinematic chain). Classification accuracies for the arm gestures are similar to previous work in which specific muscle sites are targeted and a LDA classifier with time-domain features is used, though they seem to be somewhat lower than other reports considering the relatively small number of gestures considered. Kuiken et al., for example, recognized 11 gestures at 97% average accuracy, though they used 12 sensors (compared to 6 used here) [KLL⁺09].

One-way repeated measures analysis of variance (ANOVA) performed on the participant data for the four conditions (α level of 0.05 being considered statistically significant) revealed a significant difference ($p = 0.007$), so post-hoc pairwise two-tailed Student’s t -tests were performed on each of the pairs of conditions with Bonferroni correction. Significant differences between conditions are indicated in Figure 3.5. All pairs of conditions are significantly different, with the exception of leg P1 and leg P2. This is likely because the gestures were performed in the exact same manner in P1 and P2 with similar partially

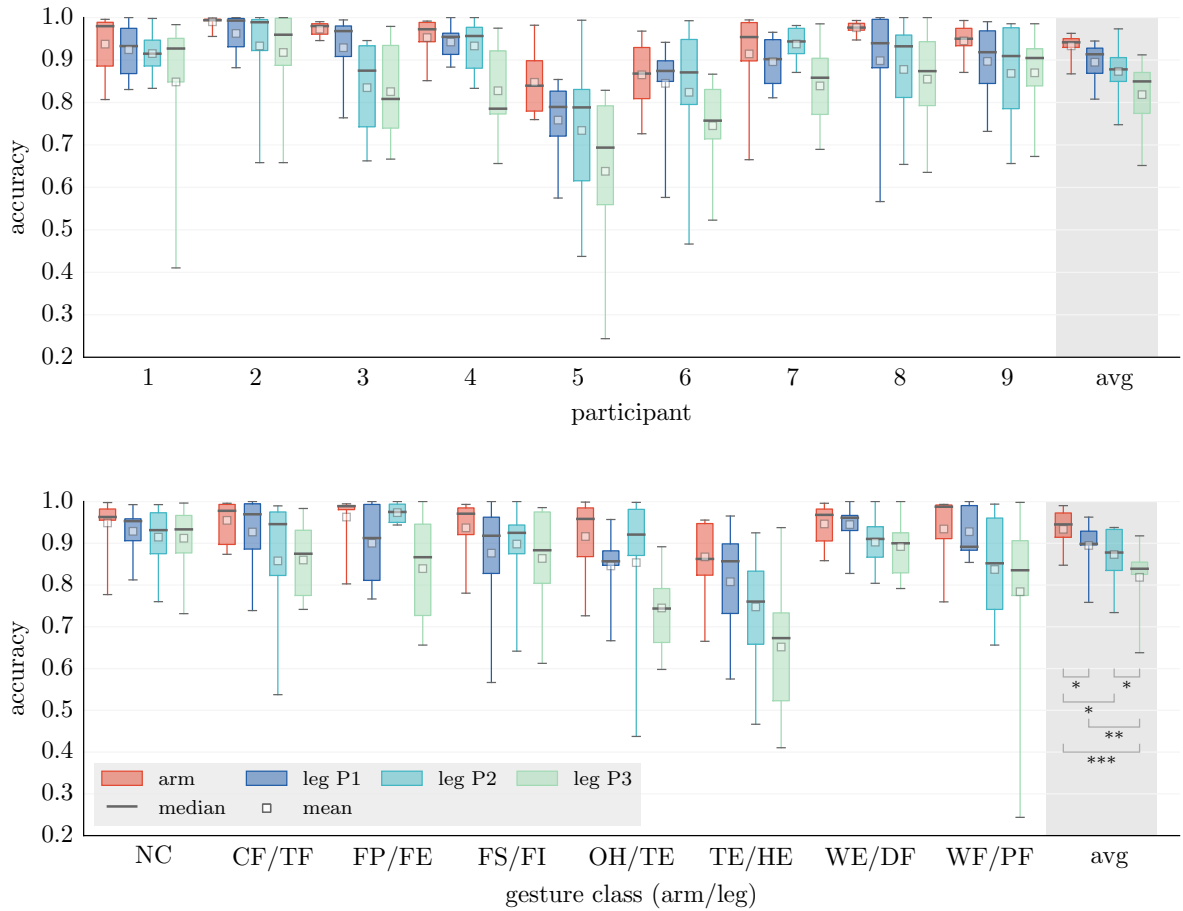


Figure 3.5: Classification accuracy for each participant distributed across gesture classes (top) and for each gesture class distributed across participants (bottom) in the four experimental conditions. Whiskers show the full extent of the data (no outliers for clarity). Stars in the “avg” column indicate significant differences between conditions (*: $p < 0.05$, **: $p < 0.01$, ***: $p < 0.001$).

closed kinematic chain conditions. Of primary interest in this study is the difference in accuracy between the arm configuration and the leg configuration in P1. The mean reduction across participants is 3.9%, however this is negligible for some participants (less than 2% decrease). In leg P1, all but two of the nine participants achieved accuracies above the mean (89.5%) and four had accuracies above 92%. Participant 5 was a low performer overall, with all accuracies for the leg configuration uncharacteristically low compared to the other participants. Across gesture classes, thumb extension/hallux extension (TE/HE) had the lowest accuracy overall, though it was particularly low in the leg configuration for all positions. We attribute this to hallux extension being the most

unnatural foot gesture of the set — some subjects had difficulty smoothly transitioning from rest to the hallux extension final position and holding that position statically, and this resulted in unusable classification accuracies for these specific subjects (< 60%). Both representations of accuracy (across participants and across gesture classes) indicate that the leg P2 and leg P3 conditions tended to have more variability and lower accuracy than the other conditions.

When radial/ulnar deviation (foot adduction/abduction) gestures are included in the classification analysis, the accuracies in the leg configuration decrease. We ran pairwise two-tailed *t*-tests to compare the arm and leg P1 conditions with and without these gestures added. When they are included in the analysis, there is a small decrease in classification accuracy for the arm configuration (-1.6% , $p = 0.046$), whereas there is a large decrease in accuracy for the leg configuration in P1 (-7.6% , $p = 0.007$). The confusion matrix shown in Figure 3.6 (leg P1) demonstrates the main issue — the classifier confuses foot inversion and foot adduction for one another as well as foot eversion and foot abduction. Furthermore, Figure 3.7 demonstrates that classifier predictions are sometimes correct or incorrect for *entire trials*. In the example shown, every instance of the foot inversion gesture in the second trial was misclassified as foot adduction, obviously affecting the classification accuracy tremendously.

3.3.5 Conclusions

An unforeseen consequence of rigidly segmenting the recordings based on the prompted onset and offset times was that participants were not consistent in matching the timing of their movement to the prompt. Subjects tended to anticipate the prompts, so we were forced to cut off the recordings short of the full three seconds in which the gesture was supposed to be held. Furthermore, despite explicit instruction to relax completely in the first two seconds of recording (before the onset prompt), some participants would occasionally move their arm or leg during this window, causing the rest class (NC) to have lower classification accuracy than is typical in gesture recognition studies. This issue may be alleviated to some extent by systematically determining onset and offset times in each recording, similar to the threshold-based approach in Chapter 2.

	predicted class									
	NC	TF	FE	FI	TE	AD	HE	AB	DF	PF
actual class	NC	91.9	1.3		1.0	1.3		1.3	1.4	
TF		90.1			2.3		3.8	2.0		
FE	1.1		77.4		2.4	1.3			15.1	
FI		5.4	1.2	74.5		15.5		1.0		
TE			1.0		81.4		4.4	4.6	6.2	
AD	3.6	4.7		17.1		69.9	1.7	1.3		
HE	1.9	6.5		2.1	3.9	2.1	80.1	1.3	1.7	
AB	5.3		15.5	1.9	3.7	2.6		69.0		
DF				1.0	2.6				93.7	
PF				1.0	4.6		1.7	1.3		90.6

Figure 3.6: Confusion matrix for the leg configuration in P1 including the two “problematic” gestures: foot adduction (AD) and abduction (AB). The matrix is generated by cross validation (two cycles for training data, two cycles for testing data) averaged across subjects. The main sources of error are the off-diagonals outlined. For clarity, numerical values less than 1% are not shown.

One issue with using leg gestures for upper limb prosthesis control is that users would need to be able to walk without unintentionally activating the arm. Toggling the device on and off could be implemented with a switch, such as a physical button pressed with the shoulder or an EMG switch controlled by an unused muscle such as the auricularis posterior behind the ear [LJ13]. It could instead be implemented automatically — Resnik et al., for example, have developed an IMU-based technology called Walk Detect which has been shown to help alleviate this issue for their foot-controller [RKEF14]. There is also notable degradation in performance when the foot is not in contact with the ground. This is similar to the limb position effect in upper limb gesture recognition, where a change in arm position can greatly affect classification accuracy [FSC⁺11]. Using a mixed training set as done here (e.g. one cycle of P1 as a base and adding a cycle of P2 or P3) can improve classification accuracy, but determining the optimal classifier training procedure to handle arbitrary limb configuration is an open problem. Since leg P1 and leg P2 conditions were not significantly different, the difference in evaluation procedures

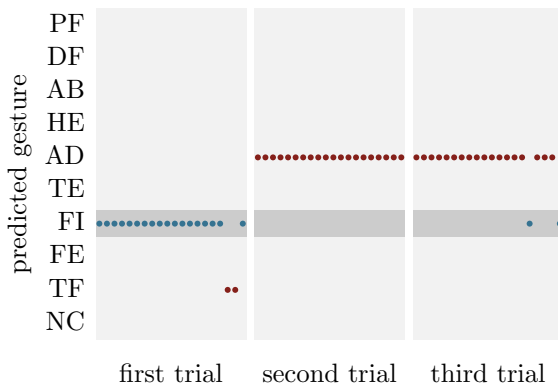


Figure 3.7: Example classifier predictions over time illustrating poor recognition of the foot inversion (FI) gesture being performed (leg P1 data shown here). Most participants had trouble producing foot inversion and foot adduction gestures distinguishably from one another. This plot illustrates that the correct and incorrect predictions take place mostly on a whole *trial* basis, hinting that feedback could be a way to improve the poor classification accuracy of the problematic gestures.

is assumed to have little to no role.

Two relatively important gestures for high-level amputees are elbow flexion and extension. If the ankle represents the wrist, the knee would represent the elbow, but controlling a prosthetic arm's elbow joint with knee movements would be impractical unless subjects learned to produce reliable isometric contractions of the upper leg muscles. If the amputee has residual biceps brachii and triceps brachii muscles, it may be preferable to utilize a proportional style control scheme to manipulate a prosthetic elbow, allowing for hand and wrist gestures to be controlled by the foot simultaneously with elbow movement. However, for patients with no residual arm muscles (e.g. shoulder disarticulation), elbow movements would need to be controlled through some other means. It seems reasonable that a deviation from the strict ankle-wrist mapping could be warranted as long as it doesn't considerably disserve usability and intuitiveness. To this end, we included foot adduction and abduction gestures, corresponding directly to radial and ulnar deviation, though they could instead map to elbow flexion and extension. However, as demonstrated in Figure 3.6 and Figure 3.7, we have not shown sufficient classification accuracies when the eversion/inversion and adduction/abduction degrees of freedom are both included in

the analysis. We speculate that this is caused by the kinesiological coupling between the gestures misclassified for one another. That is, foot adduction is a somewhat difficult gesture to produce without also inverting the foot to some extent (in open kinematic chain), since these movements are components of supination, a more natural movement [HB11]. Figure 3.7 illustrates this, showing that foot inversion (the prompted gesture) can be misclassified as foot adduction for an *entire trial*. This suggests that the classification accuracy could be improved with feedback, so that subjects could make corrections to the gesture being performed if they see that the classifier is consistently predicting an undesired gesture. If, after receiving feedback, subjects produce a second set of training data, we hypothesize that the adduction/inversion and abduction/eversion pairs will interfere with each other to a lesser extent. Finally, for shoulder disarticulation and scapulothoracic amputees, there may be a need to control a motorized shoulder. This could be facilitated with methods similar to those used by Kuiken et al., such as EMG control from residual deltoid and latissimus dorsi muscles [KLL⁺09]. A mode switch similar to that used by Resnik et al. could be another solution [RKEF14].

This study demonstrated that foot and ankle gestures produced by novice users can successfully be recognized via lower leg surface electromyography. It also showed that an intuitive mapping between the arm and leg exists, as subjects produced all gestures with upper limb image prompts and needed less than five minutes to fully understand this mapping. To my knowledge, this is the first report of electromyographic recognition of ankle and foot gestures from lower leg muscles and the first application of surface EMG to record extrinsic toe flexors and extensors. From the outset of this work, it was not known whether or not EMG signals could be recorded reliably enough from difficult-to-reach muscles such as the extensor hallucis longus for recognizing toe movements.

All classification was performed offline, and the participants received no feedback during the session. While there are a number of recent studies which have investigated electromyographic gesture recognition with only offline testing [AGJ⁺14, PQC⁺13, YSRH13], the value of feedback became apparent — the results showed that entire recording trials were being misclassified unbeknownst to the subject. In online classification testing, a

classifier is trained in the same way as done here (subjects produce gestures to the best of their abilities with no feedback), then some kind of feedback is given while subjects perform a real-time task with the trained system. This experimental paradigm allows for more realistic measures of performance to be used (e.g. task completion time) and it takes many more factors into account than a simple offline system can, such as participant learning over time, control delay, and movement overshoot and correction. The type of feedback presented ranges from simple display of the classified gesture [BK12, SLK09], to virtual prosthesis control [YZJL12, OCHB14, HSEH10, TYS⁺14], to physical prosthesis control [KLL⁺09]. In some cases, after the subject learns to repeat required gestures more reliably having received feedback information, classifier training is performed again so the subject not only becomes better at producing the gestures but may also provide the classifier with better training data [BK12]. Online testing is seen as a much more accurate representation of a classification system’s ability to act as a functional prosthesis control interface and motor learning research suggests that external focus is critical for improvement in task performance [MWC00]. It has also been shown that within the domain of classification systems known to work well in offline testing, offline performance does not strongly correlate with online performance [OCBH13]. For these reasons, we followed this study with a new experiment in which subjects could use leg movements to control a simulated robotic arm in real time.

3.4 Experiment: Initial Real-Time Control Testing

3.4.1 Introduction

In this study, inexperienced able-bodied subjects used leg gestures, recognized by techniques similar to those of the previous section, to control a simulated robotic arm in real time. They also performed the task using an analogous recording configuration on the arm for comparison. The target achievement control (TAC) test [SHLK11b] was used to evaluate real-time performance in controlling the arm. Since we found previously that including the foot adduction/inversion and abduction/eversion pairs in the gesture set can result in reduced classification accuracy, we specifically tested control with three and

four degrees of freedom separately (one configuration with adduction/abduction and one without).

3.4.2 The Target Achievement Control Test

The target achievement control (TAC) test was used to evaluate real-time control performance [SHLK11b]. The TAC test is similar to a cursor-to-target task, but the motion commands are sent to a simulated robotic arm and the targets are specific joint configurations. The TAC test has the advantage of providing realistic visual feedback for control of an arbitrary number of degrees of freedom, where cursor-to-target tasks are generally limited to two or three degrees of freedom. The arm (ABB IRB140) and hand (BarrettHand) used in this experiment were simulated in V-REP [RSF13], as shown in Figure 3.8. At the beginning of each trial, a translucent “reference arm” moved into the target posture, then an indicator changed color to prompt the user to begin moving the controlled arm to the target. Segments of the arm corresponding to the controlled joints (elbow, forearm, wrist, and hand) changed from grey to green if the joint moved to a position within the tolerance of the target joint angle. Once the controlled arm remained within $\pm 10^\circ$ tolerance of the target angle (60°) for all joints for a dwell period of 2 s, or if the target could not be achieved within 15 s, the trial ended. Joint limits were set to 10° beyond the target (plus tolerance) to allow for overshoot. A decision-based velocity ramp controller with a ramp length of 10 (500 ms) was used to help attenuate undesired movements due to misclassifications [SHLK11a]. The top 10 mean absolute value features for each class from the training data were averaged to obtain the boost values for the controller such that the maximum output velocity for a given joint would be $100^\circ/\text{s}$.

TAC test performance is typically measured using several different metrics which measure different aspects of control performance. They are completion rate, completion time, and path efficiency [SHLK11b]. Completion rate is the percentage of trials successfully completed before the trial timeout (in this experiment, the timeout was 15 s). Completion time is the amount of time from movement initiation to the moment the target is entered for the last time on a successful trial, hence excluding reaction time and target dwell time. Path efficiency is the straight-line distance to the final arm position divided

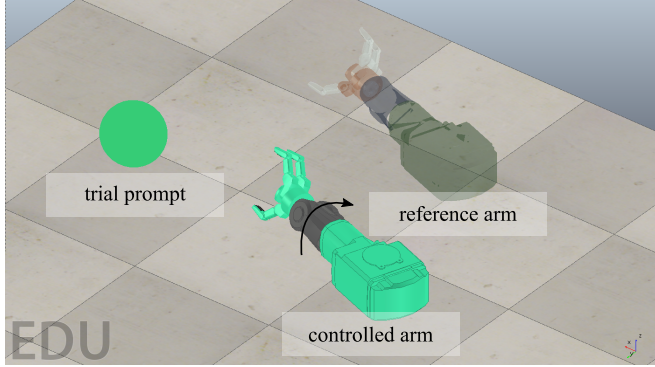


Figure 3.8: Target achievement control test environment simulated with V-REP. The subject is being prompted to supinate the forearm in this image.

by the cumulative distance travelled by the arm to get to the target, measured in joint angle space. This means 100% efficiency is achievable with 1-DOF targets if the subject generates a stream of classification decisions that move the arm in only one direction and stop inside the target.

3.4.3 Experiment Design

Eight able-bodied subjects with no myoelectric control experience participated in the study: five male, six right hand dominant (interface was reversed for left-handed subjects), ages 20–23.

The exact same EMG hardware was used and the electrodes were placed in the same manner as in the previous offline classification study. Signals in this case were sampled at 5120 Hz in 50-sample segments, bandpass filtered with a fourth order digital Butterworth filter between 8 Hz and 512 Hz, then downsampled to 2560 Hz. For this study, the software from the offline study was extended to facilitate real time classification and communication with the V-REP robotics simulation platform [RSF13]. This software is available online at <https://github.com/ixjlyons/pygesture/tree/v1.0>.

Subjects remained seated throughout the session and removed footwear during the leg control portion. They performed each gesture four times for three seconds in randomized order to generate classifier training data. In all cases, the subjects were prompted with an image of the corresponding arm gesture as in the offline study. The middle two-second section of each recording was extracted for processing, and these portions were segmented

into 150 ms windows with 100 ms overlap. The popular time domain feature set was extracted from each window (mean absolute value, waveform length, slope sign changes, and zero crossings) [HPS93], and linear discriminant analysis (LDA) was used to classify gestures.

Half of the subjects started the session in the arm configuration and the other half started in the leg configuration. Both configurations were tested in a single session. Subjects were given approximately 10 minutes of guided practice controlling the simulated prosthetic arm before starting the first recorded cycle in order to become familiar with the nature of pattern recognition control and the simulation environment. In each limb configuration, subjects performed two different TAC test tasks. In the first condition, six motion classes were used to train the classifier (3-DOF active) and every possible target was repeated four times in randomized order (24 trials). The active DOFs included forearm pronation/supination, wrist extension/flexion, and open hand/closed fist. In the second condition, elbow flexion and extension were added to the classifier (4-DOF active) and every possible target was repeated 3 times (24 trials). In both cases, the target posture involved a single movement (1-DOF target), though erroneous activation of other degrees of freedom and overshoot required correction. The distinction between these two conditions is especially important for the leg configuration, as we found previously that classification accuracy can be heavily affected by the inclusion of the foot adduction and abduction gestures.

Classification accuracy was obtained by leave-one-out cross validation with whole recording trials as the unit of train/test splitting (data from a single recording was never split into training and testing sets). TAC test performance metrics were computed as described above. An ANOVA was performed for each performance metric with subject as a random factor and number of active DOFs (3 or 4) and limb (arm or leg) as fixed factors. The significance threshold was set at $\alpha = 0.05$. Significant factors prompted follow-up paired *t*-tests repeated for each level of the factor.

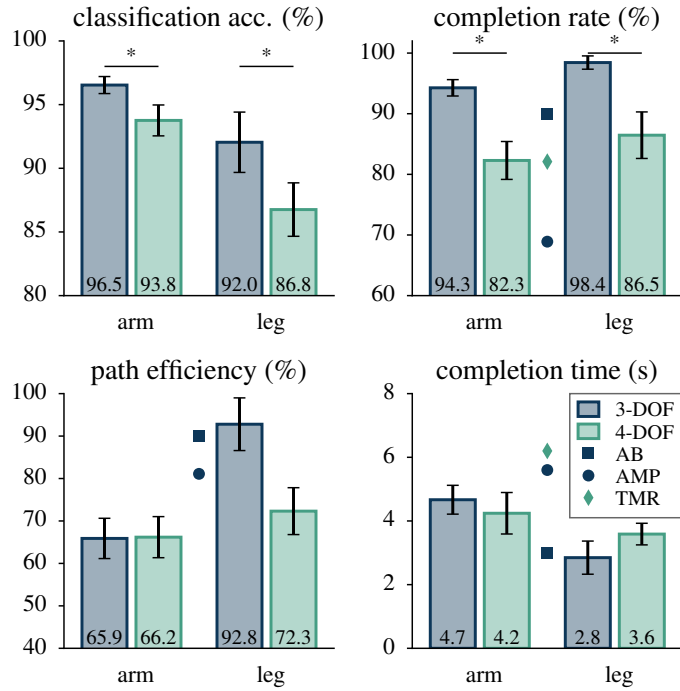
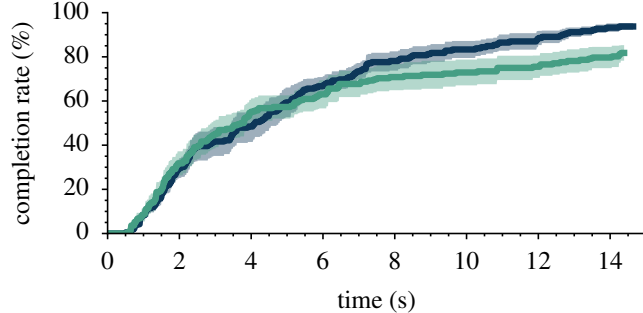


Figure 3.9: Summary of results averaged across participants. Error bars indicate standard error of the mean. Results from comparable studies are also shown: AB (inexperienced able-bodied subjects with sensors on the arm, 3-DOF active [SHLK11a, SHLK11c]), AMP (experienced amputees with sensors on the residual limb, 3-DOF active [SHLK11b]), TMR (experienced TMR subjects, 4-DOF active [SHLK09]).

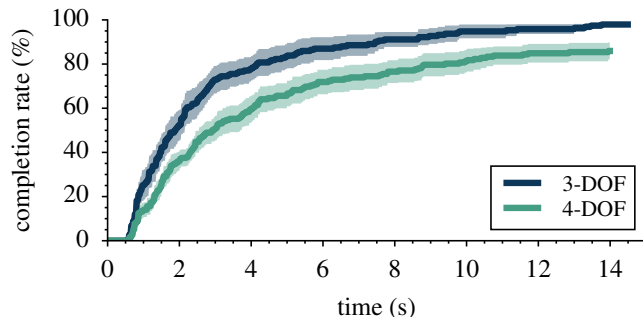
3.4.4 Results

A summary of the results is given in Figure 3.9. Average classification accuracy was generally higher than 90%, except in the leg configuration with 4-DOF active. An ANOVA showed that number of active DOFs was a significant factor ($p = 0.003$), and post-hoc t -tests indicated a significant decrease from 3-DOF to 4-DOF for both the arm and the leg configurations ($p = 0.017$ and $p = 0.012$ respectively). Although limb was only a marginally significant factor ($p = 0.050$), there does seem to have been a systematic drop in classification accuracy in the leg configuration, especially in the 4-DOF case.

Completion rate similarly decreased in the 4-DOF active case for both limb configurations ($p = 0.005$ for arm, $p = 0.023$ for leg). ANOVA failed to show limb to be a significant factor ($p = 0.155$), though completion rates in the leg configuration were slightly higher overall. Path efficiency was somewhat low (compared to similar studies) across all cases except in the leg configuration with 3-DOF active. This interaction between limb and



(a) Arm configuration



(b) Leg configuration

Figure 3.10: Cumulative completion rates averaged over participants. Filled areas represent ± 1 standard error of the mean.

number of active DOFs was significant ($p = 0.037$). No significant differences were found for completion time. Figure 3.10 shows the completion rate calculated at artificial trial cutoff times, referred to as cumulative completion rate. In the leg configuration with 3-DOF active, there was a notably rapid increase in completion rate over the first four seconds. Otherwise, cumulative completion rate curves were similar across all conditions.

3.4.5 Conclusions

Most studies using the TAC test to measure performance of prosthesis control schemes use a task with 3-DOF active and 1-DOF targets, with a few including multi-DOF targets [OCHB14, YSRH14] and only one including four active DOF [SHLK09]. It is somewhat difficult to directly compare results between studies because of differences in subject type (able-bodied, amputees, TMR patients), levels of experience with myoelectric control, recording setup, and TAC test parameters. We selected our methods for gesture classification and TAC test parameters to facilitate comparison with other studies, a few

of which are shown in Fig. 3.9. Note that upper limb amputees with intact legs would not likely show significantly different performance from able-bodied subjects, in contrast to the drop in performance typically found in myoelectric control work. However, cortical reorganization following amputation and the effects of prosthesis use may lead to differences [LGB⁺99].

The main finding from this initial study was that the real-time performance in the leg configuration is as good as or perhaps better than in the arm configuration. One of the concerns we initially had was that performance in the leg configuration would drop along with classification accuracy with the foot adduction/abduction gestures included (4-DOF active). Since this work overall aims specifically to help high-level amputees, it is necessary to evaluate performance with elbow control included, and the 3-DOF and 4-DOF conditions were used to explicitly test for the effect of the added gesture classes. While the drop in performance moving to 4-DOF is not too different from the arm configuration, it is worth noting that some subjects struggled to actuate the elbow correctly while others did not. The effect on performance may have been reduced to some extent by experience with 3-DOF active before moving on to 4-DOF. Regardless, we found that feedback is a vital part of effectively using the foot adduction and abduction gestures for control, at least for inexperienced subjects.

Subjects tended to be more efficient in the leg configuration, and it was noted that several subjects had some difficulty in the arm configuration with low levels of muscle activity being classified as forearm supination. Despite the use of a decision-based velocity ramp controller, these misclassifications resulted in the need to correct the arm position with forearm pronation. These corrective motions had an inflating effect on both the completion time and path efficiency metrics in the arm configuration. In contrast, subjects exhibited notably fast and accurate movements with 3-DOF active in the leg configuration.

3.5 Experiment: TAC Test with Two-Dimensional Targets

3.5.1 Introduction

Overall, the results of the previous preliminary real-time control experiment showed promise for myoelectric upper limb prosthesis control via leg movements. To follow this study, the study design was enhanced by including targets in two dimensions. In addition, the industrial robotic arm of the previous study was replaced with a prosthetic limb model, many improvements to the software platform were made, and a new research-grade wireless EMG hardware system was acquired.

3.5.2 Improved Simulation

A model of the Modular Prosthetic Limb (MPL) [JBB⁺11] was developed for simulation in the V-REP [RSF13] simulation environment, and is shown in Figure 3.11. A 3D model of the arm was obtained and imported into V-REP, then the assembly was configured and motors were added such that each joint could be directly velocity controlled. This model was developed in order to improve the realism for subjects, since the previous study used an industrial robotic arm that was available for drag-and-drop use within V-REP and was not a particularly realistic prosthetic limb. The software written to implement the TAC test experiment is available online at <https://github.com/ixjlyons/pygesture/tree/v2.0>.

3.5.3 Experiment Design

Eight able-bodied subjects (four male and four female, 18 to 21 years old, all right-hand dominant) performed a target achievement control (TAC) task [SHLK11b] in order to further evaluate the methods of the previous section for real-time control of a simulated prosthetic arm. Similar to the previous TAC test study, participants performed the task seated with EMG sensors on the leg in addition to a benchmark setup on the arm for comparison—able-bodied subjects facilitated this within-subjects design. Two additional subjects participated in the experiment, but they seemed to have trouble fully understanding the nature of velocity control and were dismissed after struggling to complete

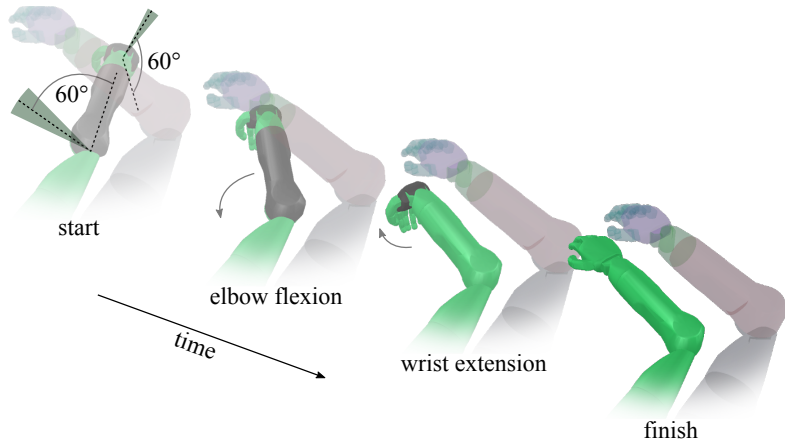


Figure 3.11: Progression of a 2-DOF TAC test trial depicted using serial screenshots of the V-REP interface. A translucent, multi-colored “reference arm” was shown to the subject to display the resting (target) posture. Each DOF involved in the trial was initially displaced by 60 degrees and the task involved bringing the arm back to the resting posture with ± 10 -degree tolerances in each joint. Arm segments corresponding to joints outside the target were colored grey and turned green when the joint reached the target.

any TAC test trials.

Six Delsys Trigno wireless EMG sensors were placed in the same locations as in the previous experiment, though these sensors have “dry” electrodes with fixed inter-electrode spacing, kept in place with double-sided stickers designed for the sensors. Overall, the signal processing and gesture classification techniques were similar to those of the previous experiment. The EMG signals were sampled at 2 kHz and a fourth-order Butterworth bandpass filter with cutoff frequencies of 10 Hz and 500 Hz was used to condition the recordings. Data was acquired in 216 ms windows with 108 ms overlap. Time domain features and linear discriminant analysis were used to classify the gestures. A decision-based velocity ramp controller [SHLK11a] was applied to the stream of LDA classification decisions to help attenuate the effect of misclassification. The joint velocities output by the controller were then directly applied to the simulated prosthetic arm.

Subjects produced classifier training data for the TAC test trials similarly to the methods used in the offline experiment, and the instructions during this portion of the experiment were the same. Four repetitions of each gesture were performed in randomized order. Subjects were prompted to perform the gesture at 2 seconds into the trial and hold

the gesture for three seconds. The section of each recording from 2.5 seconds to 4.5 seconds was used as training data. In this experiment, the rest class data came from separate trials rather than the beginning portion of non-rest trials.

After the classifier was trained, the online portion of the test began. An example TAC test trial is illustrated in Figure 3.11. During TAC test trials, a translucent “reference arm” was shown just above the “controlled arm” to demonstrate the neutral posture (joints at zero degrees). At the beginning of a trial, the controlled arm disappeared while it moved into the target posture, which consisted of either: a single joint movement by 60° (1-DOF target), or a two-joint movement by 60° each (2-DOF target). The controlled arm then reappeared in the offset posture, and an indicator changed color to prompt the user to begin moving the controlled arm back to the neutral posture. Segments of the arm corresponding to the controlled joints (elbow, forearm, wrist, and hand) changed color depending on the state of the joint—if the joint moved to a position within the tolerance of the target joint angle, the arm segment changed from grey to green. Once the controlled arm remained within the tolerance angle of the target for all joints for a dwell period of 2 s, or if the target could not be achieved within 20 s, the trial ended. The tolerance angle was set to 10° . Joint limits were set at $\pm 80^\circ$ with respect to the neutral posture. The averages of the top 10 mean absolute value features from the training data for each class were used to calculate boost values [SHLK11a] for the decision-based velocity ramp controller such that the maximum output velocity for a given joint would be $100^\circ/\text{s}$, and joint velocities were explicitly limited to this velocity.

The experiment consisted of two sessions, one for each limb configuration, separated by at least 24 hours. Half of the subjects started in the arm configuration and the other half started in the leg configuration, but tests for differences between these groups were not included in the statistical analyses. After generating classifier training data (about five minutes), subjects were given approximately 10 minutes of guided practice controlling the simulated prosthetic arm in order to become familiar with the nature of pattern recognition control and the simulation environment. Subjects controlled the arm with three and four active degrees of freedom. In the 3-DOF active condition, subjects con-

trolled forearm pronation/supination, wrist extension/flexion, and open hand/closed fist (i.e. no elbow flexion/extension). In the 4-DOF active condition, control was augmented with elbow flexion/extension. Subjects practiced with two repetitions of every possible target requiring only one motion class (1-DOF targets) with 3-DOF active control. They then moved on to two repetitions of every possible 1-DOF target with 4-DOF active. After practice, subjects alternated between blocks of 3-DOF and 4-DOF active conditions, where each block consisted of one repetition of every possible 2-DOF target (includes all 1-DOF targets). Subjects were told before each block whether or not control of elbow flexion/extension would be enabled. In total, subjects completed 4 blocks with 3-DOF active ($4 \times 18 = 72$ trials) and 3 blocks with 4-DOF active ($3 \times 32 = 96$ trials). The exact same procedure was carried out in the second session, but with the other limb configuration. The “no forearm” condition from the offline classification experiment was not used in the target achievement control experiment.

Performance metrics for the TAC test were computed as described in Section 3.4.2. For each performance metric, an ANOVA was performed with subject as a random factor and target degrees of freedom (minimum number of movement classes needed to reach a target—either 1 or 2), active degrees of freedom (number of degrees of freedom controllable by the subject—either 3 or 4), and limb configuration (either arm or leg) as fixed factors. The significance threshold was set at $\alpha = 0.05$.

3.5.4 Results

3.5.4.1 TAC Test Performance

TAC test performance in the arm and leg configurations are shown in Figure 3.12. With 3 active degrees of freedom, subjects performed remarkably similarly in the arm and leg configurations. Performance in the leg configuration dropped, however, when elbow control was enabled (4-DOF active). This is reflected in completion rate but not completion time or path efficiency because the latter two metrics are only computed for successful trials, and in the trials that were successful, subjects tended to perform well with the leg configuration. Furthermore, this difference can be almost entirely explained by a single subject’s inconsistent performance with 4-DOF active control in the leg configuration.

Unlike the other two subjects dismissed during the session, this subject seemed to only have difficulty with the leg configuration with elbow control enabled.

For completion rates, the number of active degrees of freedom was a significant factor ($p = 0.009$) as well as the number of target degrees of freedom ($p \ll 0.001$). There were also significant interactions between limb and number of active DOFs ($p = 0.033$) and number of active DOFs and number of target DOFs ($p = 0.008$). Similarly, for completion time, active DOFs was significant ($p < 0.001$) as well as target DOFs ($p \ll 0.001$). Furthermore, the interactions between limb and active DOFs ($p = 0.001$) and between limb and target DOFs ($p = 0.008$) were significant. The three-way interaction between limb, active DOFs, and target DOFs was also found to be significant ($p = 0.012$). For path efficiency, active DOFs ($p < 0.001$) and target DOFs ($p \ll 0.001$) were found to be significant main effects and the interaction between limb and active DOFs was also significant ($p = 0.008$). Although not shown in Figure 3.12, we tracked initiation time (time from presentation of the target to first non-rest class output), but found it to be essentially constant (~ 1.2 s) across all conditions except a slight systematic increase for 2-DOF targets. This increase was likely due to subjects deciding which of the two gestures should initiate the trial. No difference was found between the arm and leg configurations.

3.5.4.2 Trial Completion Timing

As in previous TAC test studies, we examined the number of trials completed at incrementally increasing artificial cutoff times, known as the cumulative completion rate (Figure 3.13). Below the cumulative completion rate curves, we also show a kernel density estimate of the distribution of all completion times (for all subjects) in order to show the time at which subjects tended to complete the trials for the different conditions. For both the arm and leg configurations and across 3-DOF active and 4-DOF active cases, it is clear that 2-DOF targets tend to take longer to reach than 1-DOF targets (as expected with serial control). In the 3-DOF active case, the completion curves are nearly identical, with a slightly faster initial rise in the leg configuration for 1-DOF targets. With four active degrees of freedom, subjects tended to complete 1-DOF target trials roughly as quickly in both the arm and leg configurations, though there was more subject variability

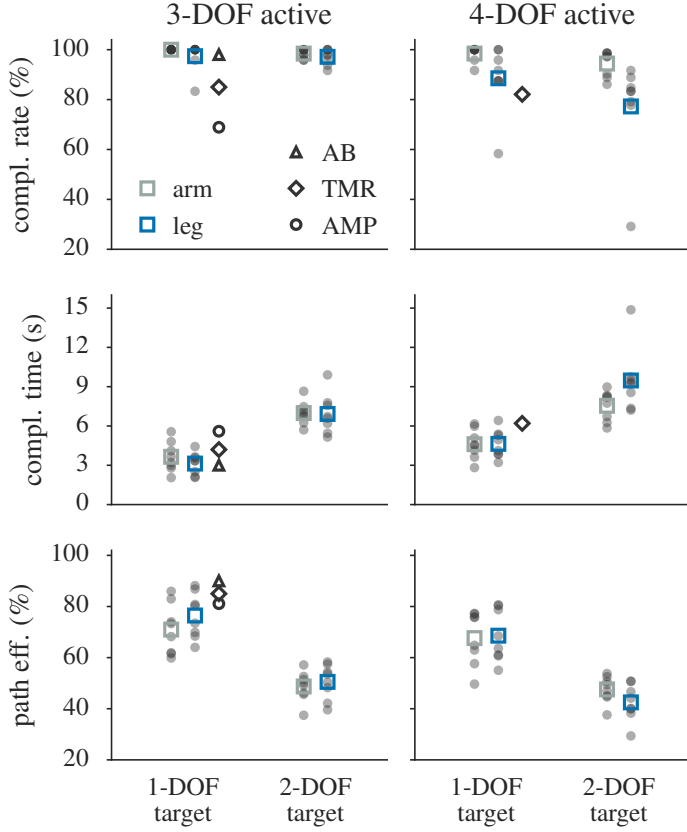


Figure 3.12: Subject performance in the target achievement control task. Each subject’s performance is shown with a translucent grey dot, and across-subject means are indicated as squares. Completion time and path efficiency correspond only to successful trials. Data from comparable studies are also shown near the corresponding configurations: AB (inexperienced able-bodied subjects with sensors on the arm [SHLK11a]), TMR (experienced TMR subjects [SHLK11a, SHLK09]), AMP (experienced amputees with sensors on the residual limb [SHLK11b]).

and an overall lower percentage of trials completed. With 2-DOF targets, this difference was amplified, and the curve for the leg configuration climbs steadily over the entire 20-second trial duration without a sharp initial increase. The density estimate shows a general grouping of trial completion times around 6 seconds and another grouping just before trial termination (20 seconds).

3.5.4.3 Improvement Over Time

In order to investigate whether or not subjects improved performance over time, we analyzed each of the TAC test metrics split into the blocks from the experiment design (each block contains all possible 1-DOF and 2-DOF targets in the given number of active

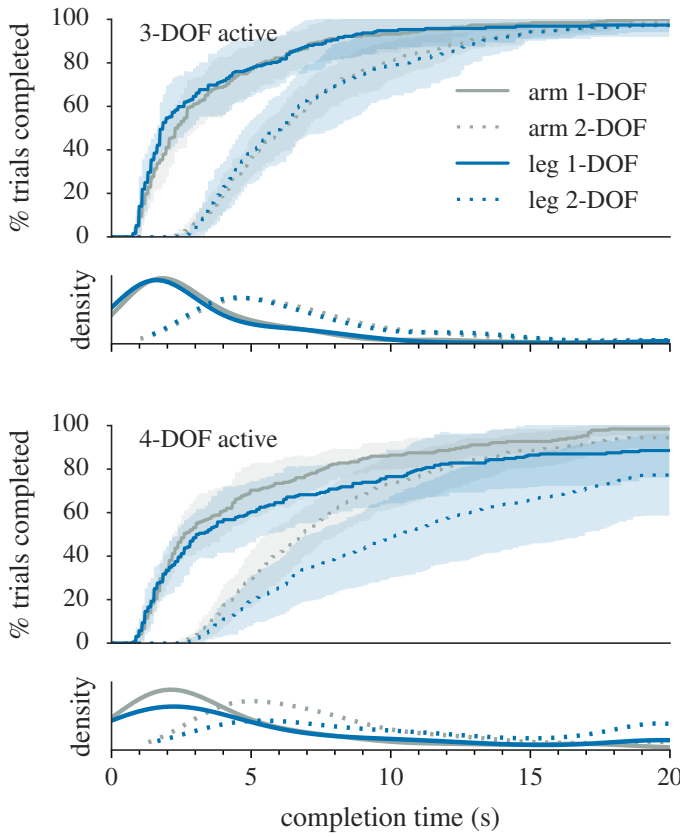


Figure 3.13: Cumulative completion rate: the percentage of trials completed across the range of completion times. Kernel density estimates of completion rates are plotted below to highlight the time at which most of the trials were completed for each condition.

degrees of freedom). This is shown in Figure 3.14. Although target DOF was a significant factor in all three metrics, each block contained a randomized ordering of 1-DOF and 2-DOF targets, and similar changes over time were observed for both 1-DOF and 2-DOF targets. From Figure 3.14, there is a clear, albeit slight, increase in completion rate in the leg configuration with 4-DOF active. The large variance across subjects is caused primarily by the single low-performing subject. A repeated measures t -test with Bonferroni correction confirmed that the completion rate in block 3 was significantly higher than in block 1 ($p = 0.013$), though the differences between blocks 1 and 2 as well as blocks 2 and 3 were not found to be significant.

3.5.4.4 Comparison to Other Studies

The results with 3-DOF active control toward 1-DOF targets are compared to the results of similar studies in Figure 3.12. Note that every study using the TAC test uses slightly

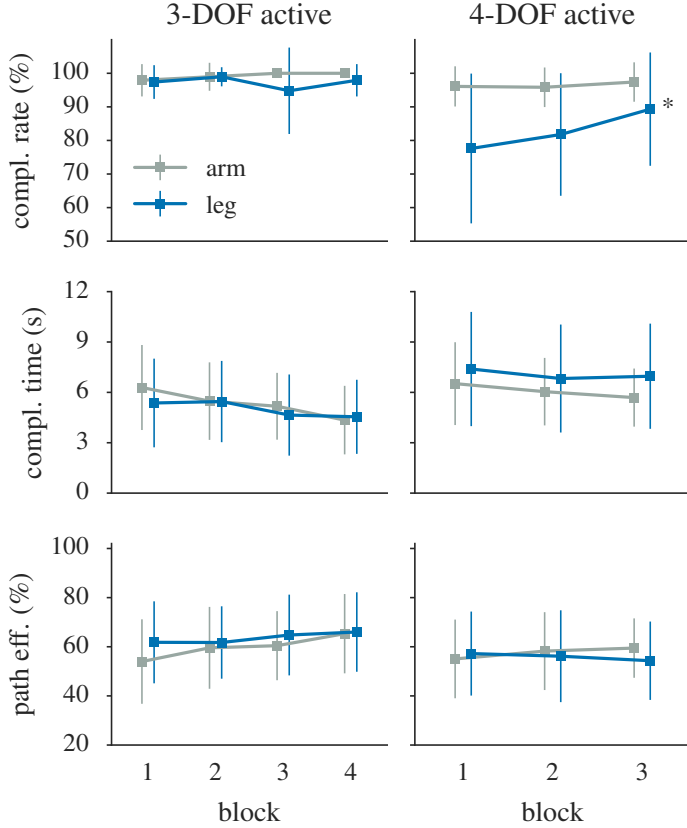


Figure 3.14: Subject performance in the target achievement control task across trial blocks. Each point is the mean over subjects and target DOFs, and error bars indicate standard deviation of the mean across subjects. Only completion rate in the leg configuration with 4-DOF active showed a significant change over the session (marked with *).

different parameters, including trial cutoff time, target distance (with respect to maximum joint angular velocity), and target size (joint angle tolerance). Most notably, the comparable studies used a 15-second cutoff time (compared to 20 seconds for our study), but Figure 3.13 shows that the final five seconds account for only a small portion of the successful trials. Performance in the arm configuration is well-matched to similar studies with inexperienced able-bodied subjects [SHLK11a], validating the end-to-end operation of our experimental procedures, hardware, and software. Interestingly, performance in the leg configuration in this condition (3-DOF active, 1-DOF target) was overall on par with the benchmark arm configuration and sometimes slightly better. We attribute this to a challenge some subjects faced in the arm configuration in commanding the arm to

rest without inadvertently pronating. This did not seem to heavily impact performance, though path efficiency was somewhat reduced compared to the leg configuration as well as the other comparable studies. In contrast, movements with 3-DOF active in the leg configuration were notably fast and accurate. Compared to amputees using residual muscles of the forearm [SHLK11b] as well as a set of six TMR patients [SHLK11a], our 3-DOF control results are favorable. While we tested only able-bodied subjects, we hypothesize that amputees with intact legs will perform just as well as able-bodied subjects, though this would need to be investigated further.

Control with 4-DOF active does not seem to be commonly studied, so there is little to compare our results to in this condition. One study involving two TMR patients [SHLK09] implemented 4-DOF active control, and the patients achieved substantially different completion rates (92.2% and 71.9% with a velocity ramp controller). The average is indicated in Figure 3.12. While performance with 4-DOF active dropped in the leg configuration, all but one of our subjects surpassed 85% completion rate, with two completing 100% of the 4-DOF active/1-DOF target trials with the leg. Control in four degrees of freedom with 2-DOF targets has, to our knowledge, not been tested elsewhere. Strong conclusions should not be drawn from these comparisons, but they serve to validate the system overall, especially in light of the fact that our subjects started with no myoelectric control experience and produced these results after less than one hour, including setup (\sim 20 minutes), classifier training (\sim 5 minutes), and real-time control familiarization (\sim 10 minutes). This is in contrast to the time for recovery, rehabilitation, and training involved with targeted reinnervation surgery.

While we cannot directly compare quantitative control performance of the proposed system to the IMU-based controller of Resnik et al. [RKEF14], we can address the functionality provided by each. As demonstrated, the current EMG-based system can provide fairly reliable control of three degrees of freedom, and most subjects obtained good performance with four degrees of freedom. In addition, hallux extension has been investigated previously as a potential gesture for controlling a secondary grip [LJ15]. The IMU-based controller provides all of these functions, and some instantiations add the ability to cycle

through six different grips (via mode switch) as well as directly control the direction of hand movement via coordinated actuation of the elbow and shoulder (endpoint control). These additional features come at the cost of increased control complexity, however, as they overload foot movements to command different functions depending on the current control mode, and typically a single arm is controlled using both feet. It is worth noting that this kind of mode switch could be added to the current EMG-based controller while remaining under control via a single leg (as opposed to both feet). In addition, we have demonstrated that EMG can be used to detect several toe movements [LJ15], which the IMU system cannot do.

3.5.5 Conclusions

The results of the offline classification study (Fig. 3.6) showed that inclusion of foot inversion/eversion in addition to adduction/abduction in the gesture set can be problematic, at least with the current sensor configuration and signal processing/classification techniques. We speculate that this was caused by three factors. First, there is biomechanical coupling between the movements misclassified for one another. For example, foot adduction is a somewhat difficult gesture to produce without also inverting the foot to some extent—the more natural movement for the foot is supination, which is a triaxial movement comprised of simultaneous adduction, inversion, and plantarflexion. A similar argument can be made for pronation. Users could potentially improve distinguishability of these two gesture pairs with practice, and Fig. 3.14 provides indirect evidence that this may occur within a single session. Second, the sensor configuration used was not heavily optimized and could potentially be improved, though the arm configuration was also non-optimized. Finally, users received no feedback during the offline experiment, so misclassifications occurred without subjects taking corrective action. Our motivation for including 4-DOF active control in the TAC test experiment was to determine if real-time visual feedback could help subjects produce the gestures with fewer misclassifications. While performance using the leg control scheme indeed dropped with elbow control enabled, this seems to be driven primarily by a single subject performing especially poorly. This may have been caused by an inability to adapt during the familiarization period or anomalous sensor

preparation. The problems this poorly performing subject faced, however, were also observed by the researchers during testing of other subjects, albeit to a much lesser extent. Control of the elbow seemed to involve one of two problems: it was either difficult to avoid actuating the elbow unintentionally, or it was difficult to avoid actuating other joints while controlling the elbow. The two dismissed subjects understood the arm-leg mapping from the beginning, but despite producing the correct movements, they could not generate a reliable stream of classification decisions. This seems to indicate that, while high classification accuracy is not necessary for real time performance, especially low classification performance can make the system difficult to use. Future work should investigate alternative electrode configurations and gesture training procedures to improve performance in recognizing lower leg gestures via surface EMG.

The slight improvement over the session in the leg configuration with 4-DOF active (Fig. 3.14) could be due to several factors. First, subjects could be learning overt strategies for completing trials in order to overcome poor classification performance. Two specific strategies we identified during testing were: avoiding problematic gestures when possible, and waiting to correct for errant movements at the end of a trial rather than stopping the primary movement to fix issues before moving on. The latter strategy was especially beneficial to completion rate for subjects that had difficulty with unintentionally flexing the elbow. Second, subjects could be learning to improve classification performance itself by producing more distinguishable gestures. In future experiments, a final post-training classification accuracy assessment could be used to detect the presence or absence of this effect. Finally, the subjects could be learning the mapping from the leg to the arm. While we cannot definitively discount this as a potential factor, the lack of change in completion time and path efficiency seems consistent with strategy learning as opposed to mapping learning. That is, subjects learned to complete trials more often, but they could not do so more quickly or more efficiently. If subjects were able to reliably produce a stream of classification decisions but were confused as to which gesture to produce, improvements in the latter would lead to lower trial completion times with more direct trajectories.

The decision to employ the gesture classification methods (LDA and time domain fea-

tures) and real-time evaluation task (TAC test) commonly used in targeted muscle reinnervation studies was primarily driven by the desire to maintain comparability between our work and the only other high-functionality myoelectric prosthesis control approach for high-level amputees (i.e. excluding mode-switch control). The results seem to indicate that these techniques are compatible with leg muscles and movements, so it seems likely that more recent advances in intent recognition from arm muscles could also benefit this upper limb prosthesis control idea. For example, a common problem in myoelectric control is the limb position effect [FSC⁺11]. Weightbearing and changing leg position (e.g. sitting, standing, lying down, etc.) could be regarded as similar to the limb position effect, and techniques designed to overcome this issue could potentially be applied to obtain accurate recognition of leg gestures in different positions [GZL12]. Furthermore, it could be beneficial to use automatic gesture onset and offset detection methods to segment the recordings used to train the classifier. This would produce a richer data set by including segments of dynamic as well as static contraction for each gesture class [SE13].

However, since the leg is different from the arm in many ways—musculature, dexterity of control, types of muscle fibers—future work should treat it as such in order to more thoroughly evaluate its control output capacity. Recording surface EMG from the leg is commonly used in a number of clinical and research settings, such as motor coordination (gait analysis), sport science, and neurological disease. In the context of gait analysis, for example, the rich temporal information in EMG signals may be used in combination with joint angle measurements to detect abnormalities in muscle activations during the gait cycle [FC09]. Leg EMG is also used in lower limb prosthetics research, which has recently been taking advantage of leg EMG as an additional sensor for improved control over other active devices which work only with “kinesthetic” and “proprioceptive” sensors [GLS13]. There has also been some recent work using supervised classification of leg movements for volitional control of lower limb prostheses in non-weight-bearing situations [HVG11, HSL⁺13]. Interestingly, Hargrove et al. found that a small number of lower leg movements (plantarflexion/dorsiflexion and external/internal tibial rotation) can be recognized with EMG sensors placed only on upper leg muscles in both able-

bodied subjects and transfemoral amputees [HSL⁺13]. Optimization efforts specifically for control using leg EMG could target the persistent problem of confusion between inversion/adduction and eversion/abduction. It is also worth noting that using surface EMG to record from the extrinsic toe extensors and flexors has, to our knowledge, not been done before. More experience is needed to ensure reliable and clean recording from these muscles, especially in developing methods for daily application by a non-expert (i.e. the prosthesis user).

While the basis of this work is on the natural mapping between upper and lower limb movements, there have been several studies suggesting that, with training, performance with a nonintuitive mapping from EMG to interface action can approach that of a more intuitive mapping [RBJ08, AIA14]. These results are interesting, but it remains unclear if or how they extend to control in more than two degrees of freedom. It is likely that the training time required to match performance with a nonintuitive mapping increases along with increased control complexity. There seem to be no obvious benefits to forcing the use of a nonintuitive mapping when an intuitive one is available, though perhaps the mapping discovery process promotes a deeper understanding of the system and is beneficial to the user’s ability to adapt to perturbations or nonstationarities. One of the goals of this study was to minimize training time needed to begin functional control of a prosthetic arm, and maintaining a mapping that can be rapidly learned was the primary factor in working toward this goal.

One potential avenue for expanding on this work is to consider hybrid controllers utilizing multiple modalities, such as combining EMG and inertial measurements. In these control schemes, the benefits of each sensor modality can be used to improve intent recognition and/or to control distinct aspects of the robot’s motion [NR15]. While EMG is a somewhat noisy sensor modality, the advantages of detecting toe movements and not necessarily requiring recalibration following changes in foot orientation or loading could make it a valuable component of such a hybrid system. Furthermore, EMG recordings capture control signals “upstream” of end effector states that other sensors like IMUs or foot switches measure, hence containing potentially much richer information. For exam-

ple, surface EMG signals can be decomposed into motor unit action potentials [DAW⁺06], giving access to neural commands which are difficult or impossible to measure once the “musculoskeletal filter” [Bur16] has applied and the limb has interacted with the external world. EMG signals from antagonistic pairs of muscles could also be used to infer properties like joint stiffness, which is not possible to measure via joint movement alone without applying known external forces. Ultimately, however, measuring both neural drive and kinematic parameters would enable better stiffness estimation than either measurement alone. Signal processing and machine learning techniques for myoelectric control continue to progress toward detecting subtler and more fluid user intentions, making EMG a promising sensor modality despite the ability to reliably measure limb movements or forces directly using other sensors.

One of the benefits of targeted reinnervation is that, in addition to efferent neural pathways for output of control signals that map intuitively to prosthesis function, some sensory feedback is restored as a result of the surgery. Indeed, specific surgical techniques for enhancing the quality of this restored somatosensory feedback have been developed [HOM⁺14]. This presents an exciting opportunity to provide dense anatomically relevant feedback, which is a critical step toward sensorimotor integration of prosthetic limbs [RCP⁺14]. With our proposed control scheme and mapped feedback signals (e.g. mapped tactile feedback to the toes corresponding to prosthetic fingers), it would be interesting to investigate the potential for cortical reorganization associated with limb substitution for both feedback and control.

3.6 Outcomes

Although ambulation would interfere with the ability to use the leg for upper limb prosthesis control, many activities of daily living (ADLs) that require the use of both arms are performed in a stationary position, such as eating at a table, washing dishes, or folding laundry. Furthermore, the use of both arms while walking often involves one or both arms being held in a static posture, such as carrying a box. Transitioning between standing and walking can be detected automatically, and this could trigger the arm to lock in place. Re-

gardless of the solutions to these practical issues, there will always be a trade-off between the merits of the control capabilities achieved and the burden of the system's intrusiveness. This trade-off is not unique to the idea of controlling a prosthetic arm with the leg, as all prosthesis control interfaces have benefits and drawbacks. While many of the practical concerns associated with a foot-based controller have been addressed by Resnik et al. for their controller based on inertial measurement unit sensing of foot movements [RKEF14], it would be interesting to see how they could be addressed for this system by developing techniques specifically optimized for the application, testing the system with amputees and conducting usability studies, and eventually testing with physical robotic arms or prostheses. Although TMR is a fascinating technique and it has been shown to work well in practice, there isn't a single system that will work for everyone. In my view, working on alternative approaches only helps to identify additional solutions that could work for those who can't or don't want to undergo invasive procedures.

The experience of running this study showed that feedback can improve control (e.g. comparing the whole trials with misclassifications in the offline study to performance in the online studies), but it may still not be enough if subjects *don't know how to influence the feedback they're seeing*. This was particularly noticeable in observing subjects attempt to actuate the elbow in the TAC test by moving the foot toward the midline of the body (adduction) and seeing the simulated arm do everything *but* flex the elbow. Classification-based systems are great when the output stream matches the intended movement, but in my experience, they can be difficult to operate once things change such as when muscles fatigue or the foot loading changes (as in sitting, standing, etc.). This realization formed the basis of my motivation to learn more about how we learn to adapt to unforeseen changes.

Chapter 4

Visuomotor Adaptation with Proportional Myoelectric Control

Preface

Based on my experience running experiments with pattern recognition control, both with the arm and the leg, it became clear to me that an important idea influencing the performance of myoelectric control is often ignored: the fact that humans readily learn and adapt. In myoelectric control, things change for many reasons: electrodes shift, muscles fatigue, skin impedance changes (e.g. because of sweat), etc. This is a major problem for static pattern recognition control. Subjects just seem to be lost and unable to determine what needs to change in order to make the classifier to correctly output the class of the movement they're clearly making with the arm or leg. This chapter presents published [LJ18a] and unpublished experimental work aimed at investigating a somewhat counterintuitive theory from motor adaptation literature that increased neuromuscular “noise” leads to faster adaptation to perturbed movements. The goal is to better understand how exactly we are able to adapt to novel situations and continue making accurate movements. By better understanding this process, it may be possible to design myoelectric control schemes or training protocols to exploit the plasticity of the neuromuscular system.

4.1 Bayesian Integration Theory of Motor Adaptation

One concept from motor learning that has recently been studied with myoelectric control is the notion of an adaptation rate, describing the proportion of an error the subject corrects for in the subsequent trial or trials. A classic type of experiment illustrating this process is prism goggles adaptation [Hel65]. Healthy individuals are capable of quickly and accurately pointing to a target placed in front of them after some practice. If you suddenly apply goggles which shift the angle of their vision, their first movement after the shift will have a large error. On the next trial, much of this error will be compensated for. And on the trial after that, the error will further be reduced, etc. This kind of visuomotor adaptation is the basis of a large body of work in the field of motor learning and has been used in the demonstration of some of the hallmarks of learning like savings and interference [WF16].

Not only are we able to adapt to novel scenarios adeptly, but we can do so in the presence of various forms of uncertainty. There is noise and uncertainty in every part of the process of generating movements and sensing the world, yet we are somehow capable of producing accurate movements [FSW08]. The exact mechanisms by which the neuromuscular system does this are not fully understood, but one model of how we learn from errors made in the presence of such noise is Bayesian integration. This model predicts that the amount by which we adjust our movements after being presented with a perturbation depends on sensory uncertainty as well as the variability of past experiences performing reaching movements [KW04]. The model relies on the idea of a forward model in the brain which maps motor commands to predicted motion and/or sensory feedback [SSK10], and according to this probabilistic model, increased sensory uncertainty should result in more reliance on the forward model to form an estimate of state such that when a perturbation is suddenly applied, the noisy feedback is treated as unreliable and the subject doesn't adjust to the perturbation. This behavior has been demonstrated in a planar reaching tasks with step perturbation [BEB08] as well as trial-by-trial random perturbations [WK10], where the adaptation rate is defined as the proportion of the perturbation seen in trial

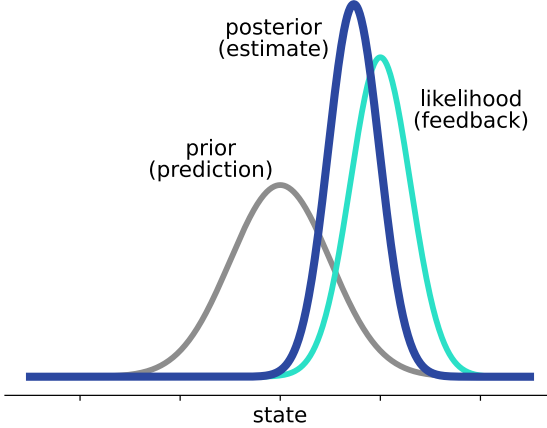


Figure 4.1: Illustration of the Bayesian update. The prior represents the subject’s initial prediction of reach position. When an observation is made that is incongruent with the prior, the estimate is shifted away toward the observation, depending on the relative strength of the prediction from the forward model and the feedback received.

$k - 1$ corrected for in trial k . It has also been shown that displaying randomly scattered feedback in a one-dimensional myoelectric control task leads to reduced adaptation to trial-by-trial perturbations [JKHS14]. The other main prediction of the Bayesian integration model is that increased model uncertainty, whether it arises from motor noise or modeling errors, *increases* our reliance on feedback because our forward model predictions are not trustworthy. This has been demonstrated less robustly than the effect of sensory uncertainty [KM11], but there is at least some evidence that there is an effect through direct or indirect modifications of model uncertainty [BEB08, WK10, HLA⁺16].

Several questions remain open regarding model uncertainty and the effects on sensorimotor learning. In the case of myoelectric control specifically, it is unclear if adding additional uncertainty to an already noisy control interface could drive a change in adaptive behavior. It is also not known whether an increased tendency to adapt to perturbations is *useful*, as it fundamentally means a forward model is not well formed or is not trusted. An alternative view is that uncertainty in the mapping is a mechanism by which one learns this forward model, which produces better long-term performance [WMC⁺14, SSS17]. One example of the intentional addition of control signal variability driving favorable behavior comes from Thorp et al., who showed that applying noise to only a subset of a redundant control system’s inputs results in subjects avoiding use of those inputs [TKMI17].

This kind of intervention could be used in training procedures to reduce the reliance on dominant inputs and promote exploration of less-used input space [WMC⁺14]. The experiments in this chapter were designed to evaluate the influence of noise introduced to a proportional myoelectric control mapping on adaptation.

4.2 Proportional Myoelectric Control

Since we are interested in tracking adaptation behavior, we need subjects to be able to express trust or distrust in an internal model on a continuous scale. Much of the current work on myoelectric control uses gesture classification to discretize the output and provide intuitive and low-noise control of a number of commands [RRFA14]. The main disadvantage of this approach is that execution of complex, multi-degree-of-freedom movements must be broken down into a series of simpler movements. Attempts at training “multi-gesture” classes can work [YSRH13], but this decreases classification performance and requires additional training time (to generate data corresponding to the gesture combinations). Proportional control is fundamentally a simple approach by which EMG signal amplitudes are used more directly to control the output. For example, the rectified and filtered amplitude of the EMG signals from wrist extensor and flexor muscles can be used to directly control the velocity of a robotic wrist. This is essentially the original myoelectric prosthesis control technique [SS91], and while it offers control that is more similar to our natural movements than the classifier-based approach, it comes at the cost of much noisier output [IA15]. The situation is further complicated by the fact that surface EMG sensors do not typically record a single muscle in isolation, and are instead amplifying the potentials generated by neighboring muscles which may have distinct functions with respect to the muscle of interest. This makes the obvious approach of directly mapping EMG sensor amplitude to an output variable like a robotic joint velocity difficult when working in more than one or two degrees of freedom.

One approach to this problem is to have the subject generate EMG signals while moving (or, in the case of amputees, contracting muscles while imagining movements), then use machine learning techniques to build a mapping from EMG space to output space.

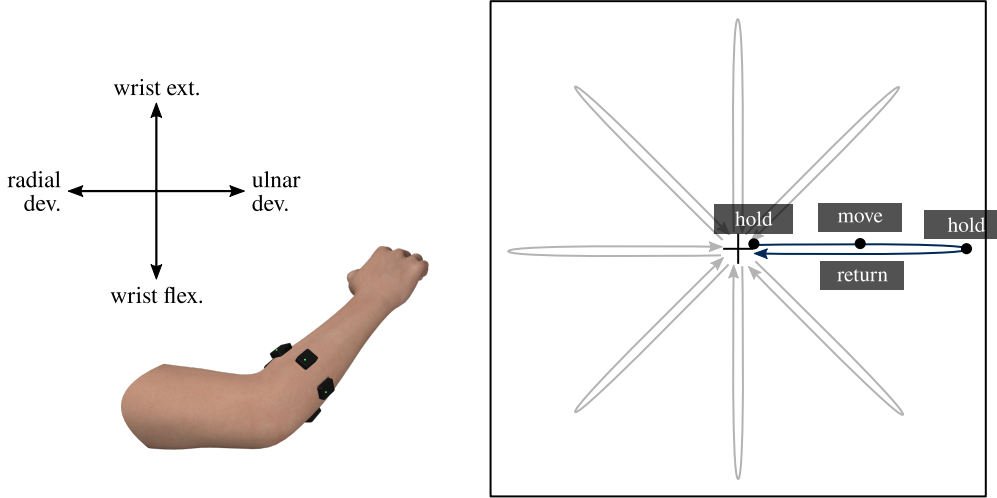


Figure 4.2: Illustration of the cursor following process. The subject watches a cursor on the screen move out to some target location and back while following it with the hand. The assumption is that windows of EMG signals correspond to the cursor position at each moment.

Fundamentally, this is not all that different from the classification approach—subjects respond to a prompt, we assume they’re producing consistent muscle activations corresponding to the prompt, then let a machine learning algorithm work to find a mapping to relate the two. The key difference is that in proportional control, the machine learning algorithm is performing regression rather than classification, so it is able to produce continuously varying output. Data is typically captured by having the subject watch a cursor move on the screen in an out-and-back trajectory while “following” it with the hand. An example is shown in Figure 4.2, which is how the cursor following task was specified in the experiments described in this chapter.

4.3 Experiment: Adaptation Following Training with Mapping Noise

4.3.1 Introduction

In this study, subjects were exposed to a new form of mapping uncertainty in which the vertical components of a linear mapping between EMG signal amplitude and two-dimensional cursor position was randomized on every trial during a cursor-to-target familiarization task. A control group performed the same task, but without the mapping

variability. After familiarization, the mapping was held fixed and subjects made movements to a target without feedback until the end of the movement, when a perturbed cursor position was shown briefly. We found that subjects in the mapping noise group overall adapted faster to the perturbations, as predicted by the Bayesian integration model. These results suggest that adaptation rate can be driven by increased mapping uncertainty, which could be a useful mechanism for getting a user to explore the input space.

4.3.2 Experiment Design

Twelve subjects participated in the experiment: 8 female and 4 male, 10 right hand dominant and 2 left hand dominant, 18 to 26 years old. The subjects were split into two groups of six: a noise group and a control group.

Subjects were fitted with six wireless EMG sensors (Delsys Trigno system), placed approximately one third of the forearm length distal to the elbow on the dominant arm, which would be a reasonable sensor arrangement for a transradial amputee. An illustration of the sensor placement is shown in Figure 4.3. The first two electrodes were placed on either side of the ulna, then the rest of the sensors were placed approximately equidistantly around the remaining space. Throughout the session, subjects were seated with the elbow resting on an arm rest with the arm held parallel to the floor and pronated so the palm faced downward. Subjects were instructed to keep the forearm still and move only the wrist.^o

In all experimental tasks, subjects viewed a computer screen with a square cursor interface drawn on it (26.8 cm wide). The center of the interface was marked with a small cross and the edges were defined to be one unit away from the origin in all four directions (normalized coordinate system). The cursor diameter was 0.04 units and the target diameter was 0.2 units. For the two left-handed subjects, the cursor interface was mirrored horizontally for all tasks so that the same wrist movements could be used by all subjects in the adaptation task.

The EMG signals were recorded at a sampling rate of 2000 Hz in chunks of 50 ms. These chunks were centered to have zero mean and then filtered with a fourth-order But-

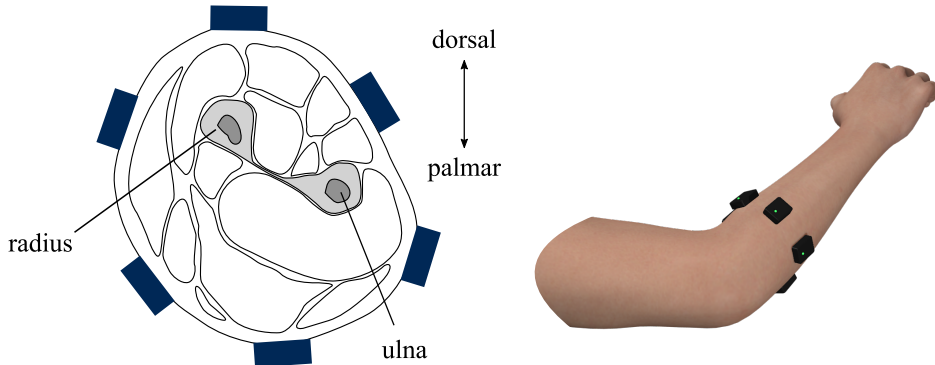


Figure 4.3: Electrode placement in the adaptation experiments. Six Delsys wireless sensors were spaced equidistantly around the forearm.

terworth bandpass filter with cutoff frequencies of 10 Hz and 450 Hz. Windows of 200 ms were then formed (150 ms overlap between adjacent windows) and the root mean square (RMS) of each channel in the window was computed to form a six-dimensional feature vector representing the magnitude of activation of each channel. This and the experiment of the next section were implemented using AxoPy, a framework for implementing human-computer interface experiments based on processing of electrophysiological signals (<https://axopy.readthedocs.io>).

4.3.3 Experimental Tasks

4.3.3.1 Mapping

In the mapping task, the cursor automatically moved from the origin out to a target location and back while the subject aimed to follow this movement by moving the wrist. Eight targets, arranged in 45° increments around a circle 0.9 units from the origin, were presented once each in a block in random order. Seven blocks of trials were performed. Each trial started by displaying the cursor in the center and the target. The cursor held the position at the center for 1 s, moved out to the center of the target in a sinusoidal velocity profile over 2 s, remained in the target for 4 s, then returned to the origin. Subjects were instructed to follow the cursor's position as closely as possible by actuating the wrist in extension/flexion and radial/ulnar deviation (Figure 4.4b), using a moderate amount of effort at the target position.

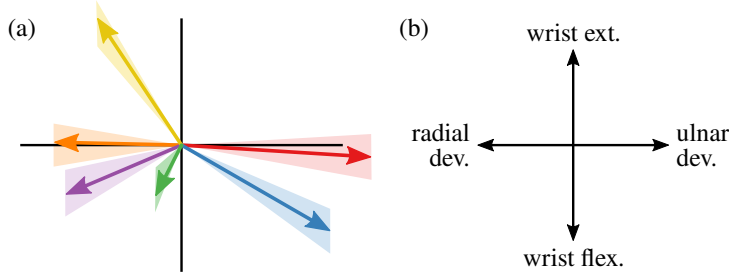


Figure 4.4: (a) Cursor control mapping from a representative subject. Each arrow represents a single EMG channel's effect on the cursor position. For the noise group, new mappings were formed on each trial by perturbing the mapping vectors vertically. (b) Wrist movements subjects used to move the cursor in the four cardinal directions (assuming right hand dominant).

After completing the mapping task, the RMS values in each channel were scaled to the range $[0, 1]$. In subsequent tasks, the scaling factors were applied to the RMS values computed in real time, and the scaled values were put through an exponentially weighted moving average filter with a decay rate of 0.5. The scaled RMS features and corresponding cursor positions from the mapping task were fit to a linear model via ordinary least squares regression, producing a 2×6 matrix mapping scaled RMS values to a two-dimensional cursor position. This is referred to as the *base mapping*. An intercept term was not included in the regression since the inputs were scaled to $[0, 1]$. Scaling the features and fitting a model without an intercept enables applying modifications to the mapping without introducing bias—i.e. relaxing the arm with low muscular activity always places the cursor at the origin.

4.3.3.2 Familiarization

In the familiarization task, subjects used the proportional control scheme to move the cursor to targets as quickly as possible, with veridical feedback throughout the trial. Eight targets arranged in a circle were again presented one at a time, this time at 0.54 units from the center of the cursor interface (60% of the distance used in the mapping task). Each target was presented once per block in random order, and 10 blocks were completed. After the target was presented, the subject had 10 s to move the cursor to the target and dwell inside it for 500 ms, otherwise the trial timed out.

On each trial, the mapping matrix was formed by adding six samples (one for each

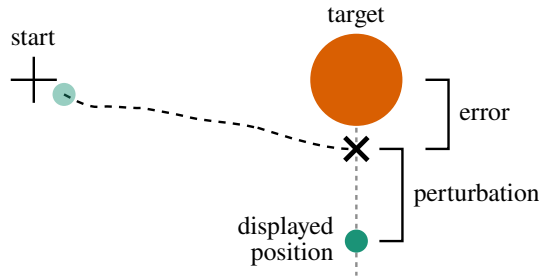


Figure 4.5: Illustration of an adaptation trial to the target at 0° . The cursor begins at the starting location (center of the screen) then disappears as the subject moves in the target direction. Once the cursor passes an invisible line perpendicular to the target direction, its position is perturbed and displayed.

channel) from a zero-mean Gaussian distribution to only the y component of each column of the base mapping, illustrated in Figure 4.4. The variance of the distribution was set either to 0.01% (control group) or 1% (noise group) of the median magnitude of the columns of the base mapping matrix. This constituted the only difference between the control and noise groups. The intended effect of this mapping update was to change the effect of each EMG channel in the vertical direction only without directly affecting the subject's ability to hold the cursor in a small region (as adding random input or output noise would). While the variance seems low, small changes to the input in the null space of the mapping matrix (i.e. different inputs leading to the same cursor position for the base mapping) can cause large variations in the vertical component of the cursor position once the mapping is changed.

4.3.3.3 Adaptation

In the adaptation task, only two targets were used: 0° and 90° (measured counterclockwise from the right). The cursor started in the center, then as it moved beyond 0.1 units from the origin, it disappeared so that subjects were required to move toward the target without feedback. Once the cursor passed through an invisible line perpendicular to the target direction at the target center, the cursor's position was perturbed along that line and the perturbed position was displayed for 1 s before returning to the center for the next trial. An illustration of a typical trial is shown in Figure 4.5. Perturbations were randomly drawn from the set $\{-0.3, 0, 0.3\}$ units. The task proceeded in a block structure, where each block consisted of two repetitions of the three perturbations in random order, followed

by a null trial in which the cursor's final position was not displayed. Each of the two targets were allocated 10 blocks in random order, for 140 trials total. Mapping perturbations were disabled for both groups in the adaptation task, since these would potentially introduce additional variability in the feedback.

4.3.4 Analysis

4.3.4.1 Path Efficiency

Cursor trajectories from the familiarization task were analyzed to uncover potential differences between groups as well as the two targets of interest in the adaptation task. One informative measure of control capability is path efficiency, defined as the ratio of the cumulative distance traveled over the course of a trial to the straight line distance to the final cursor position. It encapsulates both directness of the cursor trajectory and the ability to hold the cursor position steady once it reaches the target position. To analyze path efficiency over the course of the practice task, we combined blocks (as they were presented) such that each block contained two repetitions of each target instead of one.

4.3.4.2 Adaptation Rate

The trial-by-trial adaptation behavior was viewed through the lens of a Kalman filter [WK10], which is a special case of Bayesian integration. The subject's estimate of the target position on trial k is $\hat{x}_{k|k-1}$, and this is assumed to be directly recorded as the cursor position at the end of the movement (before perturbation is applied). Once the perturbation is applied and the feedback is received, the subject updates the estimate by applying the Kalman filter update:

$$\hat{x}_{k|k} = \hat{x}_{k|k-1} + K_k y_k \quad (4.1)$$

where K_k is the Kalman gain and y_k is the innovation, which is in our case the experimentally applied perturbation (the feedback position minus the true cursor position). Rearranging (4.1) and making the simplifying assumption that the dynamic model is unity, we get a relationship between the change in true cursor position from one trial to the next and the perturbation:

$$\delta_{k,k-1} = K_k y_k \quad (4.2)$$

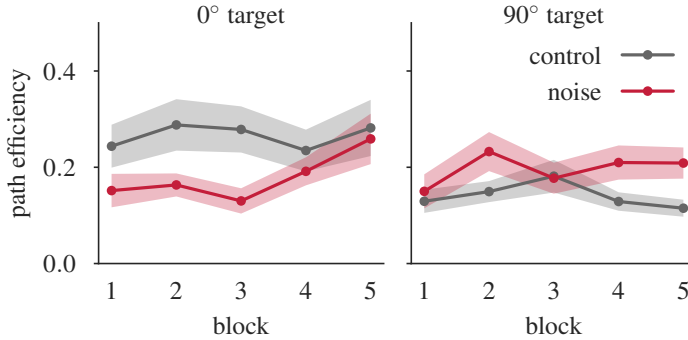


Figure 4.6: Path efficiency by block in the familiarization task. Each block consists of two repetitions of each target. Points represent subject averages and filled regions represent \pm one standard error of the mean.

The adaptation rate is then the coefficient of a linear regression fit to the true cursor position change versus the perturbation from the previous trial. Higher adaptation rate indicates a willingness to trust feedback over forward prediction. An adaptation rate was computed for each subject and each of the two targets (0° and 90°). A mixed effect analysis of variance (ANOVA) model was then used to test for differences between groups (random effects factor), target angle (fixed effects factor), and the interaction between the two. Significance was determined with $\alpha = 0.05$.

4.3.5 Results

4.3.5.1 Familiarization

Early in the experiment, we noticed that some subjects seemed to have more difficulty reaching and remaining inside the 90° target. This led to an analysis of the path efficiency during the familiarization task, which is shown in Figure 4.6. As expected from our observations, the control group's path efficiency for the 90° target was lower. Furthermore, the noise group's motion to the 0° target was affected by the vertical trial-by-trial mapping perturbations introduced, giving indirect evidence that the magnitude of the mapping noise was sufficient to drive a change in behavior. Movement to the correct vertical location for the 90° target with a changing mapping should involve only minor adjustments to the strength of muscle contraction, whereas correcting the vertical position out at the 0° target could require more complex manipulations. It appears from Figure 4.6 that this is the only condition in which learning occurred over the course of the familiarization

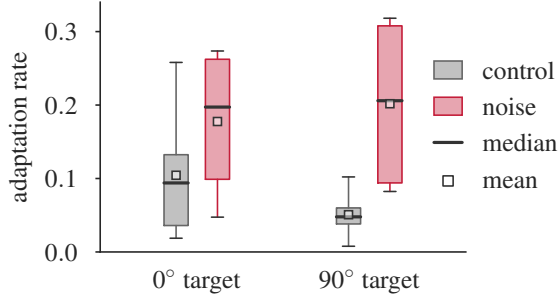


Figure 4.7: Adaptation rates for the two groups and two targets in the adaptation task. Each subject’s data for the given condition is averaged, then subject means are combined to form the boxes.

task.

4.3.5.2 Adaptation

Adaptation rates are shown in Figure 4.7. The mixed effect ANOVA showed that group was a significant factor ($P = 0.026$), whereas the target angle and the interaction between group and target angle were not found to be significant ($P = 0.626$ and $P = 0.214$, respectively). Surprisingly, adaptation rates in the noise group tended to be higher for both targets, rather than only the 0° target. It was also unexpected to find such low adaptation rates in the control group, as compared to adaptation rates found in similar myoelectric control experiments with low feedback uncertainty [JKHS14].

4.3.6 Conclusions

Our main finding is that trial-by-trial changes in a linear, proportional myoelectric control interface’s mapping during a familiarization phase led to increased adaptation rate, even though the mapping was fixed in the adaptation phase. We attribute this effect to the use of *mapping uncertainty* as opposed to adding random or signal-dependent noise to the cursor position during familiarization. Because the mapping itself changed from trial to trial, subjects were forced to produce different EMG activation profiles to achieve the same target. This caused the internal model of how motor commands influenced cursor position to be more uncertain and therefore less trustworthy than the feedback.

The secondary finding that the anisotropic (vertical only) mapping noise did not affect adaptation to the two target directions differently is somewhat surprising. In planar

reaching experiments, He et al. showed that adaptation rate is higher for more distant targets because they are associated with decreased proprioceptive precision, hence subjects are more uncertain of their feedforward prediction and rely more on the previous trial’s feedback [HLA⁺16]. In our case, perhaps the mapping uncertainty equalized control difficulty in both directions, whereas the control group tended to find the 0° target somewhat easier to reach and dwell inside. This doesn’t, however, explain the lack of difference in adaptation rate between the two targets for the control group.

One limitation of this study design is that we did not block the subject’s hand from sight. While the hand position or wrist angle does not necessarily correlate perfectly with cursor position, receiving this un-perturbed feedback could cause the adaptation rate to decrease, potentially explaining the low adaptation rates observed in the control group (or overall). Furthermore, the use of eight targets in the familiarization task likely reduced the effect of the mapping uncertainty overall. Another limitation is the small number of subjects (six per group). With relatively high variability between subjects in myoelectric control tasks, a larger sample would be appropriate for future work. Finally, a more thorough investigation of the mapping noise variance would help to more fully evaluate the Bayesian integration model.

While we have demonstrated the ability to modify adaptation behavior via a simple intervention potentially applicable to many myoelectric control schemes, the higher-level goal is to improve the ability of individuals with disabilities to interact with their environment, which becomes an issue of skill learning rather than adaptation. However, if mapping uncertainty is a mechanism through which exploratory behavior is encouraged, it may be possible to increase the robustness and reliability of myoelectric control through user training.

4.4 Experiment: Rotational and Randomized Mapping Noise

4.4.1 Introduction

This experiment was designed to more fully evaluate the effects of training with mapping noise on adaptation. Three different forms of variability were presented to different subjects during a practice task: random independent rotations of each vector in the linear EMG-to-cursor-position mapping, random rotation of the entire mapping, and random rotation of the target about the origin with no mapping variability. Following practice, subjects attempted to hit a target with no visual feedback during the movement and random visual perturbations. Feedback noise in the form of scattered cursors were also presented [JKHS14]. Finally, subjects performed a transfer task in which they attempted to hit targets with the arm and the cursor interface rotated 180°. This simulates a somewhat extreme form of the limb position effect [FSC⁺11], and we hypothesized that subjects practiced in hitting targets with a variable mapping would be able to perform better in the transfer task.

4.4.2 Experiment Design

In total, 30 subjects participated in this experiment. They were split into three different groups, where the difference between the groups was only in how variability was added during cursor-to-target practice. Four of the subjects were left-hand dominant. For these subjects, EMG sensors were applied to the left arm and the interface was mirrored.

Similarly to the previous study (Section 4.3), six Delsys Trigno wireless EMG sensors were placed around the forearm approximately one third of the way from the elbow down to the wrist. Subjects were seated in a chair with a customized arm rest that could be adjusted so that the subject could sit comfortably with the dominant forearm resting such that the hand could move freely in all directions. This time, a cover was placed over the arm to block the subject’s view of the hand.

The signals from the sensors were sampled at 2 kHz in windows of 400 samples with 300 samples of overlap (giving a 20 Hz update rate). The windows were preprocessed with

a fourth-order Butterworth bandpass filter (cutoff frequencies at 10 and 450 Hz). The root mean square of each channel was then computed and, in the case of the cursor control tasks, scaled to the range [0, 1] and mapped to a two-dimensional cursor position with a linear mapping computed through the procedure described next. Finally, an exponentially weighted moving average filter was applied to smooth cursor motions:

$$y[n] = \begin{cases} x[0], & n = 0 \\ \alpha x[n] + (1 - \alpha)y[n - 1], & n > 0 \end{cases} \quad (4.3)$$

where $x[n]$ is the input coordinate after mapping at time n and $y[n]$ is the output coordinate after smoothing. The smoothing factor α was set to 0.5.

4.4.2.1 Cursor Following

The subjects started with a cursor following task similarly to the previous study. Eight target locations located at the edges of the working interface (1 unit from the center in the normalized coordinate system) and equally spaced around a circle were presented in random order once per block. One block was used as practice. Next, the subjects were asked to supinate the arm so that the *back* of the forearm sat on the arm rest and they performed the cursor following task for two more blocks. Finally, four more blocks with the arm pronated (default position) were performed. Using the displayed cursor positions and the corresponding scaled RMS values during the four blocks of pronated cursor following, a linear mapping was fit using ordinary least squares. No intercept term was included, as in the previous study.

4.4.2.2 Pre-Test

After building a mapping, subjects were in control of the cursor for the remainder of the experiment and attempted to hit targets. In all cases, the targets were placed at 70% of the distance used in cursor following to help avoid fatigue. To establish a baseline performance level for each subject, a pre-test was performed before adding any variability. Four targets (0° , 90° , 180° , and 270°) were presented in random order 10 times each, and the subject was given as much time as needed to reach the target. In contrast to the previous experiment, subjects were *not* required to hold the cursor inside the target for a

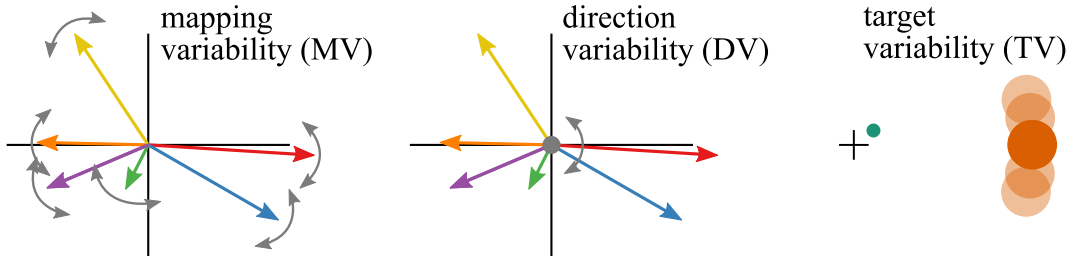


Figure 4.8: The three types of variability added, corresponding to the three different experimental groups. Mapping variability refers to sampling mapping vectors randomly from a symmetric 2D Gaussian. Direction variability refers to the entire mapping matrix being rotated randomly. Target variability refers to the target being rotated about the center of the interface randomly.

dwell period—simply touch the target with the center of the cursor was sufficient to end the trial.

4.4.2.3 Practice

After the pre-test task, the main practice task began. Only the target at 0° (directly to the right for right-handed subjects) was shown. Here, the linear mapping was modified on every trial, like in the previous study. This task was the only one with any differences between the groups. The three different kinds of variability are shown in Figure 4.8. In the mapping variability (MV) group, each vector of the mapping matrix was *independently* rotated by a random value sampled from a Gaussian distribution with zero mean and 20° standard deviation. In the direction variability (DV) group, the entire mapping matrix was randomly rotated by an amount sampled from a Gaussian with 20° standard deviation. In the target variability (TV) group, the target was rotated about the center of the interface by an amount sampled from the same distribution as in the direction variability group. This means that the DV and TV groups are *actually doing the same task*—on a given trial, they may have to change what direction they move in order to reach the target—but the feedback is different. For the direction variability group, the feedback during practice does not match their anticipated movement, whereas the target variability group knew at the beginning of each trial whether or not they needed to move up or down with respect to the previous trial. 8 blocks of 20 trials each were performed, giving the subjects substantial time to internalize the nature of the trial-by-trial variability.

4.4.2.4 Adaptation

In the adaptation task, only the 0° target was shown, and the subject was instructed to attempt to hit the target. The cursor was never displayed until the end of the trial. The invisible cursor was required to remain in a small area around the origin, and a fixation cross located at the origin changed color to indicate whether or not the subject was relaxed sufficiently to initiate movement. As soon as the cursor left a circular area centered at the origin and encompassing the target center (70% of the distance from the origin to the screen edge), the cursor position was perturbed by an angle randomly chosen from the set $\{-20^\circ, 0, 20^\circ\}$ and displayed. On half of the trials, the cursor was shown as a single circle, as in the previous experiment. On the other half of the trials, 5 circles were displayed along the radius of the underlying cursor position on screen with angles randomly selected from a Gaussian distribution centered at the perturbed angle with standard deviation 20° . Scattering the displayed cursor position in this way is a form of feedback uncertainty and is similar to the feedback uncertainty introduced in previous studies [WK10, JKHS14]. Subjects were told to locate the center of this “cloud” of cursors to estimate the true cursor position, and they were not told that perturbations were occurring. Each combination of perturbation and feedback uncertainty level (6 possible combinations) were presented 5 times per block in random order over 4 blocks for a total of 120 adaptation trials.

4.4.2.5 Post-Test and Transfer Task

Immediately following the adaptation task, the pre-test was re-run (10 repetitions of 4 targets) with no variability added, and this is referred to as the post-test. Finally, the post-test was re-run with the arm supinated 180° , and this is referred to as the transfer task. In the transfer task, the mapping built from the *prone* cursor following task was used, just as with the other tasks in the experiment, but the cursor interface was rotated 180° . This means that if the subject flexed the wrist in the supine position (palm facing upward), the hand moved upward and the cursor also theoretically moved upward. That is, subjects were *not* required to learn a 180° transformation of the interface.

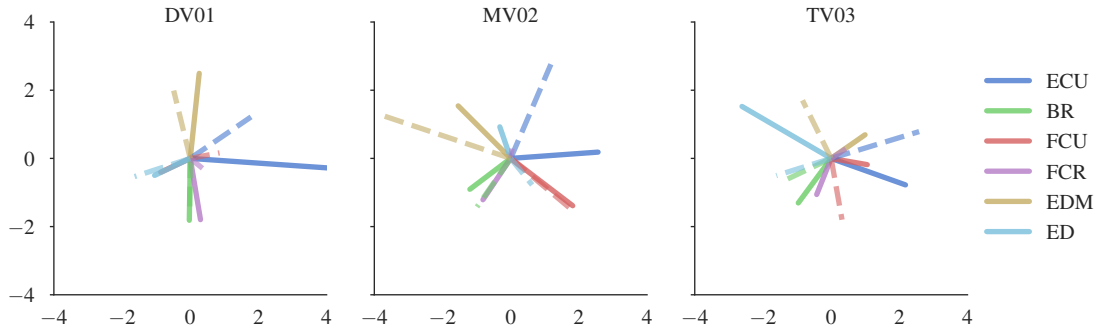


Figure 4.9: Representative mappings generated by subjects. The solid lines are the mapping vectors in the prone (default) position, and the dashed lines are the corresponding vectors fit to data generated while the subject had the arm in the supine position. Each color is a different EMG channel named after the primary muscle being recorded (extensor carpi ulnaris, brachioradialis, flexor carpi ulnaris, flexor carpi radialis, extensor digitorum minimi, extensor digitorum).

4.4.3 Results

4.4.3.1 Generated Mappings

The mappings generated during the cursor following task for a few representative subjects are shown in Figure 4.9. The solid lines indicate the mapping vectors generated with the forearm prone (“belly” of the forearm resting on the arm rest) and the dashed lines show the corresponding mapping vectors (matched by EMG channel) with the arm in the supine position. Note that in the supine cursor following task, the target directions were rotated 180° so that the “up” target was 270°. Mappings appear to be fairly similar across subjects, implying that electrode placement was consistent and that subjects tended to use similar muscle activation strategies to one another in order to move the hand in different directions. The effects of supinating the arm had a dramatic effect for some mapping vectors and not others. When the forearm rotates 180°, the radius and ulna (the two bones of the forearm) twist around each other and the musculature is displaced relative to the skin surface as a result. Differences like this underlie the limb position effect, and it is clear from the large changes in mappings that changing limb position would adversely affect performance in classification-based myoelectric controllers.

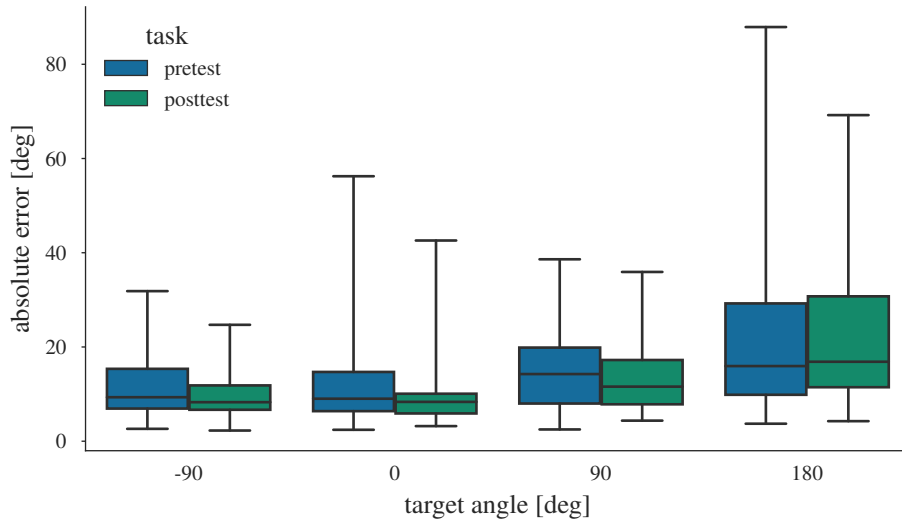


Figure 4.10: Absolute errors across target directions in the pre and post test tasks, averaged across subjects in all groups. Boxes extend to the upper and lower quartiles, while the whiskers show the full extent of the data.

4.4.3.2 Differences Between Target Directions

In the previous study, we looked at path efficiency as a measure of cursor-to-target performance. In this experiment, however, subjects did not have to dwell inside the target, so instead we can use the absolute angular error between the target angle and the cursor endpoint. The endpoint errors across all groups for each of the target directions in the pre and post test tasks are shown in Figure 4.10. Two results are clear from this analysis. First, similar to what was observed in the previous study, movement direction influenced task performance. Notably, the 180° target (to the left for right-handed subjects—radial deviation) was particularly difficult for some subjects to move toward accurately, and this varied greatly by subject. Observations made during the experiment indicated that several subjects had difficulty moving the cursor far enough in that direction to end the trial, so they resorted to ballistic movements to generate a large EMG signal, resulting in many trials with large errors. Second, there is essentially no change in performance after the practice and adaptation trials, even for the 0° target, which subjects had extensive practice with.

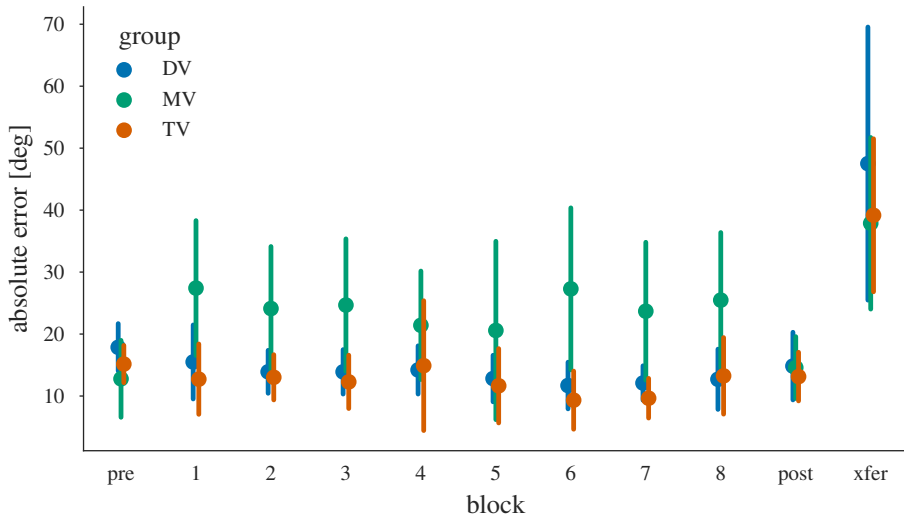


Figure 4.11: Absolute endpoint errors made averaged across subjects in each group in the pre-test, all practice blocks, post-test, and transfer tasks. Error bars indicate standard deviation across subjects.

4.4.3.3 Errors During Practice

The absolute errors in all tasks but the adaptation task are shown in Figure 4.11. As expected, there was little difference between groups in the pre-test, since all conditions were the same for all subjects in this task. In the practice blocks, however, there is a clear difference between the mapping variability group and the other two. Since every one of the 6 mapping vectors was rotated independently on each trial, the task became extremely difficult. Over the 8 blocks of practice, there was inconsistent change in endpoint error and overall little improvement from block 1 to block 8 for all three groups. Notably, post-test performance was essentially identical to pre-test performance. This is likely because the practice involved moving repeatedly to only the 0° target, so subjects were not practicing acquiring the other three targets. Performance in the transfer task (arm supinated and interface rotated to match) was poor overall and varied greatly across subjects, so group averages may not be representative of a much larger subject sample.

In addition to endpoint error, which is a measure of target acquisition performance, we can look at the angle between the cursor's position and the target at the midpoint of the trial as it relates to the endpoint error. Comparing these two errors gives a measure of

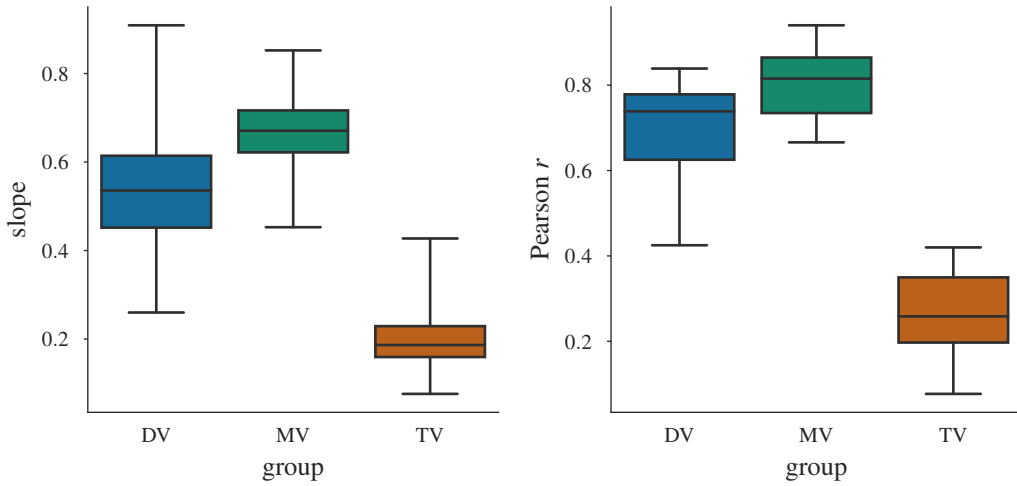


Figure 4.12: Slope and Pearson correlation coefficient of the linear regression between endpoint errors and midpoint errors in the practice task.

within-trial adaptation. Shown in Figure 4.12 are the slope and Pearson correlation coefficients from linear regressions between endpoint and midpoint errors for subjects in each group. The combination of these two plots shows that the endpoint errors are relatively uncorrelated with midpoint errors for only the target variability group. The direction variability group, however, showed high correlation between midpoint and endpoint error with an average slope of 0.53. This implies that positive midpoint errors tended to produce *smaller* positive endpoint errors, indicating adaptation to errors observed after initiating movement. For the mapping variability group, the midpoint and endpoint errors were highly correlated with a higher slope, indicating that they also adapted to some extent, but less than the DV group. One-way ANOVA on both slope and Pearson r showed significant differences ($p \ll 0.001$ for both). Post-hoc pairwise t -tests with Bonferroni correction indicated that both DV and MV had higher slope and Pearson r than TV ($p \ll 0.001$ for both), but differences between DV and MV were not found to be significant.

4.4.3.4 Trial-By-Trial Adaptation

Trial-by-trial adaptation rate, as defined in the previous study, is shown in Figure 4.13. For reference, the adaptation rate here is the slope of a linear regression between the

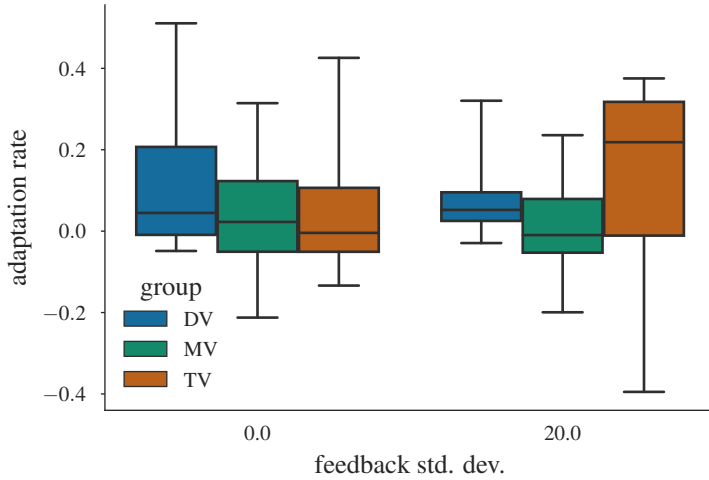


Figure 4.13: Adaptation rates for each group, split into trials with and without feedback uncertainty (scattered cursors). This adaptation rate is defined by the change in endpoint error as a function of previous perturbation.

change in endpoint from trial $k - 1$ to trial k versus the perturbation on trial k . Clearly, this definition of adaptation rate is suspect since subjects had both positive and negative adaptation rates, and none of the experimental manipulations had much of an effect. A negative overall adaptation rate would imply that the subject responded to perturbations by moving in the *same direction* as the perturbation. There is also an issue with this adaptation rate definition intuitively: it seems more likely that subjects would base their estimate of the true cursor position on the error they observed on the previous trial rather than the perturbation.

An alternative adaptation rate definition could be posed as the slope of the change in endpoint from trial $k - 1$ to trial k versus the previously displayed error. Let this form of adaptation rate be called the *observation adaptation rate*. The result of using this definition is shown in Figure 4.14. Most notably, there are no longer negative adaptation rates. Interestingly, the target variability group showed higher observation adaptation rate than the other two groups. Subjects in the direction variability and mapping variability groups may have “given up” on adaptation, albeit for slightly different reasons. After practicing extensively with the movement direction changing every trial, the DV group could have treated the perturbations as being equivalent to the practice task. Without

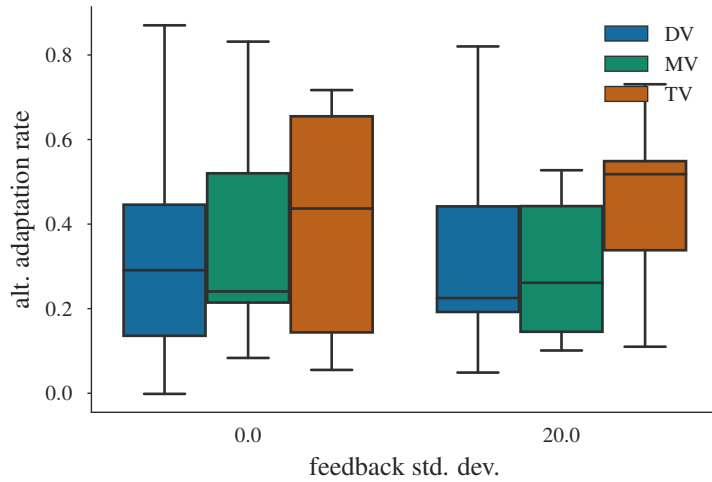


Figure 4.14: Observation adaptation rate. Here, the adaptation rate is the change in endpoint error as a function of the previously observed error.

feedback during the movement, they would have no way of knowing whether the cursor would go too low or too high on a given trial, so they took the optimal approach of choosing the average in order to minimize errors, leading to nearly zero adaptation. In the MV group, control was extremely difficult on most trials unless the random independent rotations of each mapping vector happened to be small. With such variability of control, attempting to adapt to errors may have been viewed as pointless.

4.4.4 Conclusions

One of the major flaws of this study was that the mapping variability was likely too high to bring about the subtle changes in perception necessary to affect adaptive behavior. Future studies should more explicitly examine how to add an appropriate amount of variability such that the variability actually affects cursor motion but doesn't make the task too difficult. One idea for implementing this would be to gather baseline variability for an individual subject and choose a mapping variability parameter that increases this to some desired level.

Perhaps the most important difference between this experiment and the previous one is that subjects were not required to dwell inside the target during practice. The reasoning behind removing this requirement was that it would allow for analysis in terms of endpoint

errors. The consequence, however, was that many subjects seemed to lose motivation to actually acquire the target. The main evidence explanation for this is Figure 4.12, which shows that subjects in the target variability group decreased their endpoint errors with respect to their midpoint errors overall, whereas the direction variability group did not. Since these two groups performed fundamentally the same task (similar inputs were required to reach the target) except for the feedback mismatch for the direction variability group, it could be that the visual feedback of the cursor on the screen was overridden by the subject’s proprioceptive sense of hand position. For the MV and DV groups, the mismatch between what was shown on screen during practice and what was felt in the wrist could have caused subjects in these groups to disregard the visual feedback displayed and trust the proprioceptive sense more. Requiring the subject to dwell inside the target would help reinforce the idea that the EMG signals are what drive the cursor, not necessarily hand position. It would also be interesting in the future to run the study with amputee subjects or able-bodied subjects with the wrist in a rigid brace to eliminate the potential for this override of the provided visual feedback.

4.5 Outcomes

In running these two experiments, I have become skeptical of the Kalman filter model as it pertains to this exact experiment design. Alternatively, perhaps the Kalman filter model is a good model of adaptive behavior, but this experiment design is flawed in the attempt to expose this behavior. Most notably, the perturbations introduced are not explicitly modeled. Sudden shifts of observations which are not generated by the dynamics of the process would be considered measurement (or feedback) noise, and this is distinct from the flavor of feedback noise introduced in these experiments. In the future, it would be interesting to treat the perturbations as the feedback uncertainty and introduce Gaussian distributed perturbations, more closely matching the conditions under which a Kalman filter model is appropriate.

In addition, a crucial assumption made in this experiment design is that the true cursor endpoint on trial k is equal and opposite to their estimate of the true cursor position from

the previous trial. However, two-dimensional cursor control is rather noisy compared to intact arm reaching and we have shown evidence of biases toward certain areas of the screen. Future work should aim to obtain more reliable measures of a subject's estimates in order to investigate the true effects of feedback and mapping noise on estimation behavior.

Overall, while these experiments did not show an improvement in performance in the simulated limb position effect transfer task, I believe there is still promise in the idea of encouraging subject exploration of the EMG activation space in order to improve aspects of control, whether it is performance in target acquisition or better capability of adapting to novel scenarios.

CONCLUSION

Muscles are the actuators of the body and they produce electrical signals as a byproduct of force generation. In many cases, these signals allow us to peek inside the body to estimate the intentions of a user and map these intentions to a device to replicate or enhance normal functions. Between the human and the machine, there is the myoelectric interface. In the preceding pages, I have described a number of methods and experiments using those methods aimed at improving the techniques used in myoelectric control. The single biggest realization I have made in my time executing the work presented here is that our ability to learn and adapt is simply unparalleled by machine systems, and this is too often ignored in the effort to create “intuitive” systems that take little time to learn and use. There is also a driving goal to minimize the time the user has to spend generating training data for the machine to learn what natural movement patterns look like. Perhaps an approach to satisfying these goals simultaneously is a base system that is already capable of mapping muscle signals to device commands, but is also flexible enough to allow a user to grow into. In my estimation, the future of myoelectric control will involve an increased consideration for the human as a critical component of the overall system. I hope that advances in the field of motor control and motor learning can be translated to efforts in myoelectric control so that these systems can help as many people as possible.

REFERENCES

- [AGJ⁺14] S. Amsüss, P. M. Goebel, N. Jiang, B. Graimann, L. Paredes, and D. Farina. Self-Correcting Pattern Recognition System of Surface EMG Signals for Upper Limb Prosthesis Control. *IEEE Trans. Biomed. Eng.*, 61(4):1167–1176, May 2014.
- [AIA14] Chris Wilson Antuvan, Mark Ison, and Panagiotis Artermiadis. Embedded Human Control of Robots Using Myoelectric Interfaces. *IEEE Trans. Neural Syst. Rehabil. Eng.*, 22(4):820–827, 2014.
- [BC07] Elaine Biddiss and Tom Chau. Upper-Limb Prosthetics: Critical Factors in Device Abandonment. *Am. J. Phys. Med. Rehabil.*, 86(12):977–987, 2007.
- [BEB08] Johannes Burge, Marc O. Ernst, and Martin S. Banks. The Statistical Determinants of Adaptation Rate in Human Reaching. *J. Vis.*, 8(4):1–19, 2008.
- [BK12] Nathan E. Bunderson and Todd A. Kuiken. Quantification of Feature Space Changes With Experience During Electromyogram Pattern Recognition. *IEEE Transactions on Neural Systems and Rehabilitation Engineering*, 20(3):239–246, 2012.
- [Bur16] Thomas J. Burkholder. Model-Based Approaches to Understanding Musculoskeletal Filtering of Neural Signals. In Boris I. Prilutsky and Donald H. Edwards, editors, *Neuromechanical Model. Posture Locomot.*, pages 103–120. Springer New York, New York, NY, 2016.
- [CAW⁺14] Claudio Castellini, Panagiotis Artermiadis, Michael Wninger, Arash Ajoudani, Merkur Alimusaj, Antonio Bicchi, Barbara Caputo, William Craelius, Strahinja Dosen, Kevin Englehart, Dario Farina, Arjan Gijsberts, Sasha B. Godfrey, Levi Hargrove, Mark Ison, Todd Kuiken, Marko Marković, Patrick M. Pilarski, Rüdiger Rupp, and Erik Scheme. Proceedings of the First Workshop on Peripheral Machine Interfaces: Going Beyond Traditional Surface Electromyography. *Front. Neurorobot.*, 8(August), 2014.
- [CPL⁺07] Maria Chiara Carrozza, Alessandro Persichetti, Cecilia Laschi, Fabrizio Vecchi, Roberto Lazzarini, Pierpaolo Vacalebri, and Paolo Dario. A Wearable Biomechatronic Interface for Controlling Robots with Voluntary Foot Movements. *IEEE/ASME Trans. Mechatronics*, 12(1):1–11, 2007.
- [DAW⁺06] Carlo J. De Luca, Alexander Adam, Robert Wotiz, Donald L. Gilmore, and S. Hamid Nawab. Decomposition of Surface EMG Signals. *J. Neurophysiol.*, 96(3):1646–1657, 2006.
- [DQK93] R. B Dunn, T. F. Quatieri, and J. F. Kaiser. Detection of Transient Signals Using the Energy Operator. In *Acoustics, Speech, and Signal Processing*,

1993. *ICASSP-93., 1993 IEEE International Conference on*, pages 145–148, 1993.
- [EAM12] C. Escolano, J. M. Antelis, and J. Minguez. A Telepresence Mobile Robot Controlled with a Noninvasive Brain-Computer Interface. *IEEE Transactions on Systems, Man, and Cybernetics – Part B: Cybernetics*, 42(3):793–804, jun 2012.
- [ECK⁺15] Susannah M. Engdahl, Breanne P. Christie, Brian Kelly, Alicia Davis, Cynthia A. Chestek, and Deanna H. Gates. Surveying the Interest of Individuals with Upper Limb Loss in Novel Prosthetic Control Techniques. *Journal of Neuroengineering and Rehabilitation*, 12(53):1–11, 2015.
- [EH03] Kevin Englehart and Bernard Hudgins. A Robust, Real-Time Control Scheme for Multifunction Myoelectric Control. *IEEE Trans. Biomed. Eng.*, 50(7):848–854, 2003.
- [FC09] Carlo Frigo and Paolo Crenna. Multichannel SEMG in Clinical Gait Analysis: A Review and State-of-the-Art. *Clin. Biomech.*, 24(3):236–245, 2009.
- [FSC⁺11] Anders Fougnier, Erik Scheme, Adrian D. C. Chan, Kevin Englehart, and Øyvind Stavdahl. Resolving the Limb Position Effect in Myoelectric Pattern Recognition. *IEEE Trans. Neural Syst. Rehabil. Eng.*, 19(6):644–651, 2011.
- [FSW08] A. Aldo Faisal, Luc P. J. Selen, and Daniel M. Wolpert. Noise in the Nervous System. *Nature Reviews Neuroscience*, 9(4):292–303, 2008.
- [GLS13] Michael Goldfarb, Brian E. Lawson, and Amanda H. Shultz. Realizing the Promise of Robotic Leg Prostheses. *Sci. Transl. Med.*, 5(210):210ps15, 2013.
- [Gra74] Daniel Graupe. Control of Upper-Limb Prostheses in Several Degrees of Freedom. *Bull. Prosthet. Res.*, pages 226–236, 1974.
- [GZL12] Yanjuan Geng, Ping Zhou, and Guanglin Li. Toward Attenuating the Impact of Arm Positions on Electromyography Pattern-Recognition Based Motion Classification in Transradial Amputees. *J. Neuroeng. Rehabil.*, 9(1):1–11, 2012.
- [HB11] Peggy A. Houglum and Dolores B. Bertoti. *Brunnstrom’s Clinical Kinesiology*. F.A. Davis, Philadelphia, PA, 6th edition, 2011.
- [HDH⁺15] Janne Hahne, Sven Dähne, Han-Jeong Hwang, Klaus-Robert Müller, and Lucas Parra. Concurrent Adaptation of Human and Machine Improves Simultaneous and Proportional Myoelectric Control. *IEEE Trans. Neural Syst. Rehabil. Eng.*, 23(4):618–627, 2015.

- [HEH08] Levi Hargrove, Kevin Englehart, and Bernard Hudgins. A Training Strategy to Reduce Classification Degradation Due to Electrode Displacements in Pattern Recognition Based Myoelectric Control. *Biomed. Signal Process. Control*, 3(2):175–180, apr 2008.
- [Hel65] Richard Held. Plasticity in sensory-motor systems. *Scientific American*, 213(5):84–97, 1965.
- [HFM⁺99] Hermie J. Hermens, Bart Freriks, Roberto Merletti, Dick Stegeman, Joleen Blok, Günter Rau, Cathy Disselhorst-Klug, and Göran Hägg. European Recommendations for Surface Electromyography. *Roessingh Res. Dev. Enschede*, 1999.
- [HLA⁺16] Kang He, You Liang, Farnaz Abdollahi, Moria Fisher Bittmann, Konrad Kording, and Kunlin Wei. The Statistical Determinants of the Speed of Motor Learning. *PLOS Comput. Biol.*, 12(9):1–20, 2016.
- [HN03] Xiaofei He and Partha Niyogi. Locality Preserving Projections. In *NIPS*, volume 16, 2003.
- [HOM⁺14] Jacqueline S. Hebert, Jaret L. Olson, Michael J. Morhart, Michael R. Dawson, Paul D. Marasco, Todd A. Kuiken, and K. Ming Chan. Novel Targeted Sensory Reinnervation Technique to Restore Functional Hand Sensation After Transhumeral Amputation. *IEEE Trans. Neural Syst. Rehabil. Eng.*, 22(4):765–773, 2014.
- [HPS93] Bernard Hudgins, Philip Parker, and Robert N. Scott. A New Strategy for Multifunction Myoelectric Control. *IEEE Transactions on Biomedical Engineering*, 40(1):82–94, 1993.
- [HSEH10] Levi J. Hargrove, Erik J. Scheme, Kevin B. Englehart, and Bernard S. Hudgins. Multiple Binary Classifications via Linear Discriminant Analysis for Improved Controllability of a Powered Prosthesis. *IEEE Trans. Neural Syst. Rehabil. Eng.*, 18(1):49–57, February 2010.
- [HSL⁺13] Levi J. Hargrove, Ann M. Simon, Robert Lipschutz, Suzanne B. Finucane, and Todd A. Kuiken. Non-Weight-Bearing Neural Control of a Powered Transfemoral Prosthesis. *J. Neuroeng. Rehabil.*, 10(62):1–11, 2013.
- [HSY⁺13] Levi J. Hargrove, Ann M. Simon, Aaron J. Young, Robert D. Lipschutz, Suzanne B. Finucane, Douglas G. Smith, and Todd A. Kuiken. Robotic Leg Control with EMG Decoding in an Amputee with Nerve Transfers. *The New England Journal of Medicine*, 369(13):1237–1242, 2013.
- [HVG11] Kevin H. Ha, Huseyin Atakan Varol, and Michael Goldfarb. Volitional Control of a Prosthetic Knee Using Surface Electromyography. *IEEE Trans. Biomed. Eng.*, 58(1):144–151, 2011.

- [IA15] Mark Ison and Panagiotis Aramendis. Proportional Myoelectric Control of Robots: Muscle Synergy Development Drives Performance Enhancement, Retainment, and Generalization. *IEEE Trans. Robot.*, 31(2):259–268, 2015.
- [JBB⁺11] Matthew S. Johannes, John D. Bigelow, James M. Burck, Stuart D. Harshbarger, Matthew V. Kozlowski, and Thomas Van Doren. An Overview of the Developmental Process for the Modular Prosthetic Limb. *Johns Hopkins APL Tech. Dig.*, 30(3):207–216, 2011.
- [JKHS14] Reva E. Johnson, Konrad P. Kording, Levi J. Hargrove, and Jonathon W. Sensinger. Does EMG Control Lead to Distinct Motor Adaptation? *Front. Neurosci.*, 8(302):1–6, 2014.
- [KLL⁺09] Todd A. Kuiken, Guanglin Li, Blair A. Lock, Robert D. Lipschutz, Laura A. Miller, Kathy A. Stubblefield, and Kevin B. Englehart. Targeted Muscle Reinnervation for Real-time Myoelectric Control of Multifunction Artificial Arms. *Journal of the American Medical Association*, 301(6):619–628, 2009.
- [KM11] John W. Krakauer and Pietro Mazzoni. Human Sensorimotor Learning: Adaptation, Skill, and Beyond. *Curr. Opin. Neurobiol.*, 21(4):636–644, 2011.
- [KML⁺07] Todd A. Kuiken, Laura A. Miller, Robert D. Lipschutz, Blair A. Lock, Kathy Stubblefield, Paul D. Marasco, Ping Zhou, and Gregory A. Dumanian. Targeted Reinnervation for Enhanced Prosthetic Arm Function in a Woman with a Proximal Amputation: A Case Study. *Lancet*, 369(9559):371–380, 2007.
- [KW04] Konrad P. Kording and Daniel M. Wolpert. Bayesian Integration in Sensorimotor Learning. *Nature*, 427(6971):244–247, 2004.
- [LGB⁺99] M. Lotze, W. Grotto, N. Birbaumer, M. Erb, E. Huse, and H. Flor. Does Use of a Myoelectric Prosthesis Prevent Cortical Reorganization and Phantom Limb Pain? *Nat. Neurosci.*, 2(6):501–502, 1999.
- [Liu15] Jie Liu. Adaptive Myoelectric Pattern Recognition Toward Improved Multi-functional Prosthesis Control. *Med. Eng. Phys.*, in press:1–7, 2015.
- [LJ13] Kenneth R. Lyons and Sanjay S. Joshi. Paralyzed Subject Controls Telepresence Mobile Robot Using Novel sEMG Brain-Computer Interface: Case Study. In *IEEE Int. Conf. Rehabil. Robot. (ICORR)*, Seattle, WA, 2013.
- [LJ15] Kenneth R. Lyons and Sanjay S. Joshi. A Case Study on Classification of Foot Gestures via Surface Electromyography. In *Annu. Conf. Rehabil. Eng. Assist. Technol. Soc. Am.*, Denver, CO, 2015.
- [LJ16] Kenneth R. Lyons and Sanjay S. Joshi. Real-time evaluation of a myoelectric control method for high-level upper limb amputees based on homologous leg movements. In *Engineering in Medicine and Biology Society (EMBC), 2016 IEEE 38th Annual International Conference of the*, pages 6365–6368, 2016.

- [LJ18a] Kenneth R. Lyons and Sanjay S. Joshi. In *Engineering in Medicine and Biology Society (EMBC), 2018 IEEE 40th Annual International Conference of the*, pages 5178–5181, Honolulu, HI, 2018.
- [LJ18b] Kenneth R. Lyons and Sanjay S. Joshi. Upper Limb Prosthesis Control for High-Level Amputees via Myoelectric Recognition of Leg Gestures. *IEEE Transactions on Neural Systems and Rehabilitation Engineering*, 26(5):1056–1066, 2018.
- [Luz00] Christopher C. Luzzio. Controlling an Artificial Arm with Foot Movements. *Neurorehabil. Neural Repair*, 14(3):207–212, 2000.
- [MRMG04] J. del R. Millán, F. Renkens, J. Mouriño, and W. Gerstner. Noninvasive Brain-Actuated Control of a Mobile Robot by Human EEG. *IEEE Transactions on Biomedical Engineering*, 51(6):1026–1033, jun 2004.
- [MWC00] Nancy H. McNevin, Gabriele Wulf, and Christine Carlson. Effects of Attentional Focus, Self-Control, and Dyad Training on Motor Learning : Implications for Physical Rehabilitation. *Phys. Ther.*, 80(4):373–385, 2000.
- [NR15] Domen Novak and Robert Riener. A Survey of Sensor Fusion Methods in Wearable Robotics. *Rob. Auton. Syst.*, 73:155–170, 2015.
- [OCBH13] Max Ortiz-Catalan, Rickard Brånemark, and Bo Håkansson. BioPatRec: A Modular Research Platform for the Control of Artificial Limbs Based on Pattern Recognition Algorithms. *Source Code Biol. Med.*, 8(11):1–18, 2013.
- [OCHB14] Max Ortiz-Catalan, Bo Håkansson, and Rickard Brånemark. Real-Time and Simultaneous Control of Artificial Limbs Based on Pattern Recognition Algorithms. *IEEE Trans. Neural Syst. Rehabil. Eng.*, 22(4):756–764, 2014.
- [OP99] Greg A. O’Beirne and Robert B. Patuzzi. Basic Properties of the Sound-Evoked Post-Auricular Muscle Response (PAMR). *Hearing Research*, 138:115–132, 1999.
- [PMWJ10] C. Perez-Maldonado, A. S. Wexler, and S. S. Joshi. Two-Dimensional Cursor-to-Target Control from Single Muscle Site sEMG Signals. *IEEE Transactions on Neural Systems and Rehabilitation Engineering*, 18(2):203–209, apr 2010.
- [PQC⁺13] Angkoon Phinyomark, Franck Quaine, Sylvie Charbonnier, Christine Serviere, Franck Tarpin-Bernard, and Yann Laurillau. EMG Feature Evaluation for Improving Myoelectric Pattern Recognition Robustness. *Expert Systems with Applications*, 40(12):4832–4840, 2013.
- [RBJ08] Saritha M. Radhakrishnan, Stuart N. Baker, and Andrew Jackson. Learning a Novel Myoelectric-Controlled Interface Task. *J. Neurophysiol.*, 100(4):2397–2408, 2008.

- [RCP⁺14] Stanisa Raspopovic, Marco Capogrosso, Francesco Maria Petrini, Marco Bonizzato, Jacopo Rigosa, Giovanni Di Pino, Jacopo Carpaneto, Marco Controzzi, Timm Boretius, Eduardo Fernandez, Giuseppe Granata, Calogero Maria Oddo, Luca Citi, Anna Lisa Ciancio, Christian Cipriani, Maria Chiara Carrozza Carrozza, Winnie Jensen, Eugenio Guglielmelli, Thomas Stieglitz, Paolo Maria Rossini, and Silvestro Micera. Restoring Natural Sensory Feedback in Real-Time Bidirectional Hand Prostheses. *Sci. Transl. Med.*, 6(222):222ra19, 2014.
- [RKEF14] Linda Resnik, Shana Lieberman Klinger, Katherine Etter, and Christopher Fantini. Controlling a Multi-Degree of Freedom Upper Limb Prosthesis Using Foot Controls: User Experience. *Disabil. Rehabil. Assist. Technol.*, 9(4):318–29, 2014.
- [RM00] Joshua S. Richman and J. Randall Moorman. Physiological Time-Series Analysis using Approximate Entropy and Sample Entropy. *American Journal of Physiology. Heart and Circulatory Physiology*, 278(6):H2039–H2049, jun 2000.
- [RMC04] A. Rainoldi, G. Melchiorri, and I. Caruso. A Method for Positioning Electrodes During Surface EMG Recordings in Lower Limb Muscles. *Journal of Neuroscience Methods*, 134(1):37–43, 2004.
- [RRFA14] Aidan D. Roche, Hubertus Rehbaum, Dario Farina, and Oskar C. Aszmann. Prosthetic Myoelectric Control Strategies: A Clinical Perspective. *Current Surgery Reports*, 2(3):1–11, jan 2014.
- [RSF13] Eric Rohmer, Surya P. N. Singh, and Marc Freese. V-REP: A Versatile and Scalable Robot Simulation Framework. In *2013 IEEE/RSJ Int. Conf. Intell. Robot. Syst.*, pages 1321–1326, 2013.
- [SC14] Krishna V. Shenoy and Jose M. Carmena. Combining Decoder Design and Neural Adaptation in Brain-Machine Interfaces. *Neuron*, 84(4):665–680, 2014.
- [SE11] Erik Scheme and Kevin Englehart. Electromyogram Pattern Recognition for Control of Powered Upper-Limb Prostheses: State of the Art and Challenges for Clinical Use. *J. Rehabil. Res. Dev.*, 48(6):643–660, 2011.
- [SE13] Erik Scheme and Kevin Englehart. Training Strategies for Mitigating the Effect of Proportional Control on Classification in Pattern Recognition Based Myoelectric Control. *J. Prosthetics Orthot.*, 25(2):76–83, 2013.
- [SHLK09] Ann M. Simon, Levi J. Hargrove, Blair A. Lock, and Todd A. Kuiken. A Strategy for Minimizing the Effect of Misclassifications During Real Time Pattern Recognition Myoelectric Control. In *Proc. IEEE Eng. Med. Biol. Soc. Conf. (EMBC)*, pages 1327–1330, Minneapolis, MN, 2009.

- [SHLK11a] Ann M. Simon, Levi J. Hargrove, Blair A. Lock, and Todd A. Kuiken. A Decision-Based Velocity Ramp for Minimizing the Effect of Misclassifications During Real-Time Pattern Recognition Control. *IEEE Trans. Biomed. Eng.*, 58(8):2360–2368, 2011.
- [SHLK11b] Ann M. Simon, Levi J. Hargrove, Blair A. Lock, and Todd A. Kuiken. Target Achievement Control Test: Evaluating Real-Time Myoelectric Pattern Recognition Control of a Multifunctional Upper-Limb Prosthesis. *J. Rehabil. Res. Dev.*, 48(6):619–627, 2011.
- [SHLK11c] Lauren H. Smith, Levi J. Hargrove, Blair A. Lock, and Todd A. Kuiken. Determining the Optimal Window Length for Pattern Recognition-Based Myoelectric Control: Balancing the Competing Effects of Classification Error and Controller Delay. *IEEE Trans. Neural Syst. Rehabil. Eng.*, 19(2):186–192, 2011.
- [SLK09] Jonathon W. Sensinger, Blair A. Lock, and Todd A. Kuiken. Adaptive Pattern Recognition of Myoelectric Signals: Exploration of Conceptual Framework and Practical Algorithms. *IEEE Transactions on Neural Systems and Rehabilitation Engineering*, 17(3):270–278, 2009.
- [SRS⁺10] S. Solnik, P. Rider, K. Steinweg, P. DeVita, and T. Hortobágyi. Teager-Kaiser Energy Operator Signal Conditioning Improves EMG Onset Detection. *European Journal of Applied Physiology*, 110(3):489–498, 2010.
- [SS91] Harold H. Sears and Julie Shaperman. Proportional Myoelectric Hand Control: An Evaluation. *Am. J. Phys. Med. Rehabil.*, 70(1):20–28, 1991.
- [SSK10] Reza Shadmehr, Maurice A. Smith, and John W. Krakauer. Error Correction, Sensory Prediction, and Adaptation in Motor Control. *Annu. Rev. Neurosci.*, 2010.
- [SSS17] Ahmed W. Shehata, Erik J. Scheme, and Jonathon W. Sensinger. The Effect of Myoelectric Prostheses Control Strategies and Feedback Level on Adaptation Rate for a Target Acquisition Task. In *2017 Int. Conf. Rehabil. Robot.*, pages 200–204, 2017.
- [TKMI17] Elias B. Thorp, Konrad P. Kording, and Ferdinando A. Mussa-Ivaldi. Using Noise to Shape Motor Learning. *J. Neurophysiol.*, 117(2):728–737, 2017.
- [tmr] Targeted Muscle Reinnervation.
- [TYS⁺14] Dennis C. Tkach, Aaron J. Young, Lauren H. Smith, Elliott J. Rouse, and Levi J. Hargrove. Real-Time and Offline Performance of Pattern Recognition Myoelectric Control Using a Generic Electrode Grid With Targeted Muscle Reinnervation Patients. *IEEE Trans. Neural Syst. Rehabil. Eng.*, 22(4):727–734, 2014.

- [VJ11] S. Vernon and S. S. Joshi. Brain-Muscle-Computer Interface: Mobile-Phone Prototype Development and Testing. *IEEE Transactions on Information Technology in Biomedicine*, 15(4):531–538, jul 2011.
- [WF16] Daniel M. Wolpert and J. Randall Flanagan. Computations Underlying Sensorimotor Learning. *Current Opinion in Neurobiology*, 37:7–11, 2016.
- [WK10] Kunlin Wei and Konrad Körding. Uncertainty of Feedback and State Estimation Determines the Speed of Motor Adaptation. *Front. Comput. Neurosci.*, 4(11):1–9, 2010.
- [WMC⁺14] Howard G. Wu, Yohsuke R. Miyamoto, Luis Nicolas Gonzalez Castro, Bence P. Ölveczky, and Maurice A. Smith. Temporal Structure of Motor Variability is Dynamically Regulated and Predicts Motor Learning Ability. *Nature Neuroscience*, 17(2):312–321, 2014.
- [XZGC10] Hong-Bo Xie, Yong-Ping Zheng, Jing-Yi Guo, and Xin Chen. Cross-Fuzzy Entropy: A New Method to Test Pattern Synchrony of Bivariate Time Series. *Information Sciences*, 180(9):1715–1724, may 2010.
- [YH11] Aaron J. Young and Levi J. Hargrove. Effects of Interelectrode Distance on the Robustness of Myoelectric Pattern Recognition Systems. In *Eng. Med. Biol. Soc. EMBC, 2011 Annu. Int. Conf. IEEE*, pages 3873–3876, Boston, MA, 2011.
- [YHK12] Aaron J. Young, Levi J. Hargrove, and Todd A. Kuiken. Improving Myoelectric Pattern Recognition Robustness to Electrode Shift by Changing the Interelectrode Distance and Electrode Configuration. *IEEE Trans. Biomed. Eng.*, 59(3):645–652, 2012.
- [YSRH13] Aaron J. Young, Lauren H. Smith, Elliott J. Rouse, and Levi J. Hargrove. Classification of Simultaneous Movements Using Surface EMG Pattern Recognition. *IEEE Trans. Biomed. Eng.*, 60(5):1250–1258, 2013.
- [YSRH14] Aaron J. Young, Lauren H. Smith, Elliott J. Rouse, and Levi J. Hargrove. A Comparison of the Real-Time Controllability of Pattern Recognition to Conventional Myoelectric Control for Discrete and Simultaneous Movements. *Journal of Neuroengineering and Rehabilitation*, 11(5):1–10, 2014.
- [YZJL12] Dapeng Yang, Jingdong Zhao, Li Jiang, and Hong Liu. Dynamic Hand Motion Recognition Based on Transient and Steady-State EMG Signals. *International Journal of Humanoid Robotics*, 9(1):1–18, 2012.